Mathematical Problems in Engineering

New Trends on Modeling, Design, and Control of Chaotic Systems

Lead Guest Editor: Jesus M. Munoz-Pacheco
Guest Editors: Christos Volos, Eric Campos-Canton, Ahmad Taher Azar, Viet T. Pham, and Ahmed G. Radwan

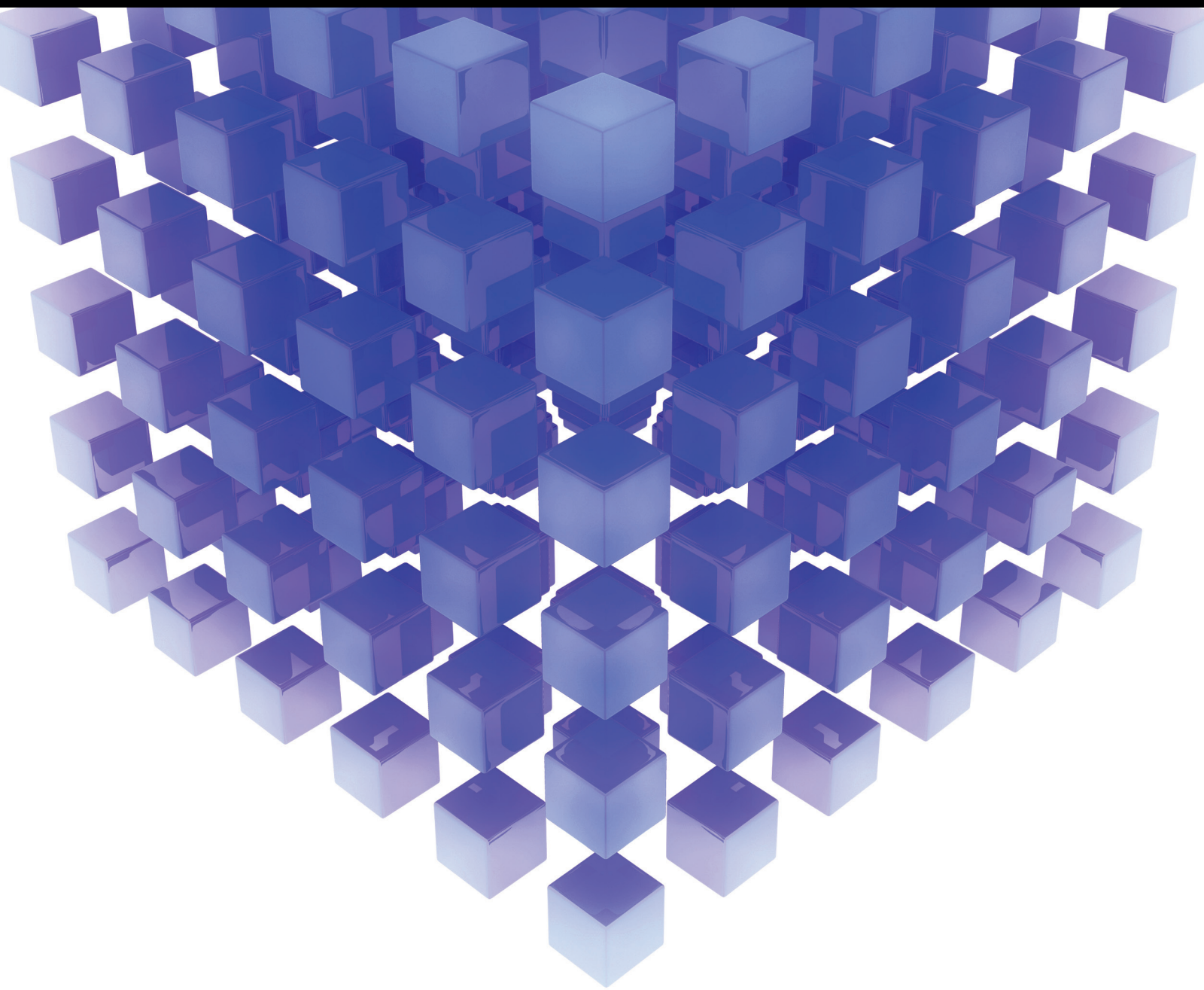

New Trends on Modeling, Design, and Control of Chaotic Systems

Mathematical Problems in Engineering

New Trends on Modeling, Design, and Control of Chaotic Systems

Lead Guest Editor: Jesus M. Munoz-Pacheco
Guest Editors: Christos Volos, Eric Campos-Canton, Ahmad Taher Azar, Viet T. Pham, and Ahmed G. Radwan

Editorial Board

Contents

Hindawi
Mathematical Problems in Engineering
Volume 2017, Article ID 3737681, 3 pages
https://doi.org/10.1155/2017/3737681

Editorial

New Trends on Modeling, Design, and Control of Chaotic Systems

Jesus M. Munoz-Pacheco,[1] Christos Volos,[2] Eric Campos-Canton,[3,4] Ahmad Taher Azar,[5,6] Viet-Thanh Pham,[7] and Ahmed G. Radwan[8]

[1]*Facultad de Ciencias de la Electrónica, Autonomous University of Puebla (BUAP), Av. San Claudio y 18 Sur, Edif. FCE1, 72570 Puebla, PUE, Mexico*
[2]*Department of Physics, Aristotle University of Thessaloniki, 54124 Thessaloniki, Greece*
[3]*División de Matemáticas Aplicadas, IPICYT, Camino a la Presa San José 2055, Col. Lomas 4a Sección, 78216 San Luis Potosí, SLP, Mexico*
[4]*Mathematics Department, University of Houston, Houston, TX, USA*
[5]*Faculty of Computers and Information, Benha University, Benha 13511, Egypt*
[6]*Nile University, Giza, Egypt*
[7]*School of Electronics and Telecommunications, Hanoi University of Science and Technology, Hanoi 100000, Vietnam*
[8]*Engineering Mathematics and Physics Department, Faculty of Engineering, Cairo University, Giza 12613, Egypt*

Correspondence should be addressed to Jesus M. Munoz-Pacheco; jesusm.pacheco@correo.buap.mx

Received 6 August 2017; Accepted 6 August 2017; Published 13 September 2017

Nowadays, one of the most studied phenomena is chaos into the nonlinear dynamical systems. For deterministic chaos to exist, a nonlinear dynamical system must have a dense set of periodic orbits and be transitive and sensitive to initial conditions. Their significance has been increased during the last decade because of several applications in diverse fields ranging from living systems, such as synchronization in neurobiology, chemical reactions among pancreatic cells, and social, economical, or political events, to nonliving systems including robotics, low power high-speed data transceivers for medical applications, chaotic electrochemical oscillators, encrypted communications, and control algorithms for motor drivers in electric vehicles. However, in order to exploit all the possible engineering applications, the open problems about chaotic systems need to be addressed by proposing novel theoretical and practical approaches focused on modeling, simulation, synthesis, design, control, and circuit implementation.

Lately, several synchronization schemes to coupling two chaotic systems, at least, have attracted increasing attention due to the fact that they are the core of many chaos-based secure communications technologies. Also, the current research interest in proposing novel multiscroll chaotic systems with self-excited or hidden attractors to increase the complexity has augmented considerably. Each new chaotic system is a potential candidate to improve chaos-based applications. Additionally, chaotic systems have been recently used to analyze financial models trying to predict the complexity of the markets with a huge effect in the global economy.

Therefore, the overall purpose of this special issue lies in gathering the latest scientific trends on the topics of chaotic systems with emphasis on real-world engineering applications. We had received a total of 28 submissions where the authors are from geographically distributed countries (China, Vietnam, Greece, Poland, Taiwan, Serbia, Iran, Tunisia, Turkey, Saudi Arabia, Egypt, Mexico, and Czech Republic). This reflects the high impact of the proposed topic and the seniority in organization of this special issue.

In the paper "Uncertain Unified Chaotic Systems Control with Input Nonlinearity via Sliding Mode Control," Z. Shen

et al. have studied the stabilization problem for a class of unified chaotic systems subject to uncertainties and input nonlinearity. Based on the sliding mode control theory, authors present a new method for the sliding mode controller design and the control law algorithm for such systems. In order to achieve the goal of stabilization unified chaotic systems, the presented controller can make the movement starting from any point in the state space reach the sliding mode in limited time and asymptotically reach the origin along the switching surface. Compared with the existing literature, the proposed controller has many advantages, such as having small chattering, having good stability, and being less conservative.

In the paper "Complexity Analysis of a Triopoly Cooperation-Competition Game Model in Convergence Product Market," L. Zhao et al. consider a tripartite cooperation-competition game model for the convergence product market, whose products are compounds of two base products or services. An early convergence product firm monopoly in this market and two potential entrants from the base products decide to cooperate with another to compete with the monopolist. Authors analyzed factors that affect existence and local stability of the Nash equilibrium. Rich nonlinear dynamic behaviors like bifurcation, chaos, and attractors are presented to explain the complex relationships between the three players. Results showed that the pulling effect on profit for the united R&D activity can significantly enlarge the stable region. Too frequently adjusted price strategy will bring the system into chaos. A parameter feedback control method is given to control the chaotic system and the authors numerically verified its effectiveness. This study has significant values to understand the fluctuations in related convergence product market.

In the paper "Hopf Bifurcation, Positively Invariant Set, and Physical Realization of a New Four-Dimensional Hyperchaotic Financial System," G. Kai et al. introduce a new four-dimensional hyperchaotic financial system on the basis of an established three-dimensional nonlinear financial system and a dynamic model by adding a controller term to consider the effect of control on the system. In terms of the proposed financial system, the sufficient conditions for nonexistence of chaotic and hyperchaotic behaviors are derived theoretically. Then, the solutions of equilibria are obtained. For each equilibrium, its stability and existence of Hopf bifurcation are validated. Based on corresponding first Lyapunov coefficient of each equilibrium, the analytical proof of the existence of periodic solutions is given. The ultimate bound and positively invariant set for the financial system are obtained and estimated. There exists a stable periodic solution obtained near the unstable equilibrium point. Finally, the dynamic behaviors of the new system are explored by theoretical analysis by using the bifurcation diagrams and phase portraits. Moreover, the hyperchaotic financial system has been simulated and implemented to confirm the results of the numerical integrations and its real contribution to engineering.

In the paper "Sliding Mode Control of Discrete Chaotic System Based on Multimodal Function Series Coupling," F. Hu has proposed a new sliding mode control model of discrete chaotic systems based on multimodal function series coupling to overcome the shortcomings of the standard PSO algorithm in multimodal function optimization. Firstly, a series coupled PSO algorithm (PP algorithm) based on multimodal function is constructed, which is optimized by multipeak solution on the basis of the standard PSO algorithm. Secondly, the improved PSO algorithm is applied to search all the extreme points in the feasible domain. Thirdly, the Powell method is used to perform the local optimization of the search results, and the newly generated extreme points are added to the extreme point database according to the same peak judgment operator. Finally, the long training time of PP algorithm can be overcome by the characteristics of fast convergence rate of the cloud mutation model. And also, both the population size and the redundancy can be reduced. Then, the clonal selection algorithm is used to keep the diversity of the population effectively. Simulation results of the sliding mode control of discrete chaotic systems have shown that the improved PSO algorithm obviously improves the response speed, overshoot, and so on.

In the paper "Synchronization in Coupled Multistable Systems with Hidden Attractors," G. PM and T. Kapitaniak present the results of coupling multistable systems which have hidden attractors with each other. Three modified Sprott systems were coupled and their synchronization was observed. The final state of the synchronized system changes with the change in the coupling strength. This was observed for two different types of coupling, one with a single variable and the other with two system variables.

In the paper "Stability and Multiscroll Attractors of Control Systems via the Abscissa," E.-C. Díaz-González et al. have established an approach to generate multiscroll attractors via destabilization of piecewise linear systems based on Hurwitz matrix. First the authors present some results about the abscissa of stability of characteristic polynomials from linear differential equations systems; that is, they consider Hurwitz polynomials. The starting point is the Gauss-Lucas Theorem, the authors provide lower bounds for Hurwitz polynomials, and by successively decreasing the order of the derivative of the Hurwitz polynomial one obtains a sequence of lower bounds. The results are extended in a straightforward way to interval polynomials; then authors apply the abscissa as a measure to destabilize Hurwitz polynomial for the generation of a family of multiscroll attractors based on a class of unstable dissipative systems (UDS) of type affine linear.

Acknowledgments

The guest editorial team would like to thank the authors of all the papers submitted to this special issue. Given the space limitations, a number of high quality contributions could not be accommodated. The editors also wish to thank the anonymous reviewers, some of whom helped with multiple review assignments. Additionally, we would like to thank the journal's Editorial Board for being very encouraging and accommodative regarding this special issue. Finally, J. M. Munoz-Pacheco acknowledges CONACYT for the financial support (no. 258880: Proyecto Apoyado por el Fondo Sectorial de Investigación para la Educación). We hope that you

will enjoy reading this special issue devoted to this exciting and fast-evolving field as much as we have done.

Jesus M. Munoz-Pacheco
Christos Volos
Eric Campos-Canton
Ahmad Taher Azar
Viet-Thanh Pham
Ahmed G. Radwan

Hindawi
Mathematical Problems in Engineering
Volume 2017, Article ID 6743734, 9 pages
https://doi.org/10.1155/2017/6743734

Research Article

Stability and Multiscroll Attractors of Control Systems via the Abscissa

Edgar-Cristian Díaz-González,[1] Baltazar Aguirre-Hernández,[1] Jorge Antonio López-Rentería,[2] Eric Campos-Cantón,[3,4] and Carlos Arturo Loredo-Villalobos[3]

[1]*Departamento de Matemáticas, Universidad Autónoma Metropolitana Iztapalapa, San Rafael Atlixco 186, 09340 CDMX, Mexico*
[2]*Departamento de Matemáticas, Universidad de Sonora, Hermosillo, SON, Mexico*
[3]*División de Matemáticas Aplicadas, IPICyT, 78216 San Luis, SLP, Mexico*
[4]*Mathematics Department, University of Houston, Houston, TX 77204-3008, USA*

Correspondence should be addressed to Carlos Arturo Loredo-Villalobos; calv@xanum.uam.mx

Received 4 January 2017; Revised 9 May 2017; Accepted 12 July 2017; Published 17 August 2017

Academic Editor: Driss Mehdi

We present an approach to generate multiscroll attractors via destabilization of piecewise linear systems based on Hurwitz matrix in this paper. First we present some results about the abscissa of stability of characteristic polynomials from linear differential equations systems; that is, we consider Hurwitz polynomials. The starting point is the Gauss–Lucas theorem, we provide lower bounds for Hurwitz polynomials, and by successively decreasing the order of the derivative of the Hurwitz polynomial one obtains a sequence of lower bounds. The results are extended in a straightforward way to interval polynomials; then we apply the abscissa as a measure to destabilize Hurwitz polynomial for the generation of a family of multiscroll attractors based on a class of unstable dissipative systems (UDS) of affine linear type.

1. Introduction

Consider the parametric dynamical system

$$\dot{\mathbf{x}} = f(\mathbf{x}, \mu), \tag{1}$$

where $\mathbf{x} \in \mathbb{R}^n$ is the state vector, $\mu \in \mathbb{R}^m$ is a parameter vector, and f is an enough smooth vector field. Several techniques have been proposed in the analysis of the solutions behavior of a dynamical system. The Hartman–Grobman theorem establishes that its internal evolution is determined by its Jacobian matrix. That is, the behavior of its solutions is described by the spectrum of its linearization. If all of the solutions of a dynamical system converge to an equilibrium point then it is said to be a *locally asymptotically stable system*. The importance of studying Hurwitz polynomials is due to its usefulness in the stability analysis of linear systems: if the characteristic polynomial of a linearized system is Hurwitz (roots with negative real part) then it is asymptotically stable. This has motivated researchers working on applications seeking such polynomials. Maxwell [1] posed the problem in the following way: How can one find the necessary and sufficient conditions to decide whether a polynomial has all its roots with negative real part? A solution was given by Hurwitz [2] and it is known as the Routh–Hurwitz criterion. Related information about Hurwitz polynomials can be found in [3–6].

The study of stability with a polynomial approach had an important impulse when Kharitonov's theorem was published in 1978. This theorem gives conditions for the stability of an interval family of polynomials (see [7]). Since then, a lot of works related to this theorem have been published (see, e.g., [8–12]). The importance of studying the stability of families of polynomials can be appreciated in applications where the presence of uncertainties in the polynomial

coefficients has to be taken into account. Other families of polynomials that have been investigated are the segments of polynomials (see [13–16]). Good references on families of stable polynomials are [3, 17–19]. The importance of knowing the abscissa of stability has been pointed out in [20–22]. Lower bounds were reported in [23, 24]; these are the first works about the abscissa of stability; and upper bounds were obtained in Bialas [25], Henrici [26], and Olifirov [27].

However, stability is not always required. For example, there is a class of chaotic dynamical systems based on unstable equilibria. Several times a structural change is given by one *bifurcation parameter* of μ that generates *bifurcation* in the solutions of the system. Generating chaotic behavior is the subject of interest in several areas in mathematics and engineering insomuch that researchers have taken the task of design systems with diverse techniques undergoing chaotic behavior with and without equilibria. One of the different chaotic behaviors is the presence of multiscroll attractor. Good references where the generation of multiscrolls has been studied are the works [28–35]. In this paper we use the abscissa of stability of Hurwitz polynomials to study the stability of systems in order to generate multiscroll attractors. To achieve the design of a chaotic system, a technique involving lower bounds for stabilizing and breaking down the stability to make multiscroll attractors arise is described. The rest of the paper is organized as follows: In Section 2, basic definitions and results needed for the development of our technique are given. In Section 3, the relation between the abscissas of stability σ_p and σ_p', of a Hurwitz polynomial $p(t)$ and its derivative polynomial $p'(t)$, respectively, is studied. Therein the relationship is the following inequality $\sigma_p' < \sigma_p$ which is used to obtain a lower bound for the abscissa of stability of a polynomial or an interval family of Hurwitz polynomials. We use the Gauss–Lucas Theorem 2 to analyze the Hurwitz stability of a polynomial and its derivative. Finally, in Section 4 an application of the lower bound to generate chaos is given.

2. Preliminaries

Consider an asymptotically stable linear system given by

$$\dot{\mathbf{x}} = A\mathbf{x}, \tag{2}$$

where $\mathbf{x}$ is the state vector of the system and $A \in \mathbb{R}^{n\times n}$ is a linear operator. Let $p(t)$ be the characteristic polynomial of A. The abscissa of stability of polynomial $p(t)$ is given by the following definition.

Definition 1. If $p(t)$ is a Hurwitz polynomial and $z_1, z_2, \ldots, z_n$ are its zeros then σ_p the abscissa of stability of $p(t)$ is defined by

$$\sigma_p = \max_{1\le i\le n} \{\operatorname{Re} z_i\}. \tag{3}$$

If $\underline{\sigma}_p$ and $\overline{\sigma}_p$ are numbers such that $\underline{\sigma}_p \le \sigma_p \le \overline{\sigma}_p$, then they are named lower and upper bound, respectively.

In Section 4 we consider a polynomial $p(t - r)$, so that, varying the parameter r, then we get destabilization of the polynomial $p(t)$ and we get the generation of multiscroll. In Section 4 we give the details. Now we present a useful theorem in our results.

Theorem 2 (Gauss–Lucas [36]). *Let K be any convex polygon enclosing all the zeros of the polynomial $f(z)$. Then the zeros of $f'(z)$ lie in K.*

Remark 3. Let us recall that a set of points is convex if it contains, with any two points P, Q in the set, the line segment joining P and Q.

The abscissa of stability σ_p of the characteristic polynomial of system (2) gives certain minimum rate of decay. Zakian and Al-Naib indicated that in computer-aided design of dynamical and control systems the numerical computation of the abscissa of stability is required (see [21, 37–39]) to warrant stability under perturbations.

3. Main Results

3.1. Abscissa of Hurwitz Polynomials: An Inequality between σ_p and $\sigma_{p'}$. Consider the polynomial $p(t) = a_n t^n + a_{n-1} t^{n-1} + \cdots + a_1 t + a_0$ with $a_i \in \mathbb{R}$ for all $i = 0, \ldots, n$.

Theorem 4. *If $p(t) = a_n t^n + a_{n-1} t^{n-1} + \cdots + a_1 t + a_0$ is a Hurwitz polynomial ($n \ge 2$) and σ_p and $\sigma_{p'}$ are the abscissas of stability of p and $p' = dp/dt$, respectively, then $\sigma_{p'} \le \sigma_p$.*

Proof. Let $p(t)$ be a Hurwitz polynomial. If $\xi_1, \xi_2, \ldots, \xi_n$ are the roots of $p(t)$ then its abscissa of stability σ_p is given by $\sigma_p = -R$, where $R = \max\{\overline{r} > 0 : \xi_1 + r, \xi_2 + r, \ldots, \xi_n + r \in \mathbb{C}^-, \forall r < \overline{r}\}$. Then $\sigma_p = -R$, where $R = \max\{\overline{r} > 0 : p(t - r)$ is a Hurwitz polynomial, $\forall r < \overline{r}\}$. Now, by the Gauss–Lucas Theorem 2 if $p(z)$ is Hurwitz then $p'(t)$ is Hurwitz. Consequently, if $p(t - r)$ is a Hurwitz polynomial then $p'(t - r)$ is a Hurwitz polynomial. This implies that $\sigma_{p'} \le \sigma_p$, as we claim. □

Example 5. Consider the polynomial $p(t) = t^3 + (19/6)t^2 + (8/3)t + 2/3$. The abscissa of stability of $p(t)$ is $\sigma_p = -0.5$ and the abscissa of stability of $p'(t) = 3t^2 + (19/3)t + 8/3$ is $\sigma_{p'} \approx -0.58$. We see that $\sigma_{p'} < \sigma_p$.

Example 6. Consider $p(t) = t^4 + (25/6)t^3 + (35/6)t^2 + (10/3)t + 2/3$. The abscissa of stability of $p(t)$ is $\sigma_p = -0.5$ and the abscissa of stability of $p'(t) = 4t^3 + (25/2)t^2 + (35/3)t + 10/3$ is $\sigma_{p'} \approx -0.57$. Therefore $\sigma_{p'} < \sigma_p$.

Example 7. Let $p(t) = t^3 + 4t^2 + 5t + 2$. The abscissa of stability of $p(t)$ is $\sigma_p = -1$ and the abscissa of stability of $p'(t) = 3t^2 + 8t + 5$ is $\sigma_{p'} = -1$. In this case we have that $\sigma_{p'} = \sigma_p$.

Remark 8. Theorem 4 leads to glimpsing the following open problem: if $p(t)$ is a Hurwitz polynomial, find necessary and sufficient conditions to make the equality $\sigma_{p'} = \sigma_p$ hold.

3.2. A Lower Bound of the Abscissa of Stability of a Polynomial

Theorem 9. *Let* $p(t) = a_n t^n + a_{n-1}t^{n-1} + a_{n-2}t^{n-2} + \cdots + a_2 t^2 + a_1 t + a_0$ *be a Hurwitz polynomial with positive coefficients and denote* $\Delta_p = [2(n-1)a_{n-1}]^2 - 8n(n-1)a_n a_{n-2}$. *The following inequalities hold:*

(a) *If* $\Delta_p \geq 0$, *then*

$$\frac{-2(n-1)a_{n-1} + \sqrt{\Delta_p}}{2n(n-1)a_n} \leq \sigma_p. \tag{4}$$

(b) *If* $\Delta_p < 0$, *then* $-a_{n-1}/na_n \leq \sigma_p$.

Proof. If $p(t) = a_n t^n + a_{n-1}t^{n-1} + a_{n-2}t^{n-2} + \cdots + a_1 t + a_0$ is a Hurwitz polynomial then $p^{(n-2)}(t) = n(n-1)\cdots 3a_n t^2 + (n-1)(n-2)\cdots 2a_{n-1}t + (n-2)\cdots 2a_{n-2}$ is a Hurwitz polynomial. By Theorem 4 we have that $\sigma_{p^{(n-2)}} \leq \sigma_{p^{(n-3)}} \leq \cdots \leq \sigma_{p'} \leq \sigma_p$. But $p^{(n-2)}(t) = 0$ if and only if $n(n-1)a_n t^2 + 2(n-1)a_{n-1}t + 2a_{n-2} = 0$. If $\Delta_p \geq 0$, then

$$\frac{-2(n-1)a_{n-1} + \sqrt{\Delta_p}}{2n(n-1)a_n} = \sigma_{p^{(n-2)}} \leq \sigma_p \tag{5}$$

and (a) is established. The proof of (b) follows in the same way. □

Example 10. For the polynomial $p(t) = 6t^5 + 43t^4 + 110t^3 + 125t^2 + 64t + 12$ we have that $n = 5$, $a_{n-2} = 110$, $a_{n-1} = 43$, $a_n = 6$, and $\Delta_p = 12736 \geq 0$. By part (a) of Theorem 9 we have that

$$\frac{-2(n-1)a_{n-1} + \sqrt{\Delta_p}}{2n(n-1)a_n} \tag{6}$$

is a lower bound of σ_p; that is, $-0.96 \leq -1/2 = \sigma_p$.

Example 11. Consider $p(t) = t^4 + 3t^3 + 5t^2 + 4t + 2$. Here $n = 4$, $a_{n-2} = 5$, $a_{n-1} = 3$, $a_n = 1$, and $\Delta_p = -156 \leq 0$. By part (b) of Theorem 9 we have that $-a_{n-1}/na_n$ is a lower bound of σ_p; that is, $-3/4 \leq -1/2 = \sigma_p$.

Remark 12. Consider

$$S_{mi} = -\left[\binom{n}{m}^{-1}\binom{n}{i}\left(\frac{a_m}{a_i}\right)\right]^{1/(i-m)} \tag{7}$$

$$\text{for } m = 0, 1, \ldots, i-1,\ i = 1, \ldots, n.$$

Note that (7) is a set of lower bounds that were obtained in [23, 24]. The bound obtained in Theorem 9(b) $-a_{n-1}/na_n$ is in the set of lower bounds given in (7): taking $m = n-1$ and $i = n$ we can see that $S_{(n-1)n} = -a_{n-1}/na_n$.

In fact, another way to obtain $S_{(n-1)n}$ is by mean of the abscissa of stability of the $(n-1)$th derivative $p^{(n-1)}(t) = n(n-1)\cdots 2a_n t + (n-1)(n-2)\cdots 2a_{n-1}$. Note that Theorem 9(a) is a new lower bound for the abscissa of stability and since it depends on three coefficients of $p(t)$ while the lower bounds in (7) only depend on two coefficients of $p(t)$, the bound in Theorem 9(a) is in some cases better than the bound in Theorem 9(b) as is illustrated by the following example.

Example 13. Consider the following polynomial $p(t) = 6t^5 + 43t^4 + 110t^3 + 125t^2 + 64t + 12$. Here $n = 5$, $a_{n-2} = 110$, $a_{n-1} = 43$, and $a_n = 6$. By item (a) from Theorem 9 we have that

$$\frac{-2(n-1)a_{n-1} + \sqrt{\Delta_p}}{2n(n-1)a_n} \approx -0.96 \tag{8}$$

is a lower bound of $\sigma_p = -1/2$ and $-a_{n-1}/na_n = -1.43 < -0.96 < -1/2 = \sigma_p$.

Example 14. Let $p(t) = 6t^3 + 19t^2 + 16t + 4$. Here $n = 3$, $a_{n-2} = 16$, $a_{n-1} = 19$, and $a_n = 6$. By item (a) from Theorem 9 we have that

$$\frac{-2(n-1)a_{n-1} + \sqrt{\Delta_p}}{2n(n-1)a_n} \approx -0.58 \tag{9}$$

is a lower bound of $\sigma_p = -1/2$ and $-a_{n-1}/na_n < -0.58 < \sigma_p$.

3.3. Lower Bounds for the Abscissa of Stability of an Interval Family of Hurwitz Polynomials. For a family of Hurwitz polynomials of degree n of the form

$$\mathcal{F} = \left\{ f(t) : f(t) = \sum_{j=0}^{n} a_{n-j}t^{n-j},\ a_i \in [\alpha_i, \beta_i],\ i = 0, 1, \ldots, n \right\} \tag{10}$$

the *abscissa of stability* is defined by $\max_{p\in\mathcal{F}}\sigma_p$.

Theorem 15. *Consider the family of Hurwitz polynomials* $f(t) = a_n t^n + a_{n-1}t^{n-1} + \cdots + a_1 t + a_0$ *with* $0 < \alpha_j \leq a_j \leq \beta_j$, $j = 0, 1, \ldots, n$; *we have that*

(a) $-\beta_{n-1}/(n\alpha_n)$ *is a lower bound for the abscissa of stability of the family of polynomials;*

(b) *if* $[2(n-1)\alpha_{n-1}]^2 - 8n(n-1)\beta_n\beta_{n-2} \geq 0$, *then* $-\beta_{n-1}/n\alpha_n$ *and*

$$\frac{-2(n-1)\beta_{n-1} + \sqrt{[2(n-1)\alpha_{n-1}]^2 - 8n(n-1)\beta_n\beta_{n-2}}}{2n(n-1)\beta_n} \tag{11}$$

are lower bounds for the abscissa of stability of the family of polynomials.

Proof. From item (b) of Theorem 9, $-a_{n-1}/(na_n)$ is a lower bound for the abscissa of stability of $f(t) = a_n t^n + a_{n-1}t^{n-1} +$

$\cdots + a_1 t + a_0$. On the other hand, since $-\beta_{n-1} \leq -a_{n-1} \leq -\alpha_{n-1}$ and $1/\beta_n \leq 1/a_n \leq 1/\alpha_n$, we have that $-\beta_{n-1}/n\alpha_n \leq -a_{n-1}/na_n$.

For item (b) of Theorem 9 suppose that $[2(n-1)\alpha_{n-1}]^2 - 8n(n-1)\beta_n\beta_{n-2} \geq 0$. From

$$\begin{aligned} \alpha_{n-2} \leq a_{n-2} \leq \beta_{n-2}, \\ \alpha_{n-1} \leq a_{n-1} \leq \beta_{n-1}, \\ \alpha_n \leq a_n \leq \beta_n, \end{aligned} \tag{12}$$

the next inequalities are obtained:

(1) $2(n-1)\alpha_{n-1} \leq 2(n-1)a_{n-1} \leq 2(n-1)\beta_{n-1}$,

(2) $8n(n-1)\alpha_n\alpha_{n-2} \leq 8n(n-1)a_na_{n-2} \leq 8n(n-1)\beta_n\beta_{n-2}$,

(3) $1/\beta_n \leq 1/a_n \leq 1/\alpha_n$,

(4) $-2(n-1)\beta_{n-1} \leq -2(n-1)a_{n-1}$,

(5) $[2(n-1)\alpha_{n-1}]^2 - 8n(n-1)\beta_n\beta_{n-2} \leq [2(n-1)a_{n-1}]^2 - 8n(n-1)a_na_{n-2}$,

(6) $1/2n(n-1)\beta_n \leq 1/2n(n-1)a_n$.

Thus

$$\begin{aligned} &\frac{-2(n-1)\beta_{n-1} + \sqrt{[2(n-1)\alpha_{n-1}]^2 - 8n(n-1)\beta_n\beta_{n-2}}}{2n(n-1)\beta_n} \\ &\leq \frac{-2(n-1)a_{n-1} + \sqrt{\Delta_p}}{2n(n-1)a_n}. \end{aligned} \tag{13}$$

This proves Theorem 15. □

Remark 16. Note that for every interval family of Hurwitz polynomials we give the lower bound $-\beta_{n-1}/(n\alpha_n)$. If additionally the family satisfies $[2(n-1)\alpha_{n-1}]^2 - 8n(n-1)\beta_n\beta_{n-2} \geq 0$ then we can give a second lower bound given by

$$\frac{-2(n-1)\beta_{n-1} + \sqrt{[2(n-1)\alpha_{n-1}]^2 - 8n(n-1)\beta_n\beta_{n-2}}}{2n(n-1)\beta_n}. \tag{14}$$

Remark 17. In Theorem 15 we have two lower bounds, but there could be more lower bounds. The abscissa is the maximum of all of them. That is, another way of obtaining the abscissa of stability is to take the maximum of the lower bounds.

Example 18. Consider the family of Hurwitz polynomials

$$f(t) = a_4t^4 + a_3t^3 + a_2t^2 + a_1t + a_0, \tag{15}$$

where $10 \leq a_0 \leq 20$, $23 \leq a_1 \leq 34$, $18 \leq a_2 \leq 19$, $5 \leq a_3 \leq 7$, and $1 \leq a_4 \leq 1$. Here $\alpha_0 = 10$, $\beta_0 = 20, \ldots, \alpha_4 = 1$, $\beta_4 = 1$, and $n = 4$.

Since $[2(n-1)\alpha_{n-1}]^2 - 8n(n-1)\beta_n\beta_{n-2} = -828 < 0$ by part (a) of Theorem 15 we have that $-\beta_{n-1}/n\alpha_n = -\beta_3/4\alpha_4 = -7/4$ is a lower bound of the abscissa of stability of the family Hurwitz polynomials.

Example 19. Consider the family of Hurwitz polynomials

$$f(t) = a_3t^3 + a_2t^2 + a_1t + a_0, \tag{16}$$

where $0.25 \leq a_0 \leq 1.25$, $0.75 \leq a_1 \leq 1.25$, $2.75 \leq a_2 \leq 3.25$, and $0.25 \leq a_3 \leq 1.75$. Here $\alpha_0 = 0.25$, $\beta_0 = 1.25, \ldots, \alpha_3 = 0.25$, $\beta_3 = 1.75$, and $n = 3$. Since $[2(n-1)\alpha_{n-1}]^2 - 8n(n-1)\beta_n\beta_{n-2} = 46 > 0$, by item (b) from Theorem 15 we have that

$$\begin{aligned} &\frac{-2(n-1)\beta_{n-1} + \sqrt{[2(n-1)\alpha_{n-1}]^2 - 8n(n-1)\beta_n\beta_{n-2}}}{2n(n-1)\beta_n} \\ &\approx -0.41, \end{aligned} \tag{17}$$

which is a lower bound of the abscissa of stability of the family of Hurwitz polynomials.

4. The Abscissa to Generate Instability and Multiscrolls Attractors

In the study of multiscroll attractors different aspects are interesting and one of them is when the multiscroll attractor exists for a particular set of system's parameters; then the interest is about robustness against parametric perturbation. For instance, we would like to know the variation of the values of parameters of a given system in order to preserve the multiscroll attractor. In this direction a polynomial approach has been used to find the maximal robust dynamics [40] and for studying the maximum range for a set of parameters to preserve the useful instability for the generation of multiscroll attractors [41]. Now, let us apply the abscissa approach for finding the lower bound of the abscissa of hyperbolicity and instability needed in UDS to generate multiscroll attractors. The linear system (2) under a control action is given as follows:

$$\dot{x} = Ax + Bu, \tag{18}$$

with Hurwitz characteristic polynomial of A, $p(t) = t^n + a_{n-1}t^{n-1} + \cdots + a_1t + a_0$. Define $f_r(t) = p(t-r)$, with $r \geq 0$. Note that $f_r(t)$ is a set of polynomials such that $f_0(t) = p(t)$ is a Hurwitz polynomial and the abscissa of stability can be calculated by

$$\sigma_{f_r} = -\max_{\bar{r}} \{\bar{r} > 0 \mid f_r(t) \text{ is Hurwitz } \forall r,\ r < \bar{r}\}. \tag{19}$$

Now, by Taylor's theorem $f_r(t) = p(t-r)$ can be rewritten as

$$\begin{aligned} f_r(t) &= t^n + \frac{p^{(n-1)}(-r)}{(n-1)!}t^{n-1} + \cdots + \frac{p'(-r)}{1!}t + p(-r) \\ &= t^n + A_{n-1}(r)t^{n-1} + \cdots + A_1(r)t + A_0(r). \end{aligned} \tag{20}$$

If $r = -\sigma_p$ then $f_r(t)$ has roots in the imaginary axis. Thence, the system is unstable in the interval $(-\sigma_p, \infty)$. Let us describe the class of instabilities by considering the following system in $\mathbb{R}^3$.

Definition 20. We have the following system:

$$\dot{x} = Ax, \tag{21}$$

where $x \in R^3$ is the state vector, $A \in R^{3\times 3}$ is a linear operator with eigenvalues λ_i, and $i = 1, 2, 3$ is said to be *dissipative* if $\sum_{i=1}^{3} \lambda_i < 0$. The system is said to be *unstable and dissipative of type I* (UDS-I) if one of its eigenvalues is a negative real number and the other two are complex conjugate numbers with positive real part; and it is said to be of *type II* (UDS-II) if one of its eigenvalues is a positive real number and the other two are complex conjugate numbers with negative real part.

This work is based on UDS-I, so a generalization of the above definition for UDS-I with dimension greater than three can be given as follows.

Definition 21. The system given by (21) where $x \in \mathbb{R}^n$, $A \in \mathbb{R}^{n\times n}$, and eigenvalues λ_i, $i = 1, 2, \ldots, n$, is said to be *dissipative* if $\sum_{i=1}^{n} \lambda_i < 0$. The system is said to be *unstable and dissipative of type I* (UDS-I) if $n - 2$ of its eigenvalues are negative real numbers and the other two are complex conjugate numbers with positive real part.

Due to the relation between the linear system like (21) and its characteristic polynomial, we shall say that an n-degree polynomial $p(t)$ is dissipative if the sum of its roots is negative. In a similar way, $p(t)$ will be a UDS-I polynomial if its roots satisfy Definition 21 for systems of type I. Notice that Definition 21 is only one possibility to define UDS considering $n - 2$ negative real numbers.

Lemma 22. *Let $p(t)$ be a real n-degree Hurwitz polynomial with roots $t_1, \ldots, t_n$. If $f_r(t) = p(t - r)$ is unstable and dissipative, then the following conditions are satisfied:*

(i) $r > -\sigma_p$.

(ii) $r < U_{diss(p)} = -(1/n)\sum_{j=1}^{n} t_j$.

Proof. The proof of (i) is obvious. We will focus on the proof of (ii). Firstly, it is not too hard to see that if the root t_j of $p(t)$ has nonzero imaginary part, then its translation $r + t_j$ and its conjugate are roots of $f_r(t)$, with $r \in \mathbb{R}$. Namely, by writing $p(t) = \prod_{j=1}^{n}(t - t_j)$, then

$$f_r(t) = \prod_{j=1}^{n}\left[t - r - t_j\right] = \prod_{j=1}^{n}\left[t - \left(r + t_j\right)\right]. \tag{22}$$

Thence,

$$\sum_{j=1}^{n}\left(r + t_j\right) = \sum_{j=1}^{n} t_j + nr, \tag{23}$$

and since $\sum_{j=1}^{n} t_j < 0$, then $-(1/n)\sum_{j=1}^{n} t_j > 0$ and

$$\sum_{j=1}^{n} t_j + nr < 0 \Longleftrightarrow \quad r < -\frac{1}{n}\sum_{j=1}^{n} t_j. \tag{24}$$

Therefore, if $f_r(t)$ is unstable and dissipative, then $r < -(1/n)\sum_{j=1}^{n} t_j$, as we claim. □

Remark 23. The previous lemma provides an upper bound for dissipativity. However, it may happen that $-\sigma_p = U_{\mathrm{diss}(p)}$ in the case when $\mathrm{Re}(t_j) = c$, for all $j = 1, \ldots, n$.

Given the fact that a Hurwitz polynomial $p(t)$ can be perturbed to be unstable for (σ_p, ∞) and that $U_{\mathrm{diss}(p)}$ is an upper bound for the dissipativity, it is possible to carry the system from stability to instability in the sense of UDS if at least one of its roots has different real part than the others. The following result is immediate from the aforementioned discussion.

Corollary 24. *Consider the Hurwitz polynomial $p(t) = \prod_{j=1}^{n}(t - t_j)$, with $n-2$ real roots and a pair of conjugate complex roots, say, t_i, t_{i+1}, for some $1 \le i \le n$. Then*

(i) *$f_r(t)$ is Hurwitz if and only if $r < -\sigma_p$.*

(ii) *If $\mathrm{Re}(t_i) \neq t_j$, $i \neq j$, then $f_r(t)$ is UDS if and only if $r \in (-\sigma_p, U_{diss(p)})$.*

In order to generate multiscroll attractors, let us consider the control system

$$\dot{\mathbf{x}} = \mathbf{A}\mathbf{x} + \mathbf{B}S + bu, \tag{25}$$

where $\mathbf{x} = [x_1, x_2, \ldots, x_n]^T \in \mathbb{R}^n$ is the state vector, $\mathbf{B} \in \mathbb{R}^n$ stands for a real affine vector, and $\mathbf{A} = [a_{ij}] \in \mathbb{R}^{n\times n}$ with $i, j = 1, 2, \ldots, n$ denotes a nonsingular linear matrix.

Let $p_A(t)$ be the characteristic polynomial of the system, $b^T = (0, 0, \ldots, 0, 1)$, and S is the following step function:

$$S = \begin{cases} s_1 & \text{for } c_1 < x_1, \\ s_2 & \text{for } c_2 < x_1 \le c_1, \\ \vdots & \\ s_m & \text{for } c_m < x_1 \le c_{m-1}, \end{cases} \tag{26}$$

where the values c_i's must be chosen in a suitable way that will be explained below. Define the linear control $u = c^T(r)x = (a_0 - A_0(r), a_1 - A_1(r), \ldots, a_{n-1} - A_{n-1}(r))x$, where $A_j(r) = p^j(-r)/j$. Then the controlled system is

$$\dot{\mathbf{x}} = \begin{pmatrix} 0 & 1 & 0 & \cdots & 0 \\ 0 & 0 & 1 & \cdots & 0 \\ \vdots & \vdots & & & 0 \\ -A_0(r) & -A_1(r) & -A_2(r) & \cdots & -A_{n-1}(r) \end{pmatrix}\mathbf{x} + \mathbf{B}S = \mathbf{A_c}\mathbf{x} + \mathbf{B}S. \tag{27}$$

Thus, the closed-loop characteristic polynomial is given by

$$\begin{aligned} f_r(t) &= t^n + A_{n-1}(r)\, t^{n-1} + \cdots + A_0(r) \\ &= t^n + \frac{p^{n-1}(-r)}{(n-1)!} t^{n-1} + \cdots + \frac{p(-r)}{0!} \\ &= p_A(t-r). \end{aligned} \tag{28}$$

When $r = 0$, A_0 is a stable matrix and $f_0(t) = p_A(t)$ but when $r > -\sigma_{p_A}$ we can obtain dissipative systems with unstable dynamics and the possibility of generating multiscroll attractors. As described in Definition 21, a system with stability index $n-2$ will be addressed as a system of the UDS type I. Besides, the following considerations have to be made in order to call (25) a UDS of type I that in addition generates an attractor $\mathfrak{A}$.

(a) The linear part of the system must satisfy the dissipative condition $\sum_{i=1}^{n} \lambda_i < 0$, where $\lambda_i, i = 1, 2, \ldots, n$, are eigenvalues of $\mathbf{A_c}$. Consider also that $n-2$ eigenvalues are negative real numbers, and two λ_i values are complex conjugate eigenvalues with positive real part $\mathrm{Re}\{\lambda_i\} > 0$, resulting in an unstable focus-saddle equilibrium $\mathbf{X}^*$. This type of equilibria presents a stable manifold $M^s = \mathrm{span}\{V_{\lambda_1}, \ldots, \lambda_{n-2}\} \in \mathbb{R}^n$ with a fast eigendirection and an unstable manifold $M^u = \mathrm{span}\{V_{\lambda_{n-1}}, V_{\lambda_n}\} \in \mathbb{R}^n$ with a slow spiral eigendirection, where V_{λ_i} corresponds to the eigenvector of $\mathbf{A}$ regarding the eigenvalue λ_i.

(b) The affine vector $\mathbf{BS}$ must be considered as a discrete function that changes depending on which domain $\mathscr{D}_i \subset \mathbb{R}^n$ the trajectory is located at. Accordingly $\mathbb{R}^n = \bigcup_{i=1}^{k} \mathscr{D}_i$. Then a switching system based on (25) is given by

$$\dot{\mathbf{X}} = \mathbf{A_c}\mathbf{X} + \mathbf{BS}(\mathbf{X}),$$

$$\mathbf{S}(\mathbf{X}) = \begin{cases} s_1, & \text{if } X \in \mathscr{D}_1; \\ s_2, & \text{if } X \in \mathscr{D}_2; \\ \vdots & \vdots \\ s_k, & \text{if } X \in \mathscr{D}_k. \end{cases} \tag{29}$$

The equilibria of system (29) are $\mathbf{X}_i^* = -\mathbf{A_c}^{-1}\mathbf{BS}$, with $i = 1, \ldots, k$, and each entry s_i of the switching system is considered in order to preserve bounded trajectories of system (29). Thence, the choice of c_i's in the definition of the step function $\mathbf{S}$ will determine the commutation regions $\mathscr{D}_i$'s that enclose each equilibrium $\mathbf{X}_i^*$.

The commuting system given by (29) induces in phase space $\mathbb{R}^n$ the flow (φ^t), $t \in \mathbb{R}$, such that each forward trajectory of the initial point $\mathbf{X}_0 = \mathbf{X}(t=0)$ is the set $\{\mathbf{X}(t) = \varphi^t(\mathbf{X}_0) : t \geq 0\}$. Furthermore, these systems have a dissipative bounded region $\Omega \subset \mathbb{R}^n$ named basin of attraction, such that the flow $\varphi^t(\Omega) \subset \Omega$ for every $t \geq 0$. The attractor $\mathfrak{A}$ is the largest attracting invariant subset of Ω.

Definition 25. Consider a system given by (29) in $\mathbb{R}^n$ and equilibrium points $\mathbf{X}_i^*$, with $i = 1, \ldots, k$ and $k \geq 2$. We say that system (29) can generate multiscroll attractors with the minimum of equilibrium points, if for any initial condition $X_0 \in \mathfrak{B} \subset \mathbb{R}^n$ in the basin of attraction the orbit $\varphi(X_0)$ generates an attractor $\mathfrak{A} \subset \mathbb{R}^n$ with oscillations around each $\mathbf{X}_k^*$.

We exemplify the theory by presenting a case in $\mathbb{R}^3$ where the following theorem holds.

Theorem 26. *Consider system (25) for the particular case where the dimension is three. That is, consider a 3D-control system with characteristic Hurwitz polynomial* $p_A(t) = (t + \zeta)(t + \bar{\zeta})(t + \rho)$, *where* $\mathrm{Im}(\zeta) \neq 0$. *If* $\mathrm{Re}(\zeta) \neq \rho$, *then the closed-loop system with the control* $u = c^T(r)x$ *is UDS for all* $r \in (-\sigma_{p_A}, U_{diss(p_A)})$.

Proof. Note that the closed-loop system (25) with the feedback $u = c^T(r)x$ has a characteristic polynomial to the polynomial family $f_r(t) = p_A(t-r)$. Then by Corollary 24 $f_r(t)$ is UDS for all $r \in (-\sigma_{p_A}, U_{\mathrm{diss}(p_A)})$. This completes the proof. □

A system satisfying the previous theorem is candidate to generate multiscroll attractors emerging from its equilibria with a suitable step function S. The number of scrolls in the attractor $\mathfrak{A}$ is due to the step function S. Next, let us illustrate the generation of multiscroll attractors. Consider the system

$$\dot{x} = \begin{pmatrix} 0 & 1 & 0 \\ 0 & 0 & 1 \\ -50 & -20 & -7 \end{pmatrix} x + \begin{pmatrix} 0 \\ 0 \\ 7.0278 \end{pmatrix} S + \begin{pmatrix} 0 \\ 0 \\ 1 \end{pmatrix} u \tag{30}$$

with step function

$$S(x_1) = \begin{cases} 3, & \text{for } 0.5 < x_1; \\ 2, & \text{for } 0.3 < x_1 \leq 0.5; \\ 1, & \text{for } 0.1 < x_1 \leq 0.3; \\ 0, & \text{for } x_1 \leq 0.1. \end{cases} \tag{31}$$

$u = (50 - p(-r), 20 - p'(-r)/1!, 7 - p''(-r)/2!)x$, where $p(t) = t^3 + 7t^2 + 20t + 50$ is Hurwitz.

The controlled system is

$$\dot{x} = \begin{pmatrix} 0 & 1 & 0 \\ 0 & 0 & 1 \\ -p(-r) & -\dfrac{-p'(-r)}{1!} & -\dfrac{-p''(-r)}{2!} \end{pmatrix} x + \begin{pmatrix} 0 \\ 0 \\ 7.0278 \end{pmatrix} S. \tag{32}$$

Denote $f_r(t) = t^3 + (p''(-r)/2!)t^2 + (p'(-r)/1!)t + p(-r)$ for $r = 0$. $f_0(t) = p(t) = t^3 + 7t^2 + 20t + 50$ is a Hurwitz polynomial

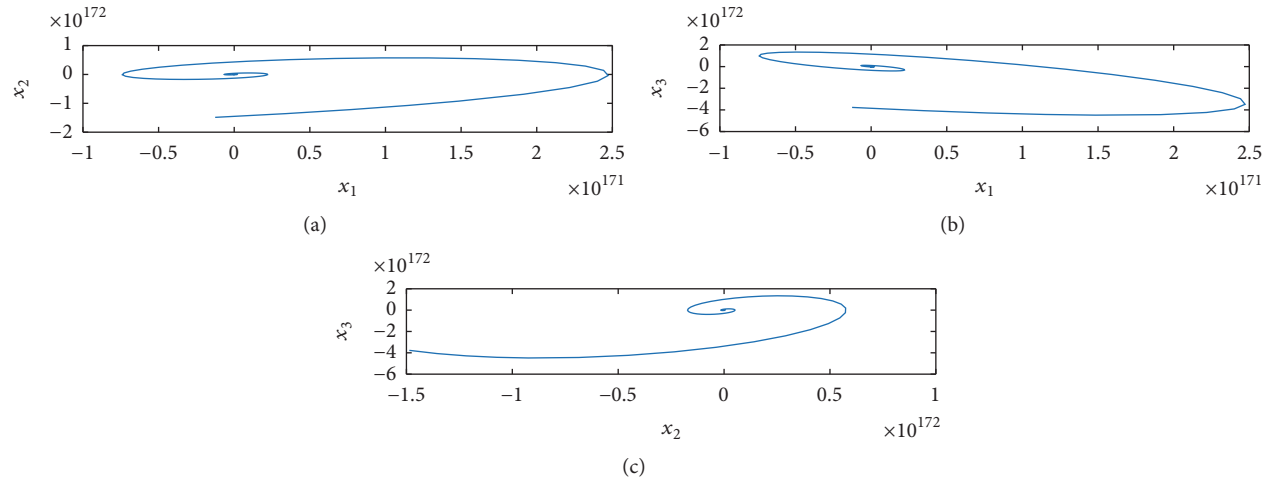

Figure 1: Projections of the solution of system (30) onto the planes: (a) (x_1, x_2); (b) (x_1, x_3); and (c) (x_2, x_3).

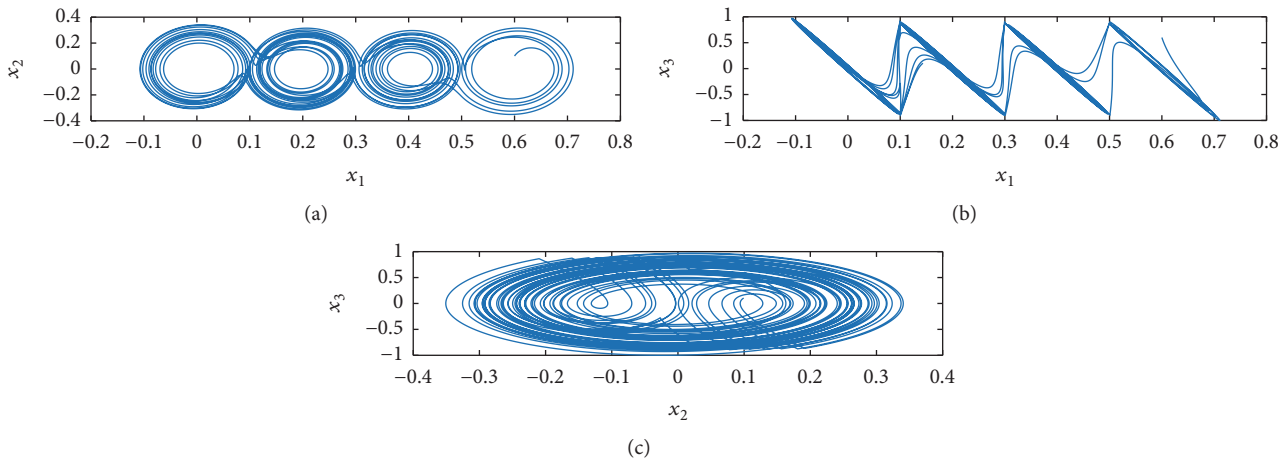

Figure 2: Projections of the attractor onto the planes: (a) (x_1, x_2); (b) (x_1, x_3); and (c) (x_2, x_3).

and there is no multiscroll. Figure 1 shows the projection of the stable solution onto the planes: (a) (x_1, x_2); (b) (x_1, x_3); and (c) (x_2, x_3).

The abscissa of $f_0(t)$ is $\sigma_{f_0} = -1$. Then other behavior could appear when $r \in (1, \infty)$. For example, for $r = 1.1$, $f_2(t) = t^3 + 3.7t^2 + 8.23t + 35.139$; hence $\sum_{j=1}^{3} t_j < 0$; consequently system (32) is dissipative when $r = 1.1$ and in Figure 2 the generation of multiscroll attractor is illustrated. Another reference where multiscroll attractors have been studied is [40].

The equilibria of the system for $r = 1.1$ are given by $\mathbf{X}_1^* = (0.6, 0, 0)^T$, $\mathbf{X}_2^* = (0.4, 0, 0)^T$, $\mathbf{X}_3^* = (0.2, 0, 0)^T$, and $\mathbf{X}_4^* = (0, 0, 0)^T$. Between equilibria, the commutation surfaces at the planes are as follows: $P_i = \{(x_1, x_2, x_3)^T \in \mathbb{R}^3 \mid x_1 = 0.1 + 0.2 * (i - 1)\}$, with $i = 1, 2, 3$, dividing the space into four domains $\mathscr{D}_{1,2,3,4}$ given by $\mathscr{D}_1 = \{(x_1, x_2, x_3)^T \in \mathbb{R}^3 \mid 0.5 < x_1\}$, $\mathscr{D}_2 = \{(x_1, x_2, x_3)^T \in \mathbb{R}^3 \mid 0.3 < x_1 \leq 0.5\}$, $\mathscr{D}_3 = \{(x_1, x_2, x_3)^T \in \mathbb{R}^3 \mid 0.1 < x_1 \leq 0.3\}$, and $\mathscr{D}_4 = \{(x_1, x_2, x_3)^T \in \mathbb{R}^3 \mid x_1 \leq 0.1\}$. Notice two important facts about the system; first the scrolls are increasing their size due to the unstable manifold; this can be better appreciated at the projection of the attractor onto the (x_1, x_3) plane from Figure 2(b). Second, the trajectory of the system oscillating around the equilibrium point $\mathbf{X}_4^*$ in $\mathfrak{A} \cap \mathscr{D}_4$ escapes from the domain $\mathscr{D}_4$ located in the left side of the commutation surface. This occurs near the unstable manifold $E^u \subset \mathscr{D}_4$ where it crosses the commutation surface and it is attracted by the stable manifold $E^s \subset \mathscr{D}_3$ to the equilibrium point $\mathbf{X}_3^*$ in the domain $\mathscr{D}_3$ located at the right side of the commutation surface P_1. The process is repeated in the inverse way forming scrolls around each equilibrium point.

5. Conclusion

In this paper we use the Gauss–Lucas theorem for obtaining an inequality between the abscissas of stability of a Hurwitz polynomial and its derivative. Then we use such inequality for getting a lower bound for the abscissa of a polynomial and for an interval family of polynomials. We have compared the lower bounds obtained with other works and we can say that the obtained bounds in this paper are easy to

calculate and sometimes are better that others. Based on the aforementioned results, an approach to generate multiscroll attractors was presented. We consider that this result is important to help in understanding the emergence of chaos in stable systems. Using the abscissa of stability we can generate multiscroll attractors from a Hurwitz polynomial. One interesting aspect is that we can generate multiscroll attractor with the change of only one parameter.

Conflicts of Interest

The authors declare that there are no conflicts of interest regarding the publication of this paper.

Acknowledgments

The first author wishes to thank CONACYT for its Ph.D. scholarship support. Jorge Antonio López-Rentería also wishes to thank CONACYT for the postdoctoral grant (Grant no. 290941-UIA) and the Iberoamerican University for the support in the realization of this paper. C. A. Loredo-Villalobos also wishes to acknowledge the support of CONACYT through the postdoctoral fellowship. Eric Campos-Cantón acknowledges the CONACYT financial support for sabbatical. He would also like to thank the University of Houston for his sabbatical support and Professor Matthew Nicol for allowing him to work with him and his valuable discussions on dynamic systems.

References

[1] J. C. Maxwell, "On Governors," *Proceedings of the Royal Society of London*, vol. 16, pp. 270–283, 1868.

[2] A. Hurwitz, "Ueber die Bedingungen, unter welchen eine Gleichung nur Wurzeln mit negativen reellen Theilen besitzt," *Mathematische Annalen*, vol. 46, no. 2, pp. 273–284, 1895.

[3] S. P. Bhattacharyya, H. Chapellat, and L. H. Keel, *Robust Control: The parametric approach*, Prentice-Hall, Upper Saddle River, NJ, USA, 1995.

[4] F. R. Gantmacher, *The Theory of Matrices*, vol. 1, Chelsea Publishing, New York, NY, USA, 1959.

[5] P. Lancaster and M. Tismenetsky, *The Theory of Matrices*, Academic Press, New York, NY, USA, 2nd edition, 1985.

[6] M. Marden, *Geometry of polynomials*, Mathematical Surveys, No. 3, American Mathematical Society, Providence, R.I., USA, 2nd edition, 1966.

[7] V. L. Kharitonov, "Asymptotic stability of an equilibrium position of a family of systems of linear differential equations," *Differentsial'nye Uravneniya*, vol. 14, pp. 2086–2088, 1978.

[8] F. Blanchini, R. Tempo, and F. Dabbene, "Computation of the minimum destabilizing volume for interval and affine families of polynomials," *Institute of Electrical and Electronics Engineers. Transactions on Automatic Control*, vol. 43, no. 8, pp. 1159–1163, 1998.

[9] F. Dabbene, B. T. Polyak, and R. Tempo, "On the complete instability of interval polynomials," *Systems & Control Letters*, vol. 56, no. 6, pp. 431–438, 2007.

[10] A. A. Kale and A. L. Tits, "On Kharitonov's theorem without invariant degree assumption," *Automatica. A Journal of IFAC, the International Federation of Automatic Control*, vol. 36, no. 7, pp. 1075-1076, 2000.

[11] R. Tempo, "A dual result to Kharitonov's theorem," *Institute of Electrical and Electronics Engineers. Transactions on Automatic Control*, vol. 35, no. 2, pp. 195–198, 1990.

[12] J. C. Willems and R. Tempo, "The Kharitonov theorem with degree drop," *Institute of Electrical and Electronics Engineers. Transactions on Automatic Control*, vol. 44, no. 11, pp. 2218–2220, 1999.

[13] B. Aguirre, C. Ibarra, and R. Suárez, "Sufficient algebraic conditions for stability of cones of polynomials," *Systems & Control Letters*, vol. 46, no. 4, pp. 255–263, 2002.

[14] B. Aguirre and R. Suárez, "Algebraic test for the Hurwitz stability of a given segment of polynomials," *Boletín de la Sociedad Matemática Mexicana 1 No. 2*, vol. 12, no. 2, pp. 261–275, 2006.

[15] S. Bialas, "A necessary and sufficient condition for the stability of convex combinations of stable polynomials or matrices," *Bulletin of the Polish Academy of Sciences. Technical Sciences*, vol. 33, no. 9-10, pp. 473–480, 1985.

[16] J.-A. López-Renteria, B. Aguirre-Hernández, and F. Verduzco, "The boundary crossing theorem and the maximal stability interval," *Mathematical Problems in Engineering*, Article ID 123403, 13 pages, 2011.

[17] J. Ackerman, *Robust Control. The Parameter Space Approach*, Springer-Verlag, New York, 2002.

[18] R. B. Barmish, *New Tools for Robustness of Linear Systems*, MacMillan Publishing Co, New York, 1994.

[19] P. Dorato, R. Tempo, and G. Muscato, "Bibliography on robust control," *Automatica. A Journal of IFAC, the International Federation of Automatic Control*, vol. 29, no. 1, pp. 201–213, 1993.

[20] O. Taussky-Todd, "On stable matrices," in *Colloques Internationaux Du Centre National De La Recherche Scientifique*, vol. 165, pp. 75–88, Paris, France, 1968.

[21] V. Zakian and U. Al-Naib, "Design of dynamical and control systems by the method of inequalities," *Proceedings of the Institution of Electrical Engineers*, vol. 120, no. 11, pp. 1421–1427, 1973.

[22] V. Zakian, "New formulation for the method of inequalities," *Proceedings of the Institution of Electrical Engineers*, vol. 126, no. 6, pp. 579–584, 1979.

[23] G. Schrack F, *Lower Bounds for the Abscissa of Stability of Stable Polynomials. Dissertation 4065 [M.sc. thesis]*, Eidgenossische Technische Hochschule, Zurich, 1967.

[24] G. F. Schrack, "Lower bounds to the abscissa of stability of a stable polynomial from symmetric functions," *SIAM Journal on Applied Mathematics*, vol. 21, pp. 373–379, 1971.

[25] S. Bialas, "Upper bounds for the abscissa of stability of a stable interval polynomial," *Bulletin of the Polish Academy of Sciences. Mathematics*, vol. 32, no. 1-2, pp. 1–9, 1984.

[26] P. Henrici, "Upper bounds for the abscissa of stability of a stable polynomial," *SIAM Journal on Numerical Analysis*, vol. 7, pp. 538–544, 1970.

[27] K. L. Olifirov, "Determination of a neighborhood of the imaginary axis which is disjoint from the spectrum of a real polynomial," *Mathematical Notes of the Academy of Sciences of the USSR*, vol. 22, no. 2, pp. 581–584, 1977.

[28] E. Campos-Cantón, J. G. Barajas-Ramírez, G. Solís-Perales, and R. Femat, "Multiscroll attractors by switching systems.," *Chaos (Woodbury, N.Y.)*, vol. 20, no. 1, p. 013116, 2010.

[29] E. Campos-Cantón, R. Femat, and G. Chen, "Attractors generated from switching unstable dissipative systems," *Chaos*, vol. 22, no. 3, Article ID 033121, 2012.

[30] J. Lü, F. Han, X. Yu, and G. Chen, "Generation 3-D multi-scroll chaotic attractors: a hysteresis series switching methods," *Automatica*, vol. 40, no. 10, pp. 1677–1687, 2014.

[31] L. J. Ontanon-García, E. Jimenez-López, E. Campos-Cantón, and M. Basin, "A family of hyperchaotic multi-scroll attractors in Rn," *Applied Mathematics and Computation*, vol. 233, pp. 522–533, 2014.

[32] C. Sánchez-López, R. Trejo-Guerra, J. M. Muñoz-Pacheco, and E. Tlelo-Cuautle, "N-scroll chaotic attractors from saturated function series employing CCII+s," *Nonlinear Dynamics*, vol. 61, no. 1-2, pp. 331–341, 2010.

[33] J. A. K. Suykens and J. Vandewalle, "Generation of n-Double Scrolls (n = 1, 2, 3, 4,. . .)," *IEEE Transactions on Circuits and Systems I: Fundamental Theory and Applications*, vol. 40, no. 11, pp. 861–867, 1993.

[34] J. A. K. Suykens, A. Huang, and L. O. Chua, "A family of n-scrolls attractors from a generalized Chuas circuit," *International Journal of Electronics and Communications*, vol. 51, no. 3, pp. 131–138, 1997.

[35] M. s. Yalcin, J. A. Suykens, J. Vandewalle, and S. Özoguz, "Families of scroll grid attractors," *International Journal of Bifurcation and Chaos in Applied Sciences and Engineering*, vol. 12, no. 1, pp. 23–41, 2002.

[36] H. S. Wilf, *Mathematics for the physical sciences*, Dover Publications, Inc., 180 Varick Street, New York, NY, USA, 1978.

[37] V. Zakian, "Computation of the abscissa of stability by repeated use of the Routh test," *Institute of Electrical and Electronics Engineers. Transactions on Automatic Control*, vol. 24, no. 4, pp. 604–607, 1979.

[38] V. Zakian, "A criterion of approximation for the method of inequalities," *International Journal of Control*, vol. 37, no. 5, pp. 1103–1111, 1983.

[39] V. Zakian, *Control Systems Design: A New Framework*, Springer–Verlag, London, UK, 2005.

[40] B. Aguirre-Hernández, E. Campos-Cantón, J. A. López-Renteria, and E. C. Díaz González, "A polynomial approach for generating a monoparametric family of chaotic attractors via switched linear systems," *Chaos, Solitons & Fractals*, vol. 71, pp. 100–106, 2015.

[41] E. C. Díaz-González, J.-A. López-Rentería, E. Campos-Cantón, and B. Aguirre-Hernández, "Maximal unstable dissipative interval to preserve multi-scroll attractors via multi-saturated functions," *Journal of Nonlinear Science*, vol. 26, no. 6, pp. 1833–1850, 2016.

Hindawi
Mathematical Problems in Engineering
Volume 2017, Article ID 5214235, 6 pages
https://doi.org/10.1155/2017/5214235

Research Article

Synchronization in Coupled Multistable Systems with Hidden Attractors

Gokul PM and Tomasz Kapitaniak

Division of Dynamics, Lodz University of Technology, Stefanowskiego 1/15, 90-457 Lodz, Poland

Correspondence should be addressed to Gokul P M; gokulnappu@gmail.com

Received 9 December 2016; Revised 17 March 2017; Accepted 20 March 2017; Published 19 April 2017

Academic Editor: Jesus M. Munoz-Pacheco

In this paper, we study the results of coupling multistable systems which have hidden attractors with each other. Three modified Sprott systems were coupled and their synchronization was observed. The final state of the synchronized system changes with the change in the coupling strength. This was seen for two different types of coupling, one with a single variable and the other with two system variables.

1. Introduction

Synchronization of dynamical systems has become a field of intense interest and hence extensive study in the last decades [1–8]. Just the dynamical systems alone have been known to exhibit a wide variety of complex behavior.

The reason why synchronization of coupled systems is gaining interest is the huge real life applications that collective behavior [9–11] of such systems has [12–15]. From social behavioral analysis to biological models like neural networks, we have seen the importance and hence the justified interest in the study of this phenomenon increasing.

Since the introduction of the concept of synchronization by Pecora and Carroll [1], there have been a lot of different approaches and therefore types of synchronization observed and documented, like the complete synchronization, phase synchronization [16], lag synchronization [17], and so forth. In our work, we will be studying complete synchronization of the system presented.

Now looking at behaviors of dynamical systems, a recent concept that is becoming increasingly interesting is the concept of multistability and hidden attractors [18–22]. Multistable systems are those dynamical systems that have more than one equilibrium point for a given set of parameters. This results in the final state of the system being very sensitive to the initial conditions and also to perturbations.

Another interesting concept is the hidden attractor. Hidden attractors are attractors whose basins do not intersect with small neighborhoods of equilibria. This results in needing special methods to find them as standard methods become insufficient. These kinds of attractors were first observed by Yang et al. [23] who, when studying a system with two stable equilibrium points, found that the same system exhibited chaotic behavior. These attractors were later called hidden attractors by Leonov et al. [24]. There have been a lot of further studies in this field, since the systems show multistability, and have resulted in hidden attractors being shown using electronic circuits by Saha et al. [25, 26]. This shows actual physical realization of the theoretical concept. Furthermore, the system introduced by Sprott [27–29], and later studied in a more generalized way by Wang et al. [30, 31], has shown similar behavior. This is important to our case as it will be the base system we will be using in our studies.

In our study, we have decided to take a multistable system with hidden attractors [30] and study the complete synchronization of three such systems coupled simply. While there have been studies done on seeing the transition between two attractors in a multistable system [32] and even on generalized synchronization of such attractor [33], we will be observing the complete synchronization of our system and how multistability of the system affects the observed synchronization.

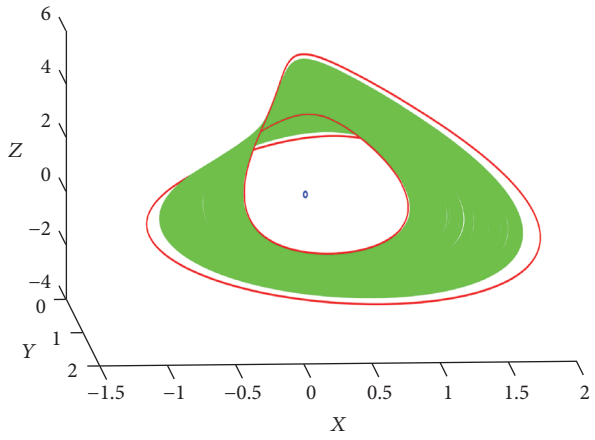

Figure 1: Phase space plot for the uncoupled system (1) where the blue point gives the stable equilibrium point, the green line gives the strange attractor which is chaotic, and the red line denotes the hidden attractor which is in period-three limit cycle.

2. System Model

In this work, we study the different synchronization of one such system proposed by Wang and Chen [30], which in itself was a more generalized version of the one proposed by Sprott [27–29]. Wang-Chen system is described by

$$\begin{aligned} \frac{dx}{dt} &= yz + a, \\ \frac{dy}{dt} &= x^2 - y, \\ \frac{dz}{dt} &= 1 - 4x, \end{aligned} \tag{1}$$

where x, y, and z are three state variables, while a is the parameter.

This system has a hidden attractor and shows multistability and the parameter a is chosen in such a way that the final state is very sensitive to the initial condition. There are three attractors in the system to begin with: a point attractor, a strange attractor, and a hidden attractor. In our system, we have chosen $a = 0.01$, so that the stable attractor converges to a point, the hidden attractor is in period-three state, and the strange attractor is chaotic as illustrated in Figure 1.

3. Single Variable Coupling

There are a variety of ways in which the system mentioned can be coupled. We have chosen a simple unidirectional coupling but with all x, y, and z being coupled one at a time. The figures below show the results, where the initial condition of the individual systems would have all taken them to the hidden attractor had there been no coupling. The plot shows how the difference, Δ_{ij} changes with the coupling strength, where

$$\Delta_{ij} = \frac{1}{N}\sum_{l=1}^{N}\sqrt{\left(x_i^l - x_j^l\right)^2 + \left(y_i^l - y_j^l\right)^2 + \left(z_i^l - z_j^l\right)^2} \tag{2}$$

with $i, j = 1, 2, 3$, and $l = 1, 2, \ldots, N$. Here l denotes the last few iterations over which we have taken the mean. In our work, the value of Δ_{ij} is corresponding to the synchronization error. For example, when the synchronization occurs the value of $\Delta_{ij} < 0 \pm 0.0001$.

It can be seen from Figure 2 that there are multiple regions of synchronization. When these regions were studied individually, they showed that the final synchronized state was not the same at all these points. It was also seen that, at every point of synchronization, there is a complete synchronization of all the variables with every other variable.

Let us take the case of unidirectional x-coupling alone, whose equation is

$$\begin{aligned} \dot{x_1} &= y_1 z_1 + a + k\left(x_2 - x_1\right), \\ \dot{y_1} &= x_1^2 - y_1, \\ \dot{z_1} &= 1 - 4x_1, \\ \dot{x_2} &= y_2 z_2 + a + k\left(x_3 - x_2\right), \\ \dot{y_2} &= x_2^2 - y_2, \\ \dot{z_2} &= 1 - 4x_2, \\ \dot{x_3} &= y_3 z_3 + a + k\left(x_1 - x_3\right), \\ \dot{y_3} &= x_3^2 - y_3, \\ \dot{z_3} &= 1 - 4x_3. \end{aligned} \tag{3}$$

After studying the individual cases, it was seen that the final region of synchronization changes from one attractor to another at the different synchronization regions (see Figure 3). Since it was seen that all variables, that is, x, y and z, synchronize whenever a single one synchronizes, we can just study the final state of a single system and conclude that all the systems are in this same state. The synchronized states start with the system being in the fixed point attractor ($k = 0.15$) which then changes to the period-three attractor (from $k = 0.32$) and finally to the chaotic attractor ($k = 0.36$), where it stays for all other increases.

Now, when we try the same using y-coupling, synchronization only occurs in a small region. Here both the regions of synchronization are where the system finally reaches the fixed point. No other regions were observed. When repeated for the z-coupling, the result was that there was a large region of synchronization like in the case of x-coupling, but the final synchronized state was always in the fixed point attractor, like in the y-coupling.

4. Two-Variable Coupling

Next we tried the same unidirectional coupling, but now with two variables. For example, the equations for xy-coupling looks like

$$\begin{aligned} \dot{x_1} &= y_1 z_1 + a + k\left(x_2 - x_1\right), \\ \dot{y_1} &= x_1^2 - y_1 + k\left(y_2 - y_1\right), \end{aligned}$$

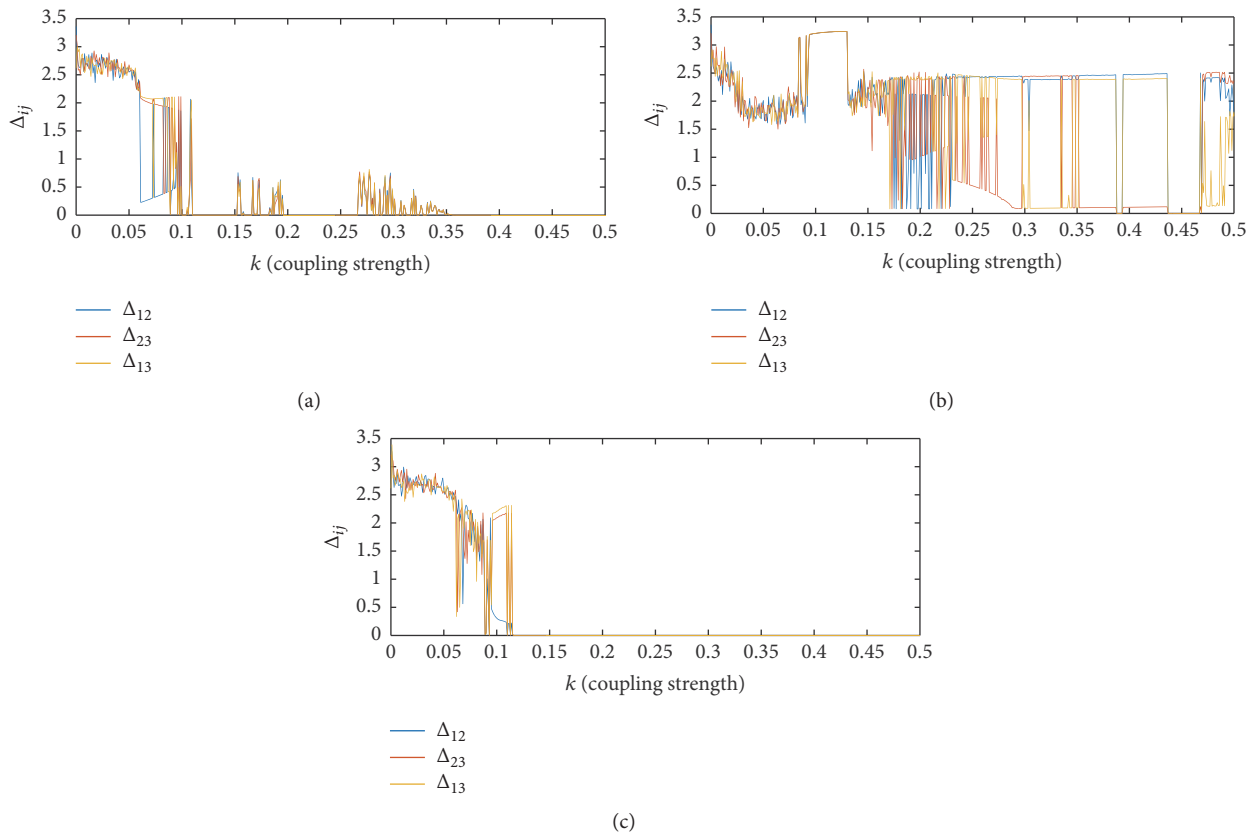

Figure 2: Change of the absolute difference between the variables Δ after a long period of time with increasing coupling strength, with (a), (b), and (c) being the plots for x-, y-, and z-coupling, respectively.

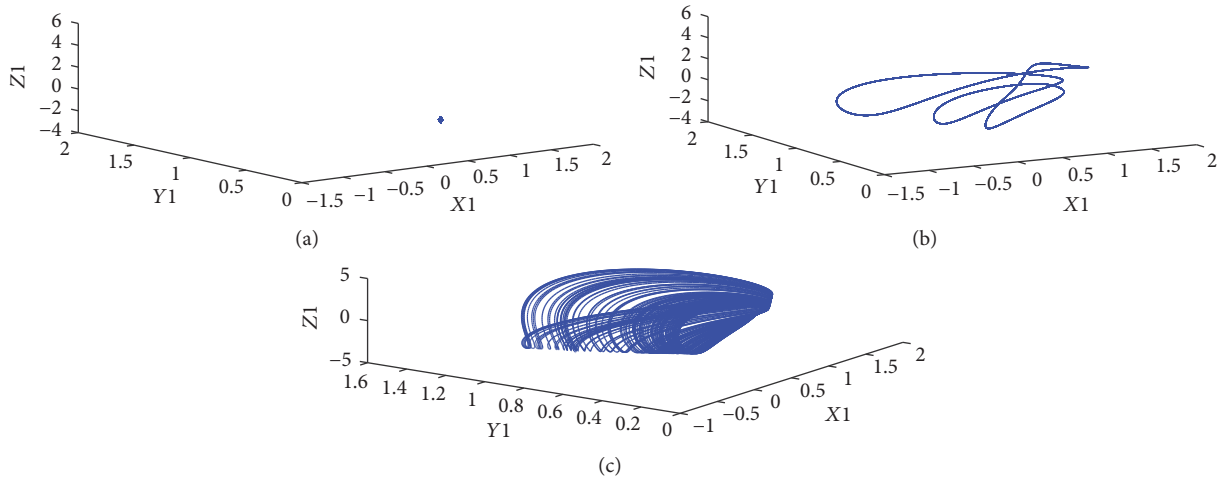

Figure 3: The final state of the variables of the first system at different coupling strength for x-coupling only. Figures (a), (b), and (c) show the phase space at $k = 0.15$, 0.32, and 0.36, respectively.

$$
\begin{aligned}
\dot{z_1} &= 1 - 4x_1, \\
\dot{x_2} &= y_2 z_2 + a + k\left(x_3 - x_2\right), \\
\dot{y_2} &= x_2^2 - y_2 + k\left(y_3 - y_2\right), \\
\dot{z_2} &= 1 - 4x_2, \\
\dot{x_3} &= y_3 z_3 + a + k\left(x_1 - x_3\right), \\
\dot{y_3} &= x_3^2 - y_3 + k\left(y_1 - y_3\right), \\
\dot{z_3} &= 1 - 4x_3.
\end{aligned} \tag{4}
$$

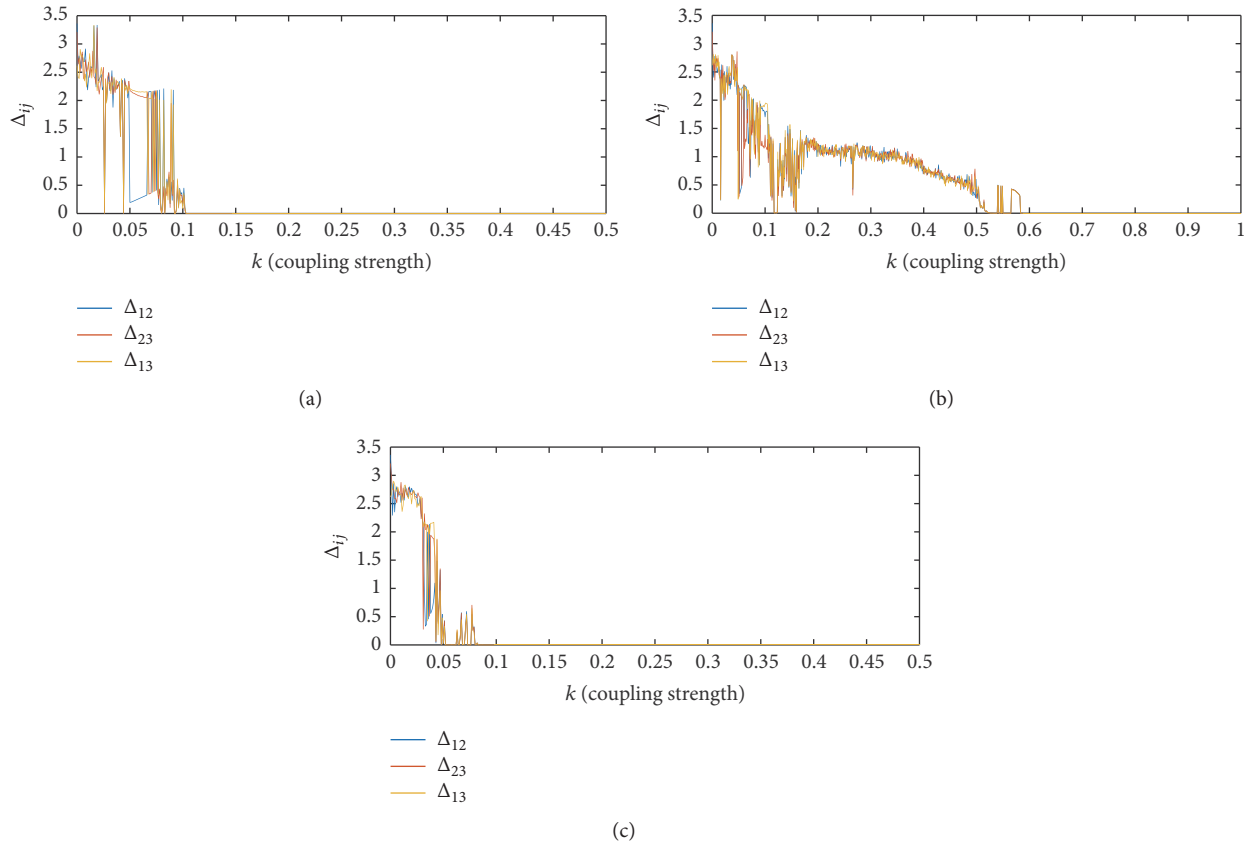

Figure 4: Change of the absolute difference between the variables Δ after a long period of time with increasing coupling strength, with (a), (b), and (c) being the plots for *xy*-, *yz*-, and *xz*- coupling, respectively.

Many regions of synchronization were observed separated by a desynchronized region. Like the previous case, we expected these regions to show different behavior, which is true, though the order is different, with the system going from point attractor to chaotic to period-three attractor as seen in Figure 4. In the case of *xy*-coupling and *xz*-coupling, that was the final synchronized state, but we saw that, for *yz*-coupling, the final synchronized state undergoes one more shift into the chaotic attractor, although this time it is without the separation of a desynchronized region. This can be seen from Figures 5 and 6, respectively.

5. Conclusion

In the model studied, we observed synchronization of three systems that were introduced by Sprott et al., in the case of two types of unidirectional coupling, using one variable and then two. We studied the case where the individual systems were in period-three hidden attractor. It was seen that, depending on the strength of coupling between the systems, not only was the synchronization affected, but also the final synchronized state was affected. While the one-variable coupling that gave the most interesting result was for *x*-coupling, where the final state shifted from point attractor to the chaotic one via the period-three attractor, the two-variable coupling gave for *xy*-coupling and *xz*-coupling the same phenomenon of transition from point attractor to chaotic attractor to period-three attractor, whereas the *yz*-coupling made one more final transition to the chaotic attractor.

Our work emphasizes this observed synchronization, which, depending on the coupling strength alone, changes its final state from a stable equilibrium point to the strange and hidden attractors in that order or vice versa depending on the type of coupling. This change is interesting and we attribute this effect to the multistability of the system which made it very sensitive to perturbations.

Since the uncoupled system is very sensitive to the initial conditions, we tried to repeat the whole process with different initial condition, where the initial uncoupled system was in different attractors, including cases where each system was in a different attractor. Similar results were observed, where the system started from the point attractor and then moved to the periodic or chaotic attractor and then again moved on to a different attractor.

Conflicts of Interest

The authors declare that they have no conflicts of interest.

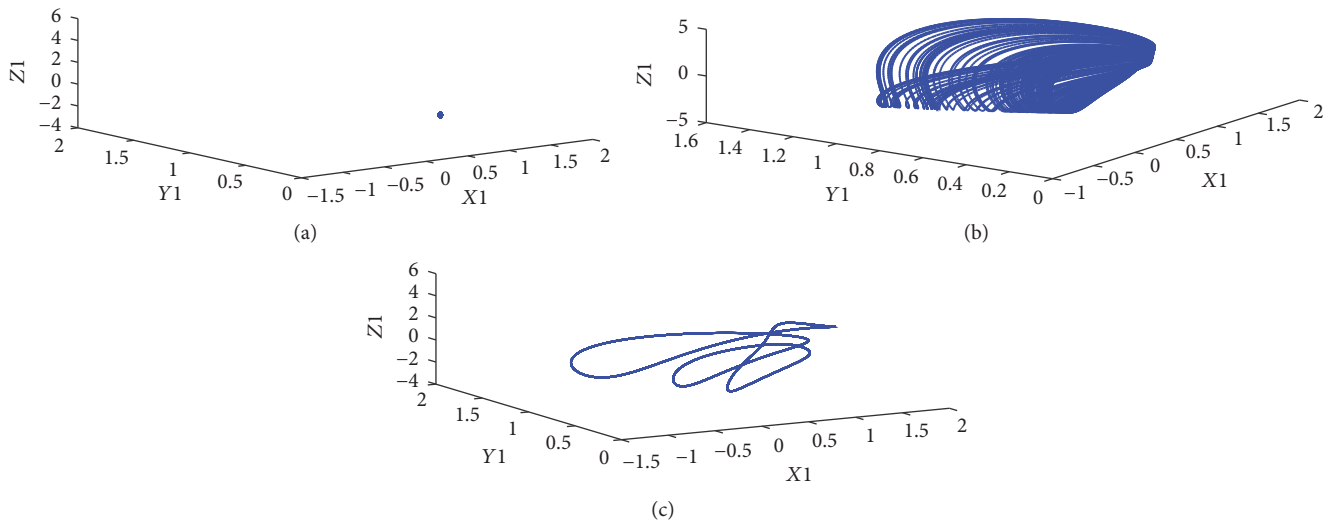

Figure 5: The final state of the variables of the first system at different coupling strength for *xy*-coupling. Figures (a), (b), and (c) show the phase space plot of one system at $k = 0.08$, 0.11, and 0.12, respectively.

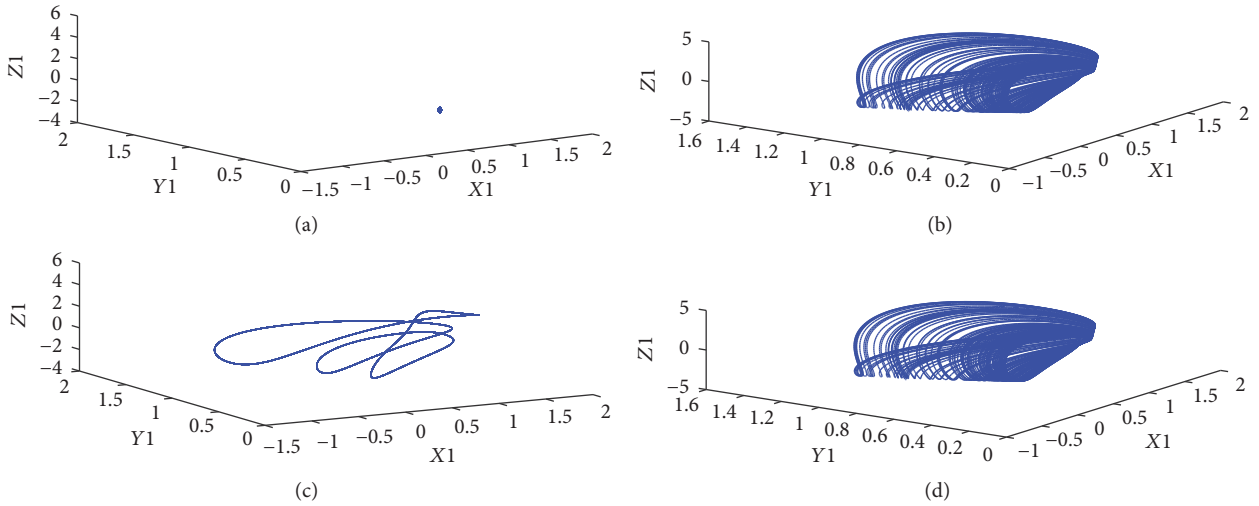

Figure 6: The final state of the variables of the first system at different coupling strength for *yz*-coupling only. Figures (a), (b), (c), and (d) show the phase space plot of one system at $k = 0.12$, 0.53, 0.849, and 2.81, respectively.

Acknowledgments

This work has been supported by the Polish National Science Centre, MAESTRO Programme, Project no. 2013/08/A/ST8/00/780.

References

[1] L. M. Pecora and T. L. Carroll, "Synchronization in chaotic systems," *Physical Review Letters*, vol. 64, no. 8, pp. 821–824, 1990.

[2] S. Yanchuk and T. Kapitaniak, "Chaos-hyperchaos transition in coupled Rössler systems," *Physics Letters, A*, vol. 290, no. 3-4, pp. 139–144, 2001.

[3] S. Yanchuk and T. Kapitaniak, "Symmetry-increasing bifurcation as a predictor of a chaos-hyperchaos transition in coupled systems," *Physical Review E*, vol. 64, no. 5, Article ID 056235, 2001.

[4] M. Kapitaniak, K. Czolczynski, P. Perlikowski, A. Stefanski, and T. Kapitaniak, "Synchronization of clocks," *Physics Reports*, vol. 517, no. 1-2, pp. 1–69, 2012.

[5] M. Kapitaniak, K. Czolczynski, P. Perlikowski, A. Stefanski, and T. Kapitaniak, "Synchronous states of slowly rotating pendula," *Physics Reports*, vol. 541, no. 1, pp. 1–44, 2014.

[6] M. Kapitaniak, P. Brzeski, K. Czolczynski, P. Perlikowski, A. Stefanski, and T. Kapitaniak, "Synchronization thresholds of coupled self-excited nonidentical pendula suspended on the vertically displacing beam," *Progress of Theoretical Physics*, vol. 128, no. 6, pp. 1141–1173, 2012.

[7] P. Kuzma, M. Kapitaniak, and T. Kapitaniak, "Coupling multistable systems: uncertainty due to the initial positions in the

attractors," *Journal of Theoretical and Applied Mechanics*, vol. 52, no. 1, p. 281, 2014.

[8] M. Kapitaniak, M. Lazarek, M. Nielaczny, K. Czolczynski, P. Perlikowski, and T. Kapitaniak, "Synchronization extends the life time of the desired behavior of globally coupled systems," *Scientific Reports*, vol. 4, article 4391, 2014.

[9] A. S. Pikovsky, M. G. Rosenblum, and J. Kurths, *Synchronization: A Universal Concept in Nonlinear Sciences*, Cambridge University Press, Cambridge, UK, 2002.

[10] S. Boccaletti, J. Kurths, G. Osipov, D. L. Valladares, and C. S. Zhou, "The synchronization of chaotic systems," *Physics Report*, vol. 366, no. 1-2, pp. 1–101, 2002.

[11] L. Kocarev and U. Parlitz, "Generalized synchronization, predictability, and equivalence of unidirectionally coupled dynamical systems," *Physical Review Letters*, vol. 76, no. 11, pp. 1816–1819, 1996.

[12] B. F. Kuntsevich and A. N. Pisarchik, "Synchronization effects in a dual-wavelength class-B laser with modulated losses," *Physical Review E*, vol. 64, no. 4, Article ID 046221, 2001.

[13] M. I. Rabinovich, P. Varona, A. I. Selverston, and H. D. I. Abarbanel, "Dynamical principles in neuroscience," *Reviews of Modern Physics*, vol. 78, no. 4, Article ID 1213, 2006.

[14] B. Blasius, A. Huppert, and L. Stone, "Complex dynamics and phase synchronization in spatially extended ecological systems," *Nature*, vol. 399, no. 6734, pp. 354–359, 1999.

[15] D. J. Watts and S. H. Strogatz, "Collective dynamics of "small-world" networks," *Nature*, vol. 393, no. 6684, pp. 440–442, 1998.

[16] M. G. Rosenblum, A. S. Pikovsky, and J. Kurths, "Phase synchronization of chaotic oscillators," *Physical Review Letters*, vol. 76, no. 11, pp. 1804–1807, 1996.

[17] M. G. Rosenblum, A. S. Pikovsky, and J. Kurths, "From phase to lag synchronization in coupled chaotic oscillators," *Physical Review Letters*, vol. 78, no. 22, pp. 4193–4196, 1997.

[18] Y. Maistrenko, S. Brezetskyi, P. Jaros, R. Levchenko, and T. Kapitaniak, "Smallest chimera states," *Physical Review E*, vol. 95, Article ID 010203, 2017.

[19] S. Brezetskyi, D. Dudkowski, and T. Kapitaniak, "Rare and hidden attractors in Van der Pol-Duffing oscillators," *European Physical Journal: Special Topics*, vol. 224, no. 8, pp. 1459–1467, 2015.

[20] A. Chudzik, P. Perlikowski, A. Stefanski, and T. Kapitaniak, "Multistability and rare attractors in van der Pol-Duffing oscillator," *International Journal of Bifurcation and Chaos*, vol. 21, no. 7, pp. 1907–1912, 2011.

[21] T. Kapitaniak and G. A. Leonov, "Multistability: uncovering hidden attractors," *European Physical Journal: Special Topics*, vol. 224, no. 8, pp. 1405–1408, 2015.

[22] J. C. Sprott, "Strange attractors with various equilibrium types," *The European Physical Journal Special Topics*, vol. 224, no. 8, pp. 1409–1419, 2015.

[23] Q. Yang, Z. Wei, and G. Chen, "An unusual 3D autonomous quadratic chaotic system with two stable node-foci," *International Journal of Bifurcation and Chaos*, vol. 20, no. 4, pp. 1061–1083, 2010.

[24] G. A. Leonov, N. V. Kuznetsov, and V. I. Vagaitsev, "Hidden attractor in smooth Chua systems," *Physica D: Nonlinear Phenomena*, vol. 241, no. 18, pp. 1482–1486, 2012.

[25] P. Saha, D. C. Saha, A. Ray, and A. RoyChowdhary, "Multistability in a single system with hidden attractors: theory and experiment," *International Journal of Physics*, vol. 2, no. 6, pp. 217–225, 2014.

[26] P. Saha, D. C. Saha, A. Ray, and A. R. Chowdhury, "Memristive non-linear system and hidden attractor," *European Physical Journal: Special Topics*, vol. 224, no. 8, pp. 1563–1574, 2015.

[27] J. C. Sprott, "Automatic generation of strange attractors," *Computers and Graphics*, vol. 17, no. 3, pp. 325–332, 1993.

[28] J. C. Sprott, "Some simple chaotic flows," *Physical Review E*, vol. 50, no. 2, pp. R647–R650, 1994.

[29] J. C. Sprott, "Simplest dissipative chaotic flow," *Physics Letters. A*, vol. 228, no. 4-5, pp. 271–274, 1997.

[30] X. Wang and G. Chen, "A chaotic system with only one stable quilibrium point," *Communications in Nonlinear Science and Numerical Simulation*, vol. 17, Article ID 12641272, pp. 1264–1272, 2012.

[31] J. C. Sprott, X. Wang, and G. Chen, "Coexistence of point, periodic and strange attractors," *International Journal of Bifurcation and Chaos*, vol. 23, no. 5, Article ID 1350093, 2013.

[32] A. N. Pisarchik, R. Jaimes-Reátegui, J. R. Villalobos-Salazar, J. H. García-López, and S. Boccaletti, "Synchronization of chaotic systems with coexisting attractors," *Physical Review Letters*, vol. 96, no. 24, Article ID 244102, 2006.

[33] A. Hu and Z. Xu, "Multi-stable chaotic attractors in generalized synchronization," *Communications in Nonlinear Science and Numerical Simulation*, vol. 16, no. 8, pp. 3237–3244, 2011.

Hindawi
Mathematical Problems in Engineering
Volume 2017, Article ID 8423413, 11 pages
https://doi.org/10.1155/2017/8423413

Research Article

Sliding Mode Control of Discrete Chaotic System Based on Multimodal Function Series Coupling

Fengjun Hu

Institute of Information Technology, Zhejiang Shuren University, Hangzhou, Zhejiang 310014, China

Correspondence should be addressed to Fengjun Hu; jainism@msn.com

Received 9 December 2016; Revised 2 March 2017; Accepted 20 March 2017; Published 12 April 2017

Academic Editor: Eric Campos-Canton

A new sliding mode control model of discrete chaotic systems based on multimodal function series coupling is proposed to overcome the shortcomings of the standard PSO algorithm in multimodal function optimization. Firstly, a series coupled PSO algorithm (PP algorithm) based on multimodal function is constructed, which is optimized by multipeak solution on the basis of the standard PSO algorithm. Secondly, the improved PSO algorithm is applied to search all the extreme points in the feasible domain. Thirdly, the Powell method is used to perform the local optimization of the search results, and the newly generated extreme points are added to the extreme point database according to the same peak judgment operator. Finally, the long training time of PP algorithm can be overcome by the characteristics of fast convergence rate of the cloud mutation model. And also, both the population size and the redundancy can be reduced. Then, the clonal selection algorithm is used to keep the diversity of the population effectively. Simulation results of the sliding mode control of discrete chaotic systems show that the improved PSO algorithm obviously improves the response speed, overshoot, and so on.

1. Introduction

Chaotic system can be divided into integer order chaotic system and fractional chaotic system. Fractional chaotic system is a very complex nonlinear system [1]. Sliding mode control has become an important branch of modern control theory because of its good robustness and antijamming characteristics [2]. Fractional chaotic system sliding mode has advantages of fractional chaotic system and sliding mode control, which can further improve the control performance of the system on the basis of traditional sliding mode control and become an important research area of modern nonlinear control.

Before introducing the sliding mode control of fractional order chaotic system, we mainly studied the control and synchronization of the fractional chaotic systems. At present, the control and synchronization of the fractional chaotic system are divided into two categories. One is the classical system stability theory and control method based on traditional integer order system. On the basis of the theory and control method, the stability analysis of the fractional order is carried out to design the integer order controller [3]. The other is to utilize the characteristics of the fractional order system to put forward the fractional order controller design method; then, the control of the fractional order system can be realized [4]. The control methods can be divided into the following areas:

(1) Feedback control based on pole placement of the fractional order system: Matignon [5] discussed the relationship between internal stability and external stability of the fractional differential equations. The system is linearized near the equilibrium point. And the author also described the characteristic equation of the system and the eigenvector based on the fractional calculus theory and the traditional algebraic polynomial, analyzed the relationship between the fractional system eigenvalues and the system matrix pole, and presented the sufficient conditions for the stability of the fractional order system.

(2) The control of Gronwall inequality based on the fractional order: the Gronwall inequality is extensively applied to the integer order differential equation, and

the solution of the system is expressed analytically. The Gronwall inequality is taken to analyze the system solution to obtain the design of the controller, which is a common control design method for integer order systems. Lazarević and Spasić [6] applied the Gronwall inequality to the fractional time-delay system, analyzed the solution of the fractional order system, and realized the finite-time stabilization control of the fractional order. N'Doye and others [7] generalized the Bellman-Gronwall inequality, analyzed a class of nonlinear affine fractional order systems, and achieved the asymptotic stability of the fractional systems. Ye et al. [8] extended the integer order Gronwall inequality to the fractional systems, proposed the generalized Gronwall inequality, and successfully implemented the asymptotic stability control for the fractional time-delay systems.

(3) Fractional order PID control: in the classical control theory and applications, PID controller has been developed very well and is widely applied to the actual system. In accordance with the PID control, the integral controller and differential controller of the PID controller can be partially extended to the fractional order; that is, the fractional integral and the fractional differential are introduced into the control design. Vasundhara Devi et al. [9] first proposed the fractional order PID controller and proved that the integer order PID controller belongs to a subset of the fractional PID controller. By adjusting the fractional order, the control effect of the fractional integral and fractional differential controller can be changed.

(4) Feedback control based on linear matrix inequality: Sabatier and others [10] gave a sufficient and necessary condition for the stability of the fractional order time-invariant interval uncertain systems. Because of the state boundedness characteristic of chaotic systems, this condition has been applied to the control and synchronization of the fractional order chaotic systems. Chen and others [11] presented a sufficient and necessary condition for the fractional order systems with parametric perturbations and applied it to the fractional order chaotic systems to achieve robust synchronization of the fractional order chaotic systems. Dadras and Momeni [2] introduced the passive theory into the fractional order system and designed the fractional integral sliding surface by the linear matrix inequality to realize the passive sliding mode control of the time-varying uncertain fractional chaotic systems.

(5) Sliding mode control of the fractional order system: the application of the integer order sliding mode to the fractional systems has been proved to be effective. The integral sliding mode surface and approach law are designed, respectively. And the effectiveness of the sliding surface is proved. The Lyapunov function is designed to analyze the stability of the fractional order system, and then, the sliding mode control law is obtained [12]. On the other hand, by combining the design idea of the integral sliding mode surface with the characteristics of the fractional system, we can design the fractional sliding mode surface, and the integer integral of the sliding surface is changed to the fractional integral [13]. Similarly, the approximation of the integer order can be extended to the fractional systems; that is, the differential equation of integer order approximation law description can be generalized into the fractional order equation, which can realize the fractional order sliding mode approximation law [14].

In this paper, a PSO multiobjective optimization algorithm is introduced. Since the algorithm is easy to fall into the local optimization, a sliding mode control of discrete chaotic system based on multimodal function series coupling is proposed combining the characteristics of multimodal function optimization problems. Simulations show the effectiveness of this method.

2. Multimodal Function Optimization Problem Modeling

In many engineering optimization, such as complex system parameters and structural optimization, neural network weights, and structural optimization, we not only need to find the global optimal solution in the feasible region but also need to search several global optimal solutions and other valued local optimal solutions. Thus, multichoices and multi-information can be provided for decision makers. The above can be classified as multimodal function optimization problem or multipeak function optimization (MFO).

The multimodal optimization problem, as shown in (1), consists of two parts: the objective function and the search range.

$$\text{Minimize} \quad f(x), \quad x = (x_1, x_2, \ldots, x_n) \in S. \tag{1}$$

In (1), the search range S that can meet all the variables is called the feasible region, and the solution in feasible region is called the feasible solution. In the feasible region, the solution with the smallest objective function is the optimal solution. The optimal solution can be divided into global optimal solution and local optimal solution. In the multimodal function optimization, not only all the global optimal solutions of the optimization problem need to be found, but also the local optimal solutions need to be found as many as possible.

For the MFO problem of the objective function minimum value solution, the fitness function is defined as

$$\text{fit}(X) = f(X). \tag{2}$$

In (2), $f(X)$ is the function value of X, and $\text{fit}(X)$ is the fitness value.

For the MFO problem of the function maximum value solution, the limit construction method is used to solve the minimization problem. The fitness function is defined as

$$\text{fit}(X) = C_{\max} - f(X). \tag{3}$$

In (3), $C_{\max}$ is the maximum estimate of $f(X)$.

From (2) and (3), we can see that the smaller the fitness value, the better the fitness.

3. Solution Algorithm of Multimodal Function Problem Based on Series Coupling

Based on PSO algorithm and Powell method, this paper presents PP algorithm based on series coupling. The PP algorithm has the maximum repetition search M ($M > 1$) to avoid the situations in which not all the extreme values can be searched in an evolutionary iteration. In each iteration, firstly, the improved PSO algorithm is used to carry out the global search of all the extreme points in the feasible region. Secondly, Powell method is used to perform the local search towards the optimal solutions found by the improved PSO to improve the accuracy of the solution. Finally, the peak judgement operator adds the newly generated extreme points to the extreme point database and rerandomizes the initialization of the particles.

3.1. PSO Algorithm Improvement. In the case of the particle swarm with the N numbers of particles in the D-dimensional search space, denote the flying speed of particle i as $V_i = (V_{i1}, V_{i2}, \ldots, V_{iD})^T$. The current position is $X_i = (X_{i1}, X_{i2}, \ldots, X_{iD})^T$, the searched optimal position of particle i is $P_i = \{P_{i1}, P_{i2}, \ldots, P_{iD}\}$, and the searched optimal position of the swarm is $P_g = \{P_{g1}, P_{g2}, \ldots, P_{gD}\}$. In order to reduce the possibility of the particles leaving the search space during the process of evolutionary iterations, the speed is limited as $V_{\min} \le V_{id} \le V_{\max}$. The standard PSO is shown in

$$V_{id}(t+1) = \omega(t) V_{id}(t) + c_1 \text{rand}() \left(P_{id}(t) - X_{id}(t)\right) + c_2 \text{rand}() \left(P_{gd}(t) - X_{gd}(t)\right). \quad (4)$$

In (4), t is the current iteration number, V_{id} represents the dth dimensional component of the particle i velocity vector V, and $1 \le d \le D$. c_1 represents the cognitive learning factor of the particle individual and c_2 represents the social learning factor. rand() is the random number generated by the uniform distribution on $[0, 1]$.

In the multimodal optimization, in order to make each local optimal value become the "only way" of some particles in PSO algorithm, this paper improves the standard PSO and obtains the improved PSO.

(1) Ideally, the self-cognition of each individual in the particle swarm represents each local optimization of the multipeak optimization. Thus, let $c_2 = 0$; we can obtain not just the global optimal values, but all the local optimal values.

(2) Consider that the random function rand() in (4) mainly increases the randomness of the particle motion so as to make the local optimal point jump out. In order to let each particle of the particle swarm converge to each local optimal value as soon as possible, rand() in (4) should be removed.

(3) The linear decreasing strategy of inertia weight is simple and intuitive and has better searching ability, which makes the algorithm balance between the global search and the local search. Therefore, ω uses the above strategy, which is shown in

$$\omega(t) = \omega_{\text{start}} - (\omega_{\text{start}} - \omega_{\text{end}}) \frac{t}{t_{\max}}. \quad (5)$$

In (5), t represents the current PSO iteration algebra, $t_{\max}$ represents PSO maximum iteration number, and ω_{start} and ω_{end} represent the maximum and the minimum value of ω.

Based on the above improvements, (4) can be changed to

$$V_{id}(t+1) = \omega(t) V_{id}(t) + c_1 \left(P_{id}(t) - X_{id}(t)\right). \quad (6)$$

The position change is performed according to (7). In order to avoid the particles leaving from the search space during the process of evolution iteration, the following condition should be satisfied: $X_{\min} \le X_{id} \le X_{\max}$.

$$X_{id}(t+1) = X_{id}(t) + V_{id}(t+1). \quad (7)$$

3.2. Nonlinear Powell Direct Search Method. The nonlinear Powell direct search method is a nonlinear direct local search method for solving unconstrained optimization problems without using derivatives. It is considered to be a relatively effective method in direct search. Powell search method is known as the direction acceleration method as well. Using this method, the calculation of the derivative is not required and only the function value is used to carry out the one-dimensional search from one point towards two directions. Then, the minimal value can be obtained. Nonlinearity means that the search direction of the initial point is not fixed, the acceleration direction will change with the change of the initial point position, and the search is not along a straight line.

The steps of the Powell search method are as follows:

Begin

Step 1. The particle of the last search generation of PSO is taken as the initial point $x^{(0)} \in S$. Set the search precision of the Powell method as ε. D numbers of initial linearly independent search directions $d^{(i)}$ are given, and $i = 0, 1, \ldots, D-1$. Set $k = 0$.

Step 2. According to (9) below, one-dimensional search is performed accurately from point $x^{(0)}$ to each search direction in turn $d^{(0)}, d^{(1)}, \ldots, d^{(D-1)}$. Thus, $x^{(0)}, x^{(1)}, \ldots, x^{(D)}$ is obtained.

$$f\left(x^{(i)} + \alpha_i d^{(i)}\right) = \min_{\alpha \in S} f\left(x^{(i)} + \alpha d^{(i)}\right), \quad (8)$$

$$x^{(i+1)} = x^{(i)} + \alpha_i d^{(i)}. \quad (9)$$

In (8), α and α_i represent the step sizes and α_i is obtained by the exact linear search; that is, α_i is the solution of the one-dimensional optimization problem above. α_i can be negative, which indicates that the exact linear search takes place over the entire real axis.

Step 3. Let $d^{(D)} = x^{(D)} - x^{(0)}$. If $\|d^{(D)}\| \le \varepsilon$, and the solution $x^{(D)}$ is obtained, calculation ends. Otherwise, the exact linear search is performed from point $x^{(D)}$ to the direction of $d^{(D)}$ to get $x^{(D+1)}$.

Step 4. According to (10), the indicator tl determined by the maximal decrease is calculated.

$$f\left(x^{(tl)}\right) - f\left(x^{(tl+1)}\right) = \max_{0\le i\le D-1}\left\{f\left(x^{(i)}\right) - f\left(x^{(i+1)}\right)\right\}. \tag{10}$$

Step 5. When (11) holds, it shows that $d^{(0)}, d^{(1)}, \ldots, d^{(D-1)}$ are still linearly independent, and the search directions of the next round are still $d^{(0)}, d^{(1)}, \ldots, d^{(D-1)}$. Then, $x^{(0)} = x^{(D+1)}$. Return to Step 2.

$$f\left(x^{(0)}\right) - 2f\left(x^{(D)}\right) + f\left(2x^{(D)} - x^{(0)}\right) \ge 2\left(f\left(x^{(tl)}\right) - f\left(x^{(tl+1)}\right)\right). \tag{11}$$

Step 6. When (11) does not hold, it shows that $d^{(0)}$, $d^{(1)}, \ldots, d^{(D-1)}$ are linearly dependent. Thus, set $d^{(tl+1)} = d^{(tl+i+1)}$ to ensure linearly independence of the new generated search direction, $x^{(0)} = x^{(D+1)}$, $k = k + 1$. Return to Step 2.

End

3.3. The Same Peak Judgement of the Extreme Points. The extreme points found by the PP algorithm are compared with all the extreme points in the extreme point database EP in turn and make the same peak judgement. If it is judged as the same peak and greater than the fitness value of the existing extreme point, the extreme point is discarded. If it is judged as the same peak but less than the fitness value of the extreme point, the extreme point is replaced. And if it is judged to be different peak, it is added to set EP.

The same peak judgement operator uses the peak exploration method to perform the same peak judgement towards the global extreme points. In this paper, the peak exploration method is applied in the same peak judgement of all the global and local extreme points. The method is as follows.

Set A as an extreme point in EP and B as the extreme point found by the PP algorithm. $(h-1)$ points are inserted between A and B, and AB is divided into h equal parts. The same peak operators of h parts are calculated, which is shown as

$$Tf(i) = \text{fit}\left(X_{i+1}\right) - \text{fit}\left(X_i\right). \tag{12}$$

In (12), X_{i+1} and X_i are two adjacent points between A and B, $1 \le i \le h$. When $i = 1$, X_1 is point A, and when $i = h$, X_{h+1} is point B. If value of Tf changes from positive to negative, it means that there is a mountain between points A and B. Then, A and B are different peak extreme points. Otherwise, they are the same peak extreme points.

3.4. Performance Analysis of PP Algorithm in Multimodal Function Optimization Problem. Let the numbers of particles N be 20~105. Set the acceleration factor $c_1 = 1.49445$. Set the inertia weight: $\omega_{\text{start}} = 0.9$, $\omega_{\text{end}} = 0.4$, and $t_{\max} = 30$, respectively. The maximal repeated search number is $M = 2$~10, and $\varepsilon = 2 \times 10^{-8}$. Select f_1 as the test function; the comparison of the results of the PP algorithm, multipopulation coevolution strategy ES, and the standard PSO algorithm is shown in Table 1.

Table 1: Comparisons of PP algorithm with other evolutionary algorithms.

Method	Number	$\overline{X}$		Mean_G	Time
		x_1	x_2		
ES	1	−2.9135	3.2658	648.9996	11.2
	2	3.2584	−1.5894	648.9996	
	3	−3.4584	−3.5814	648.9994	
	4	2.8595	2.1247	648.9991	
PSO	1	−2.9251	3.2671	648.9997	—
	2	3.2597	−1.5902	648.9998	
	3	3.4595	−3.5877	648.9998	
	4	2.8608	2.1211	648.9995	
PP	1	−2.9295	3.2613	650	2.5
	2	3.2657	−1.5945	650	
	3	3.4624	−3.5898	650	
	4	2.8695	2.1202	650	

$$f_1(x) = 660 - \left(x_1^2 + x_2 - 11\right)^2 - \left(x_1 + x_2^2 - 7\right)^2. \tag{13}$$

In Table 1, $\overline{X}$ represents the mean value of the optimal solution location at the time of the test. Mean_G is the average of the global solutions of the 50 tests.

From Table 1, we can see that, compared with ES and the standard PSO, the PP algorithm can search all four global extreme points of the function f_1 in 50 tests, and also there are no redundant or missing extreme points. The solution quality is significantly improved. Therefore, the PP algorithm has obvious advantages in search precision.

For function f_1, the standard PSO has no mean computing time, and we use "—" to express time. Time of the ES is 11.2 seconds, and time of the PP algorithm is 2.5 seconds. Thus, the PP algorithm has obvious advantages in the speed of convergence.

Then, the global convergence of PP algorithm is analyzed.

Suppose. (1) Definition domain Ω of the multimodal function optimization problem is a bounded closed region of R^n. (2) The objective function $f(X)$ is a continuous function on the region Ω.

Theorem 1. *Set $\{X(k)\}$ (k is the cumulative iteration algebra) as the population sequence generated by the PP algorithm, where $x^*(k) \in X(k)$ is the optimal point in the kth generation of the population; that is, $x^*(k) = \arg\min_{x\in\Omega} f(x(k))$. If the objective function and the feasible region of problem P satisfy hypothesis 1, $p\{\lim_{k\to\infty} f(x^*(k)) = f^*\} = 1$ holds, where $(f^* = \min\{f(x) : x \in \Omega\})$; that is, the population sequence converges to the global optimal solution with probability 1.*

Demonstration. Define the cumulative iteration algebra k as $k = t_{\max}(m-1) + t$, where m is the repeated search algebra ($1 \le m \le M$), $t_{\max}$ is the maximum iteration algebra, and t is the iterative algebra.

The change of the displacement of the two generations before and after the PP algorithm is $\Delta X_{id}(t) = \omega(t)V_{id}(t) + c_1(P_{id}(t) - X_{id}(t))$. Thus, when the population particles converge, the social cognitive part $(P_{id}(t) - X_{id}(t))$ tends to 0 and less than 1, the particle velocity will drop rapidly to 0, and the particle swarm will stop moving. Therefore, the population particles may converge on the local solution and not on the global solution. For this reason, when the population particles fall into the evolutionary stagnation state, the particles are subjected to the mutation operation through the basic normal cloud generator. And the basic normal cloud generator based on the cloud model is subject to normal distribution.

Due to the mutation operation of the basic normal cloud generator with normal distribution, the displacement of particle X_i is subject to normal distribution; that is, $\Delta X_i(t) \sim N(0, \sigma_t^2)$, where $N(0, \sigma_t^2)$ represents the normal distribution with average value 0 and variance σ_t^2.

Therefore, we can conclude that Theorem 1 holds.

4. Optimization of PP Algorithm Based on Cloud Mutation Clonal Selection

In order to solve the problems of the multimodal function optimization, based on the above improved methods, this paper utilizes the characteristics of fast convergent speed of the cloud mutation model to compensate the shortcomings of fast training time of the PP algorithm. Meanwhile, it can reduce the population size and redundancy. And the clonal selection algorithm can effectively maintain the diversity of population. Hence, a particle swarm optimization algorithm based on cloud mutation clonal selection is proposed (WCPP).

4.1. Optimization of Particle Space Distribution Based on Cloud Mutation. The cloud model has the characteristics of randomness and stability tendency. The randomness can keep the individual diversity so as to search for more local extreme points, and the stable tendency can protect the better individual to perform adaptive localization of the global optimal values. Thus, in order to improve the accuracy of the PP algorithm and expand the search range to find other extreme points, a cloud mutation operator based on cloud model is introduced on the basis of the PP algorithm to update the particles.

Thresholds ε and t_N are given. When a particle satisfies (14), that is, the particle degenerates and degradation amplitude is smaller than ε, it is considered that the particle has a generation in the evolutionary stagnation state.

$$0 < \text{fit}\left(X_i(t)\right) - \text{fit}\left(X_i(t-1)\right) < \varepsilon, \tag{14}$$

$$\varepsilon = \text{abs}\left(\frac{\text{fit}\left(X_i(t)\right)}{a}\right). \tag{15}$$

In (15), $\text{fit}(X_i(t))$ represents the fitness value of X_i in the tth generation. a is a constant. When $\text{fit}(X_i(t)) - \text{fit}(X_i(t-1)) < 0$, it indicates the evolution of particle X_i. And when $\text{fit}(X_i(t)) - \text{fit}(X_i(t-1)) > 0$, it indicates the degradation of particle X_i.

The cloud mutation condition can be defined as the degradation of a particle of t_N successive generations and the degradation amplitude is less than ε. When a particle satisfies the condition of cloud mutation, mutation operation is performed to the particle by a basic normal cloud generator. t_N is set as 5 here. Since t_N is set too small, the mutation occurs too frequently and it is easy to miss the extreme point. On the other hand, the convergent speed of the algorithm can slow down.

One-dimensional normal cloud operator can be extended to D dimensions. And the cloud mutation operator for each dimension of X_i is as follows:

Begin

For $d = 1 : D$

$Ex = X_{id}$;
En = variable search range/$cc1$;
$cc1 = 20\,\text{sqrt}(t)$;
$He = En/cc2$;
$cc2 = 10$;
A normal random number x_i is generated by the basic normal cloud generator, at the same time a random number Temp is also generated. When $\mu_i >$ Temp, X_{id} is updated by x_i.

End For

End

En represents the horizontal width of the cloud, and the greater the horizontal width, the greater the scope of the particle search. When $cc1$ is set as $20\,\text{sqrt}(t)$, the search range of the initial evolution is very large, which is helpful to find more extreme points. With the dynamic narrowing of the search range of t, it is favorable to the fine search of particles.

"Dimensional catastrophe problem" exists in dimension function. As the dimension increases, it is difficult to find the optimal solution in each dimension through the general evolutionary algorithms. The abnormal values on individual dimension lead to poor quality of the final solution or an inability to find the optimal solution to the optimization problem. Thus, in order to prevent the particles from falling into the local extreme points and failing to find the global optimal solution in high-dimensional multimodal function, the search particles are reinitialized with a certain probability p_s to find better solutions. When in the search state, the particles are rerandomly distributed in the search space as shown in

$$V_k(t+1) = \frac{(V_{\min} + V_{\max})}{2} + (V_{\min} - V_{\max})(\text{rand}() - 0.5),$$

$$X_k(t+1) = \frac{(X_{\min} + X_{\max})}{2} + (X_{\max} - X_{\min})(\text{rand}() - 0.5)\,\mathbb{k}. \tag{16}$$

After the initialization, particles are updated according to (16).

4.2. Population Diversity Optimization Based on Clonal Selection Algorithm. In order to ensure the diversity of the population, optimization is performed based on the clonal selection algorithm. The steps are divided into clonal amplification, adaptive wavelet mutation, and immune selection.

(1) Clonal Amplification. In the PSO immune system, the problem to be solved is the antigen. Each particle in the particle swarm has the potential to represent each local optimization value in the multipeak optimization. Therefore, N particles searched in the last iteration of the PP algorithm are all used as antibodies. The affinity function of antibodies and antigens uses the fitness function of the PP algorithm; that is,

$$\text{affinity}(a_i) = \text{fit}(a_i). \tag{17}$$

In (17), $\text{fit}(a_i)$ is the fitness value of particle a_i and $\text{affinity}(a_i)$ is the affinity value of the antibody a_i (the particle X_i). From (17), we can see that the smaller the affinity value of the antibody, the better the affinity.

The antibodies in the antibody population were sorted in ascending order according to the affinity value before the clonal amplification. The clonal amplification operator for the sorted ith antibody a_i is calculated according to

$$\beta_i = \text{round}\left(a_c \frac{1}{\sqrt{i}} + b\right). \tag{18}$$

In (18), a_c is a constant greater than 1, round() is a round function, and b can ensure that each antibody has a constant larger than 1 with a certain number of clones. From (18), we can see that the higher the affinity, the greater the clonal multiple. In the clonal selection algorithm, when the current iteration number is ct, the ith cloned amplified antibody a_i is changed to $a_i(\text{ct}) = \{a_{i1}(\text{ct}), a_{i2}(\text{ct}), \ldots, a_{i\beta_i}(\text{ct})\}$ after β_i times of clone.

(2) Adaptive Wavelet Mutation. Morlet wavelet has better probability distribution of upper and lower wings. Thus, Morlet wavelet is applied to immune mutation operation to make CSA have a wider range of searching, higher precision, and good regulating performance. Morlet wavelet mother function is shown in

$$\Psi_{a,b}(x) = \frac{1}{\sqrt{a}} e^{-((x-b)/a)/2} \cos\left(5\frac{x-b}{a}\right). \tag{19}$$

When $a = 1$ and $b = 0$, Morlet wavelet function is shown in Figure 1. In Figure 1, the horizontal axis is the independent variable, and the vertical axis is the wavelet mother function.

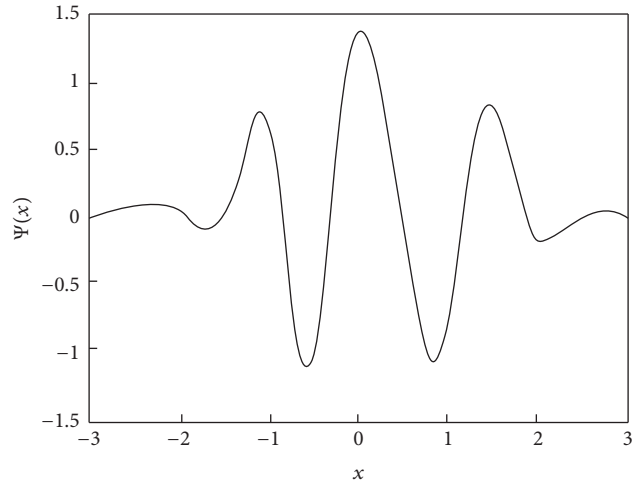

Figure 1: Morlet wavelet function.

With the progress of ct, the affinity of the antibody increases constantly. When the adaptive dynamic of the antibody mutation probability p_m reduces, the convergent speed of the algorithm can be improved. p_m is shown as

$$p_m(\text{ct}) = p_m(\text{ct}-1)\left(1 - 0.01\frac{\text{ct}}{\text{ct}_{\max}}\right). \tag{20}$$

In (20), $\text{ct}_{\max}$ is the maximum iteration number. When ct = 1, the initial value is set as 0.7. X_{id} mutation uses adaptive wavelet mutation operator based on the time-varying scale. X_{id} mutation formula is shown as follows:

$$X'_{id} = \begin{cases} X_{id} + \dfrac{X_{\max} - X_{id}}{m}\eta(\text{ct})\,\sigma(\text{ct}), \sigma(\text{ct}) \geq 0 X_{id} \\ \quad + \dfrac{X_{id} - X_{\min}}{m}\eta(\text{ct})\,\sigma(\text{ct}), \text{else}, \end{cases} \tag{21}$$

where m is an increase constant.

$$\eta(\text{ct}) = 1 - r^{(1-\text{ct}/\text{ct}_{\max})^b}. \tag{22}$$

In (22), $\eta(\text{ct})$ is the time-based mutation scale, r is the random number between $[0, 1]$, and b is the system parameter, which determines the dependency degree of the random number disturbance on ct.

$$\sigma(\text{ct}) = \frac{1}{\sqrt{a(\text{ct})}} e^{-(\varphi/a(\text{ct}))^2/2} \cos\left(5\frac{\varphi}{a(\text{ct})}\right). \tag{23}$$

In (23), $\sigma(\text{ct})$ is the wavelet mutation function, and φ is a random number between $[-3a(\text{ct}), 3a(\text{ct})]$. Function $a(\text{ct})$ is shown as

$$a(\text{ct}) = e^{-\ln(g)(1-\text{ct}/\text{ct}_{\max})^c + \ln(g)}. \tag{24}$$

In (24), c is the shape parameter of $a(\text{ct})$ and is set to 1. g is the upper limit of $a(\text{ct})$ and is set to 10000. Thus, the value of $a(\text{ct})$ increases with the increase of ct between 1 and 10000, while the range of $\sigma(\text{ct})$ shrinks with the increase of ct.

Table 2: Comparing the results of PP algorithm with WCPP algorithm.

Method	Number	Mean_G	Mean_L	Time
PP	1	3.5216	2.7526	91.5
	2	3.5259	2.7568	
	3	3.5951	2.8692	
	4	3.6059	2.8925	
WCPP	1	3.4253	2.2682	50.8
	2	3.4158	2.2481	
	3	3.4682	2.2543	
	4	3.5060	2.4988	

From (21), we can see that, at the early stage of the evolution, for smaller r, $\eta(\text{ct}) \approx 1$. When the value of $\sigma(\text{ct})$ is large, the mutation space is also large, so that the probability of searching other extreme points can be increased. And in the middle and late stages of the evolution, adaptive of $\eta(\text{ct})$ is smaller. When ct is approaching $\text{ct}_{\max}$, $\eta(\text{ct}) \approx 0$, and the value of $\sigma(\text{ct})$ is relatively small. Thus, by improving the local fine-tuning ability, the precision of the algorithm can be improved effectively.

(3) Immune Selection. Let $S_i(\text{ct}) = T_s^c(a_i(\text{ct})) = \min\{\text{affinity}(a_i'(\text{ct}))\}$, and $S_i(\text{ct}) \cup a_i(\text{ct}) \rightarrow a_i(\text{ct}+1)$. $a_i'(\text{ct})$ represents an antibody obtained by clonal amplification and mutation of the ctth iteration. Compression of population antibody is achieved by local selection, and the optimal solution of population is not deteriorated.

4.3. Performance Analysis of WCPP Algorithm in Multimodal Function Optimization. Select f_2 as test function, the result comparison of the PP algorithm and the WCPP algorithm is shown in Table 2.

$$f_2(x) = x\sin(10\pi x) + 2. \tag{25}$$

In Table 2, $\overline{X}$ represents the mean value of the optimal solution location at the time of the test. Mean_G represents the average of the global solutions of the 50 tests.

The mean value Mean_L of the local solution of the PP algorithm is larger than that Mean_L of the WCPP algorithm, which shows that the local solution of the PP algorithm has higher accuracy than the WCPP algorithm in the case that 16 local extreme points can be searched for objective function f_2.

5. Application of WCPP Algorithm to Sliding Mode Control of Discrete Chaotic Systems

5.1. Fractional Order Chaotic System Sliding Mode Control Model. Suppose a control system as $\dot{x} = f(x,u,t)$, $x \in R^n$, $u \in R^n$, $t \in R$. Switching function needs to be determined, $s(x)$, $s \in R^m$. Then, the control function can be solved as follows:

$$u = \{u^+(x), s(x) > 0 u^-(x), s(x) < 0. \tag{26}$$

In (26), $u^+(x) \neq u^-(x)$. Then,

(1) the sliding mode exists: that is, (26) holds;

(2) the accessibility condition can be satisfied, and the movement points outside the switching surface will reach the switching surface with a limited time;

(3) the stability of the sliding mode movement is ensured;

(4) the dynamic quality requirement of the control system is satisfied.

If the first three basic problems can be satisfied, we can call the control as sliding mode control.

Henon fractional chaotic system is taken as an example; the sliding mode control model of fractional chaotic system is constructed. The Henon chaotic system with control is shown as

$$\begin{aligned} x_1(k+1) &= 1 - a\left(x_1(k)\right)^2 + bx_2(k) + u(k), \\ x_2(k+1) &= x_1(k), \end{aligned} \tag{27}$$

where $x \in R^n$, $u \in R$.

Define the switching function as $s(k) = C_e[e(k), de(k)]$, where $C_e = [c_k, c_0]$. Then, $s(k+1) = C_e[e(k+1), de(k+1)]$, $de(k+1) = (e(k+1) - e(k))/\text{ts}$, where ts is the sampling time. And we can obtain (28) as follows:

$$\begin{aligned} s(k) &= c_k e(k) + c_0 de(k), \\ s(k+1) &= \left(c_k + \frac{c_0}{\text{ts}}\right) e(k+1) - \left(\frac{c_0}{\text{ts}}\right) e(k). \end{aligned} \tag{28}$$

When the fractional order chaotic system enters the ideal sliding mode, $s(k)$ can satisfy the following:

$$s(k+1) = s(k). \tag{29}$$

That is,

$$\left(c_k + \frac{c_0}{\text{ts}}\right) e(k+1) - \left(\frac{c_0}{\text{ts}}\right) e(k) = c_k e(k) + c_0 de(k), \tag{30}$$

where $e(k+1) = r(k+1) - x_1(k+1)$. Define $f(k) = 1 - ax_1^2(k) + bx_2(k)$; then, we can have $u_{\text{eq}}(k) = x_1(k+1) - f(k)$.

From the above, we can obtain the sliding mode control equivalent control part of the fractional order chaotic system $u_{\text{eq}}(k)$, which is shown in

$$u_{\text{eq}}(k) = \frac{\left(c_k + c_0/\text{ts}\right) r(k+1) - \left(c_k + c_0/\text{ts}\right) e(k) - c_0 de(k)}{c_k + c_0/\text{ts}}. \tag{31}$$

5.2. Sliding Mode Control Flow of the Discrete Chaotic System Based on WCPP Algorithm

(1) Evaluation Function Selection. The selection of the evaluation function not only needs to consider the stability, fastness, and accuracy of the system but also needs to consider the control energy problem, the form of which is shown as

$$J(p) = \int_0^\infty \left(w_1 |e(t)| + w_2 |u(t)| + w_3 t_u\right) dt. \tag{32}$$

In (32), $e(t)$ is the system error, $u(t)$ is the control variable, t_u is the initial step time, and w_1, w_2, w_3 are the weights. The smaller the value of the evaluation function $J(p)$ is, the closer the corresponding function p is to the global optimal solution. The evaluation function value decreases as the algorithm runs.

(2) Sliding Mode Control Flow of the Discrete Chaotic System Based on WCPP Algorithm. By using the WCPP algorithm, the parameters of the sliding mode controller are globally optimized to construct the sliding mode control method. The flow is as follows:

Begin

Step 1. Initialize the sliding mode controller, other parameters, and a group of particles with size N. The initialization parameters include maximum repetition search number M of hybrid algorithm and the WCPP maximum number of iterations $\mathrm{ct}_{\max}$.

Step 2. The evaluation function value of each particle is obtained by control of the discrete chaotic system according to the position of each particle and the optimal position of individual particle P_i and the optimal position of all particles P_g are recorded.

Step 3. If the repeated search algebra m is larger than M, the iteration is stopped, and the algorithm is finished. The output of the sliding mode controller controls the discrete chaotic system. Otherwise, turn to Step 4.

Step 4. **If** the WCPP algorithm iteration number $t \le t_{\max}$,

If the condition of the cloud mutation is satisfied,
the cloud mutation is performed on the particles.
Else
Speed and positions are updated on the particles.
End If
Update particles P_i and P_g, and
$t + 1$.
End If

Step 5. The particles in the last search generation of the WCPP algorithm are cloned and amplified.

Adaptive wavelet mutation operator performance is carried out.

Immune selection performance is carried out.

And, ct + 1.

End If
update particles P_i and P_g,

Step 6. $m + 1$, the positions and the speed are reinitialized.

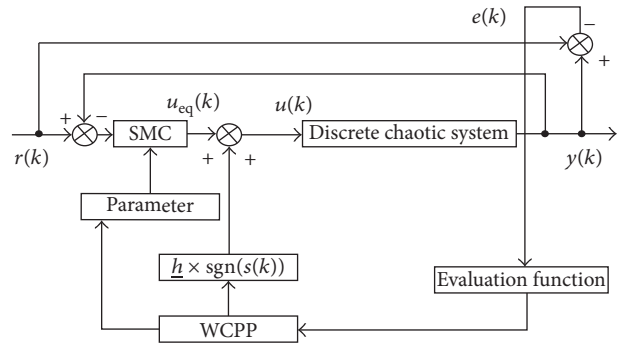

Figure 2: Sliding mode control of discrete chaotic system based on WCPP algorithm.

Step 7. The searched optimal fitness particles are assigned to the initialized particles and turn to Step 2.

End

In order to improve the fastness of the sliding mode control method for the discrete chaotic systems based on the WCPP algorithm, the values of the algorithm parameters N and M are small.

Figure 2 is the discrete chaotic system sliding mode control structure based on the WCPP algorithm.

5.3. Algorithm Simulations. A discrete chaotic system is taken as the simulation object; the model of the controlled object is shown as

$$y(k+1) = \frac{y(k)}{1 + y(k)^2 + d(k)} + u(k)^3. \tag{33}$$

For the above discrete chaotic system, simulations of step input signal $r(k) = 1$ are implemented based on the WCPP and other two algorithms, which is shown in Figure 3. In this simulation, the disturbance signal is set as $d(k) = 0$. And at this time the WCPP optimized parameters are $\{20, 1\}$.

From Figure 3, we can see that the WCPP algorithm has very strong search ability. It can search the global optimal value of the sliding mode controller parameters without overshoot, and the error, the response speed, and adjustment time all achieved the optimal performance. Therefore, the control effect of the WCPP algorithm is superior to the control effect of the PSO and the PP algorithm.

For the above discrete chaotic system, the simulations of the square wave input signal $r(k) = 0.5\,\mathrm{sign}(\sin(8\pi k \cdot \mathrm{ts}))$ are implemented by the WCPP algorithm and other two algorithms, respectively, which is shown in Figure 4.

Another discrete chaotic system is also taken as the simulation object; the model of the controlled object is shown as

$$y(k) = \frac{-0.1\,y(k-1) + u(k-1)}{1 + y^2(k-1)}. \tag{34}$$

For the above discrete chaotic system, simulations of step input signal $r(k) = 1$ are implemented based on the WCPP

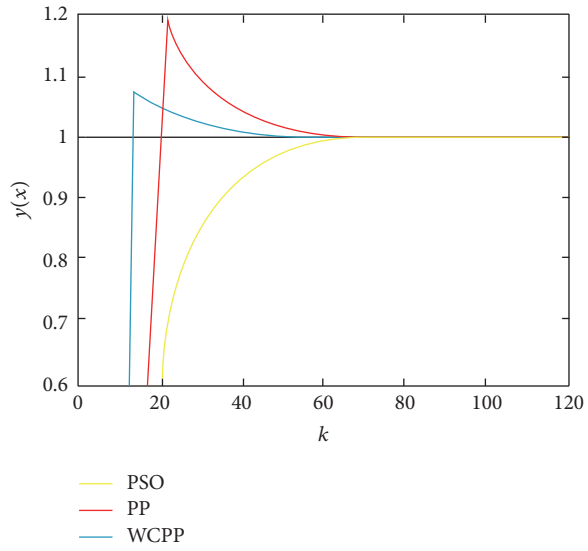

Figure 3: Simulation results of discrete chaotic systems.

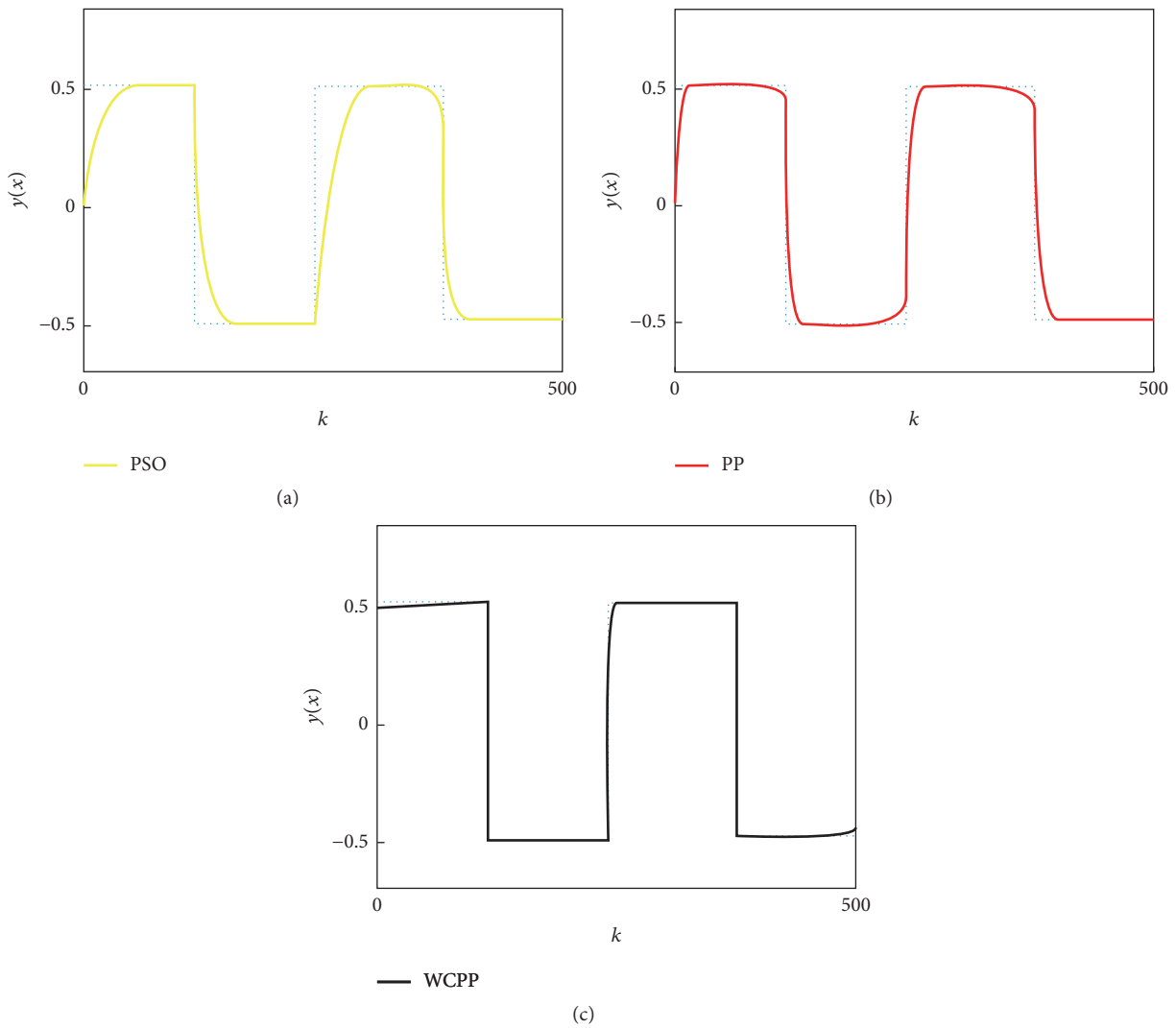

Figure 4: Square wave simulation of discrete chaotic system.

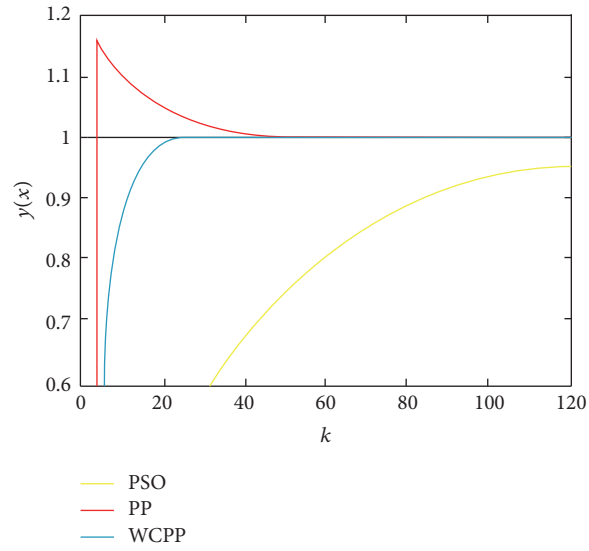

Figure 5: Simulation results of discrete chaotic systems.

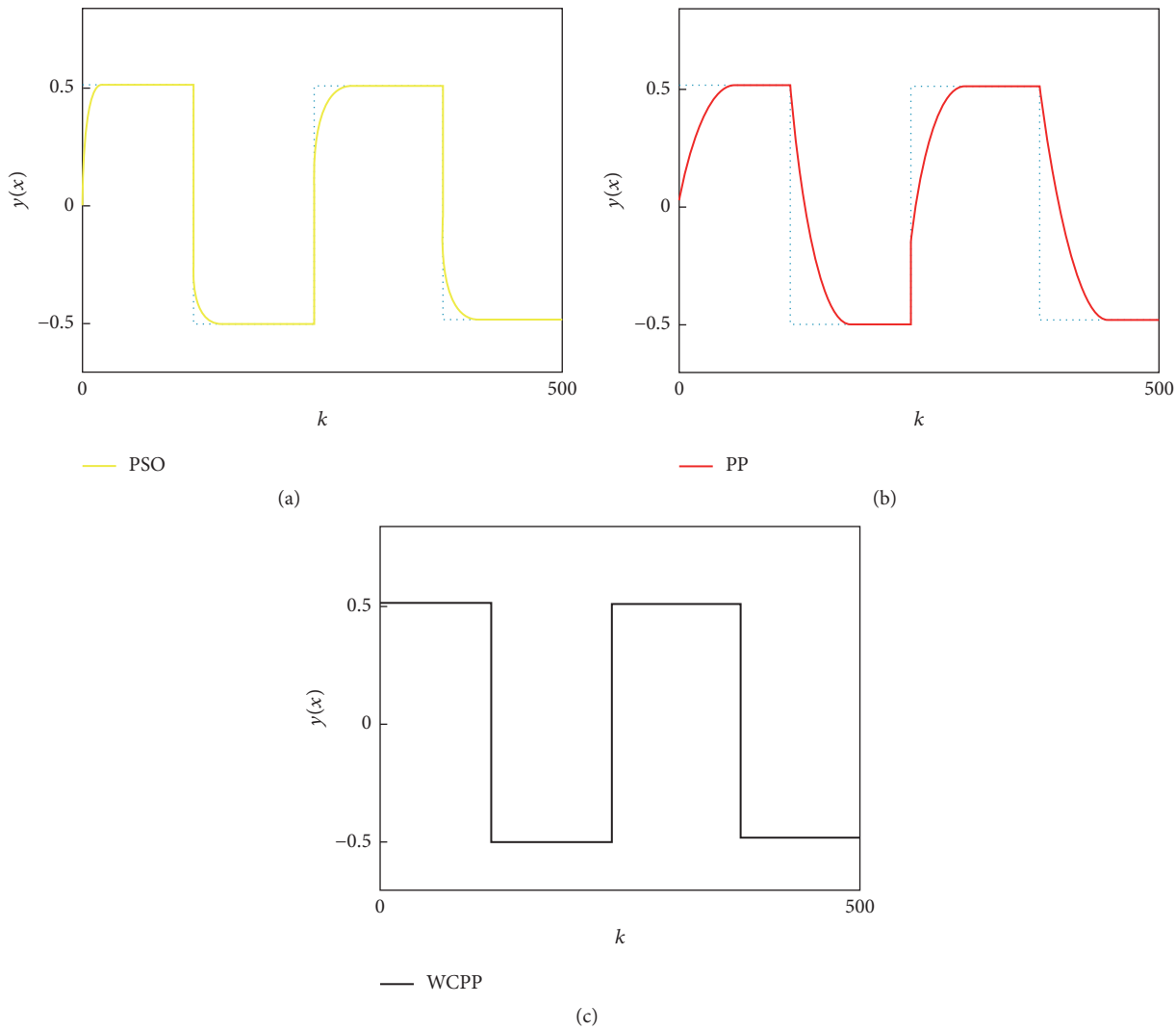

Figure 6: Square wave simulation of discrete chaotic system.

and other two algorithms, which is shown in Figure 5. The WCPP optimized parameters are {1.000, 0.001}.

From Figure 5, we can find that the WCPP algorithm is basically no overshoot and is able to achieve the desired value in the second iteration. The performances of the WCPP algorithm in error, response speed, and adjustment time are significantly better than those of PSO and PP algorithms. Therefore, WCPP algorithm has strong searching ability and good control quality.

For the above discrete chaotic system, the simulations of the square wave input signal $r(k) = 0.5\,\mathrm{sign}(\sin(8\pi k \cdot \mathrm{ts}))$ are implemented by the WCPP algorithm and other two algorithms, respectively, which is shown in Figure 6.

It can be seen from Figures 4 and 6 that the response speed, overshoot, and other performances of the WCPP algorithm have been improved significantly.

6. Conclusions

Chaos and chaos systems are widely used in physics, engineering, biology, finance, and so forth. The modeling of complex systems based on the theory of calculus can more accurately reflect the dynamic characteristics of the systems. Discrete chaotic systems can be widely used in the field of chaotic secure communications. Thus, it is of great theoretical and applicable value in the applications of control and synchronization of the chaotic dynamic systems. In order to overcome the shortcoming of the standard PSO algorithm in multimodal function optimization problems, a sliding mode control model of discrete chaotic systems based on the coupled multimode functions is proposed. The simulation results show that the improved algorithm proposed in this paper has significantly improved the response speed and overshoot performance compared with the standard PSO algorithm.

Conflicts of Interest

The author declares that there are no conflicts of interest regarding the publication of this paper.

Acknowledgments

This work was supported by the National Natural Science Foundation of China (Grant no. 51675490).

References

[1] Y.-H. Chang, C.-I. Wu, H.-W. Lin, H.-C. Chen, and C.-W. Chang, "Fractional order integral sliding-mode flux observer for direct field-oriented induction machines," *International Journal of Innovative Computing, Information and Control*, vol. 8, no. 7, pp. 4851–4868, 2012.

[2] S. Dadras and H. R. Momeni, "Fractional terminal sliding mode control design for a class of dynamical systems with uncertainty," *Communications in Nonlinear Science and Numerical Simulation*, vol. 17, no. 1, pp. 367–377, 2012.

[3] A. H. J. De Ruiter, "Adaptive spacecraft attitude control with actuator saturation," *Journal of Guidance, Control, and Dynamics*, vol. 33, no. 5, pp. 1692–1696, 2010.

[4] H. Liu, L. Guo, and Y. Zhang, "Composite attitude control for flexible spacecraft with simultaneous disturbance attenuation and rejection performance," *Proceedings of the Institution of Mechanical Engineers. Part I: Journal of Systems and Control Engineering*, vol. 226, no. 2, pp. 154–161, 2012.

[5] D. Matignon, "Stability properties for generalized fractional differential systems," *ESAIM: Proceedings and Surveys*, vol. 5, pp. 145–158, 2008.

[6] M. P. Lazarević and A. M. Spasić, "Finite-time stability analysis of fractional order time-delay systems: gronwall's approach," *Mathematical and Computer Modelling*, vol. 49, no. 3-4, pp. 475–481, 2009.

[7] I. N'Doye, M. Zasadzinski, M. Darouach, and N.-E. Radhy, "Observer-based control for fractional-order continuous-time systems," in *Proceedings of the 48th IEEE Conference on Decision and Control held jointly with 28th Chinese Control Conference (CDC/CCC '09)*, pp. 1932–1937, December 2009.

[8] H. Ye, J. Gao, and Y. Ding, "A generalized Gronwall inequality and its application to a fractional differential equation," *Journal of Mathematical Analysis and Applications*, vol. 328, no. 2, pp. 1075–1081, 2007.

[9] J. Vasundhara Devi, F. A. Mc Rae, and Z. Drici, "Variational Lyapunov method for fractional differential equations," *Computers & Mathematics with Applications*, vol. 64, no. 10, pp. 2982–2989, 2012.

[10] J. Sabatier, M. Moze, and C. Farges, "LMI stability conditions for fractional order systems," *Computers & Mathematics with Applications*, vol. 59, no. 5, pp. 1594–1609, 2010.

[11] Y. Chen, H.-S. Ahn, and I. Podlubny, "Robust stability check of fractional order linear time invariant systems with interval uncertainties," *Signal Processing*, vol. 86, no. 10, pp. 2611–2618, 2006.

[12] T. P. Sales, D. A. Rade, and L. C. G. De Souza, "Passive vibration control of flexible spacecraft using shunted piezoelectric transducers," *Aerospace Science and Technology*, vol. 29, no. 1, pp. 403–412, 2013.

[13] J. Erdong and S. Zhaowei, "Passivity-based control for a flexible spacecraft in the presence of disturbances," *International Journal of Non-Linear Mechanics*, vol. 45, no. 4, pp. 348–356, 2010.

[14] K. Lu, Y. Xia, Z. Zhu, and M. V. Basin, "Sliding mode attitude tracking of rigid spacecraft with disturbances," *Journal of the Franklin Institute. Engineering and Applied Mathematics*, vol. 349, no. 2, pp. 413–440, 2012.

Hindawi
Mathematical Problems in Engineering
Volume 2017, Article ID 2490580, 13 pages
https://doi.org/10.1155/2017/2490580

Research Article

Hopf Bifurcation, Positively Invariant Set, and Physical Realization of a New Four-Dimensional Hyperchaotic Financial System

G. Kai,[1,2] W. Zhang,[1] Z. C. Wei,[1,3] J. F. Wang,[1] and A. Akgul[4]

[1] *Beijing Key Laboratory of Nonlinear Vibrations and Strength of Mechanical Structures, College of Mechanical Engineering, Beijing University of Technology, Beijing 100124, China*
[2] *School of Mathematics and Statistics, Inner Mongolia University of Financial and Economics, Hohhot 100124, China*
[3] *School of Mathematics and Physics, China University of Geosciences, Wuhan 430074, China*
[4] *Department of Electrical and Electronics Engineering, Faculty of Technology, Sakarya University, 54187 Sakarya, Turkey*

Correspondence should be addressed to W. Zhang; sandyzhang0@yahoo.com

Received 16 December 2016; Revised 10 February 2017; Accepted 9 March 2017; Published 10 April 2017

Academic Editor: Ahmad Taher Azar

This paper introduces a new four-dimensional hyperchaotic financial system on the basis of an established three-dimensional nonlinear financial system and a dynamic model by adding a controller term to consider the effect of control on the system. In terms of the proposed financial system, the sufficient conditions for nonexistence of chaotic and hyperchaotic behaviors are derived theoretically. Then, the solutions of equilibria are obtained. For each equilibrium, its stability and existence of Hopf bifurcation are validated. Based on corresponding first Lyapunov coefficient of each equilibrium, the analytical proof of the existence of periodic solutions is given. The ultimate bound and positively invariant set for the financial system are obtained and estimated. There exists a stable periodic solution obtained near the unstable equilibrium point. Finally, the dynamic behaviors of the new system are explored from theoretical analysis by using the bifurcation diagrams and phase portraits. Moreover, the hyperchaotic financial system has been simulated using a specially designed electronic circuit and viewed on an oscilloscope, thereby confirming the results of the numerical integrations and its real contribution to engineering.

1. Introduction

In recent years, economic dynamics become very prominent in the mainstream economics, and stochastic analysis is a popular way to interpret financial time series based on the existing information. Random exogenous shocks is usually considered to be the reason of a periodic behavior of the economic system by employing stochastic analyses, caused by factors outside the system. The shortcoming of the stochastic approach is incapable to illustrate the dynamics of financial systems [1].

An effective and rapid control method is very important for the government when some chaotic phenomenon appears [2–5]. A classical three-dimensional financial dynamic model describing the time variations of state adjustment has been reported [3], which includes the interest rate, the price index, and the investment demand. Later, another three-dimensional financial chaotic risk dynamic system was constructed for management process of financial markets and proved to be controlled effectively [6]. Then Holyst and Urbanowicz [7] used the method of delayed feedback control (DFC) and proved that a chaotic financial system can be stabilized on various periodic orbits [8]. Reference [9] discussed the complex behaviors of a financial system with time-delayed feedback by numerical simulation. Normal form of a financial system with delaying has been derived, which is associated with Hopf and double Hopf bifurcations and makes the financial system more complicated [10, 11]. In addition, the positively invariant sets of the dynamic system have a basic significance in the state constraints and control constraints, which are widely applied in different kinds of field: general 3-body problem [12], delay

differential-equations [13], stability of dynamic system [14], robust attitude control schemes [15], relative motion control of the spacecraft [16], interconnected and time-delay systems [17], and permanent magnet synchronous motor system [18].

On the other hand, high dimensional control system is now a research hot topic, which has been applied in many fields. Zhang et al. introduced a three-dimensional ultimate bound and positively invariant set in which parameters are positive [19]. Wang et al. showed a smooth four-dimensional quadratic autonomous hyperchaotic system, which generated two novel double-wing periodic, quasi-periodic, and hyperchaotic attractors [20]. Wei and Zhang obtained the ultimate bound and positively invariant set is in a four-dimensional autonomous system [21]. Du et al. proposed hyperchaotic Rikitake system which was a novel four-dimensional autonomous nonlinear system and assured the existence of Hopf bifurcation [22]. A new four-dimensional quadratic autonomous hyperchaotic attractor was presented and the Hopf bifurcation at the equilibrium point was analyzed by Prakash and Balasubramaniam [23]. Therefore, the dynamical behaviors of hyperchaotic systems are more complex than chaotic systems and will have practical meanings for carrying out this research about financial systems [24]. Therefore, it is very necessary to explain complicated phenomena of financial dynamics by a thorough studying on the internal structural characteristics of hyperchaotic systems. On the viewpoint of mathematics and finance, these research points are attractive and rational. This paper constructs a new type of hyperchaotic financial system by nonlinear feedback method.

The remainder of the paper is organized as follows. Firstly, a new four-dimensional financial system is introduced by adding feedback controllers to the classic financial system in Section 2. And a sufficient condition for nonexistence of chaotic or hyperchaotic behaviors is obtained theoretically. Then the novel hyperchaotic financial system is confirmed numerically from Lyapunov exponents. Characterizations for the four-dimensional Hopf bifurcations are surveyed in Section 3. Section 4 introduces the ultimate bound and positively invariant set. The dynamic properties of the system are showed via bifurcation diagram in Section 5. In Section 6, a real contribution to engineering will be realized by an electronic circuit and oscilloscope in real time. Section 7 gives some conclusions.

2. Financial System from Classic Financial Model

2.1. Formulation of System. A financial dynamic system with different factors is reported in [3]. With the proper dimensions and appropriate coordinates, a simplified financial model is proposed:

$$\dot{x} = z + (y - a)\,x, \tag{1a}$$

$$\dot{y} = 1 - by - x^2, \tag{1b}$$

$$\dot{z} = -x - cz, \tag{1c}$$

where "x" shows the interest rate that is defined as the price or cost of money for borrowing and return to lending. "y" implies the investment demand, which will be directly affected by the interest rate. In addition, the supply and demand of the commercial goods and inflation rate cause changes of "z"; let $a > 0$, $b > 0$, and $c > 0$, respectively, be the saving amount, the cost per investment, and the elasticity of demand in commercial market.

This paper is dedicated to greatly survey the dynamical behaviors of a four-dimensional financial system which expanded from a known three-dimensional financial system and also proposes a simplified mathematical system. In this paper, we design the controlled system as follows:

$$\dot{x} = z + (y - a)\,x, \tag{2a}$$

$$\dot{y} = 1 - by - x^2, \tag{2b}$$

$$\dot{z} = -x - cz + u, \tag{2c}$$

$$\dot{u} = -dxy - ku - mz, \tag{2d}$$

where u denotes control input and economically state intervention to balance the economic environment. For example, United States interest rates are determined by the Federal Reserve with considering short term economic targets. Regulatory agencies of open markets meet at certain intervals to monitor the economic and financial situation and decide on monetary policies. To decrease inflation and increase the purchasing power of the consumers, government will increase the interest rate. As a result of this, control input is the factor that interacts with all variables. This cross relation between interest rate, inflation (this also represents the price and goods and services which are denoted as "z" in the study), and government regulations can be expressed from (2d), in which d, k, and m mean corresponding amplitudes.

Therefore, it will be expected to study some complex dynamical behaviors about the proposed four-dimensional autonomous system (2a), (2b), (2c), and (2d).

2.2. Nonexistence of Chaotic or Hyperchaotic Behaviors. In addition, chaotic solutions do not exist for certain parameter values in system (2a), (2b), (2c), and (2d). We get three positive Lyapunov exponents, and it will be beneficial for us to find hyperchaos. More precisely, the main results are obtained as follows.

Theorem 1. *A six-parameter family (a, b, c, d, k, m) of system (2a), (2b), (2c), and (2d) is considered. If the parameters satisfy $a > 0$, $b > 0$, and $c > 0$, then the following conditions are met as*

$$m = \frac{d\left(1 + ac + 2d - a^2 d + acd + d^2 - ak - ck + adk - cdk + k^2\right)}{(1+d)^2}, \tag{3}$$

$$\frac{ad + k}{1 + d} < 0,$$

and system (2a), (2b), (2c), and (2d) has no bounded chaotic solutions or hyperchaotic solutions.

Proof. From system (2a), (2b), (2c), and (2d),

$$d\dot{x} + \frac{d(k-a)}{1+d}\dot{z} + \dot{u} = (-ad - s)x + (d - m - cs)z + (-k + s)u. \tag{4}$$

Under assumption (3), (4) becomes

$$d\dot{x} + \frac{d(k-a)}{1+d}\dot{z} + \dot{u} = -\frac{ad+k}{1+d}\left[dx + \frac{d(k-a)}{1+d}z + u\right]. \tag{5}$$

Thus, we can get the expression that

$$dx + \frac{d(k-a)}{1+d}z + u = \left[dx(0) + \frac{d(k-a)}{1+d}z(0) + u(0)\right]e^{-((ad+k)/(1+d))t}. \tag{6}$$

Since $(ad + k)/(1 + d) < 0$ ($a > 0$ is the amount of saving; $b > 0$ is the cost per investment) and at least one of the following conditions is satisfied: $x(t)$, $z(t)$, or $u(t)$ is not bounded, then system (2a), (2b), (2c), and (2d) is not chaotic.

The proof is complete. □

3. Some Basic Properties and Bifurcation Analysis of the New System (2a), (2b), (2c), and (2d)

3.1. Equilibria and Stability. Firstly, the invariance of system is easily demonstrated with the transformation of coordinate $(x, y, z, u) \to (-x, -y, z, -\omega)$; namely, the system has rotated symmetry around the axis z.

We consider the equilibrium point of system (2a), (2b), (2c), and (2d) to analyze the equilibria and let

$$z + (y - a)x = 0, \tag{7a}$$

$$1 - by - x^2 = 0, \tag{7b}$$

$$-x - cz + u = 0, \tag{7c}$$

$$-dxy - ku - mz = 0. \tag{7d}$$

Combining (7a), (7b), and (7c), we obtain

$$x = \pm\sqrt{1-by},$$
$$z = \pm(a-y)\sqrt{1-by}, \tag{8}$$
$$u = \pm\sqrt{1-by}\,(1 + ac - cy).$$

Substituting (8) into (7d) yields

$$\sqrt{1-by}\,[(d - ck - m)y + k + ack + am] = 0, \tag{9}$$

where $f_y' = 0$ and

$$f_y' = -\frac{b}{2\sqrt{1-by}}[(d - ck - m)y + k + ack + am] + \sqrt{1-by}\,[d - ck - m] = 0, \tag{10}$$

$$y = \frac{2}{3b} - \frac{k + ack + am}{3(d - ck - m)}. \tag{11}$$

Substituting (11) into (10) yields

$$\sqrt{1 - \frac{b(k + ack + am)}{d - ck - m}}\left(\frac{d - ck - m}{b} + k + ack + am\right) = 0. \tag{12}$$

Hence, we can obtain the following results:

System (2a), (2b), (2c), and (2d) have only one equilibrium point $E_0(0, 1/b, 0, 0)$.

If $d - ck - m \neq 0$ and $\Gamma_1 = -d + ck + m$ and $\Gamma_2 = k + ack + am$, system (2a), (2b), (2c), and (2d) with $0 < \Gamma_1 < b\Gamma_2$ has three equilibrium points $E_0(0, 1/b, 0, 0)$ and $E_{1,2}(\pm x_0, y_0, \mp z_0, \mp u_0)$, where

$$x_0 = \frac{\Gamma_1 - b\Gamma_2}{\Gamma_1},$$
$$y_0 = \frac{\Gamma_2}{\Gamma_1},$$
$$z_0 = (ad + k)\frac{\Gamma_1 - b\Gamma_2}{\Gamma_1^{3/2}}, \tag{13}$$
$$u_0 = (d + acd - m)\frac{\Gamma_1 - b\Gamma_2}{\Gamma_1^{3/2}}.$$

In the next step, we research the stability situation of equilibria E_0 and $E_{1,2}$. By linearizing system (2a), (2b), (2c), and (2d) at the equilibrium (x_*, y_*, z_*, u_*), the Jacobian matrix is

$$J(E) = \begin{pmatrix} y_* - a & x_* & 1 & 0 \\ -2x_* & -b & 0 & 0 \\ -1 & 0 & -c & 1 \\ -dy_* & -dx_* & -m & -k \end{pmatrix}. \tag{14}$$

Obviously, the characteristic equation at the equilibrium point (x_*, y_*, z_*, u_*) is

$$\lambda^4 + (a + b + c + k - y_*)\lambda^3 + (1 + ab + ac + bc + ak + bk + ck + m + 2x_*^2 - by_* - cy_*)\lambda^2 + (b + abc + k + abk + ack + bck + am + bm + 2cx_*^2 - bcy_* + dy_* - bky_* - cky_* - my_*)\lambda + bk + abck + abm - 2dx_*^2 + 2ckx_*^2 + 2mx_*^2 + bdy_* - bcky_* - bmy_* = 0. \tag{15}$$

The following symbols are introduced:

$$a_1 = a + b + c + k - y_*, \tag{16a}$$

$$a_2 = 1 + ab + ac + bc + ak + bk + ck + m + 2x_*^2 - by_* - cy_*, \tag{16b}$$

$$a_3 = b + abc + k + abk + ack + bck + am + bm + 2cx_*^2 - bcy_* + dy_* - bky_* - cky_* - my_*, \tag{16c}$$

$$a_4 = bk + abck + abm - 2dx_*^2 + 2ckx_*^2 + 2mx_*^2 + bdy_* - bcky_* - bmy_*. \tag{16d}$$

By using the criterion initiated by Routh-Hurwitz, the real parts of all the roots are negative if and only if

$$\begin{aligned} a_i &> 0, \quad (i = 1, 2, 3, 4) \\ a_1 a_2 - a_3 &> 0, \\ a_1 a_2 a_3 - a_3^2 - a_1^2 a_4 &> 0. \end{aligned} \tag{17}$$

Therefore, the equilibrium point (x_*, y_*, z_*, u_*) is asymptotically stable when (17) are satisfied.

Remark 2. For the sake of simplification of the study of dynamical behavior of system (2a), (2b), (2c), and (2d) in the following subsections, the values of system parameters are fixed as $a = 0.9$, $c = 1.5$, $d = 0.2$, and $k = 0.05$.

(A) When $m = 0.005$, system (2a), (2b), (2c), and (2d) has three equilibria for E_0 and $E_{1,2}$:

(A_1) E_0 is asymptotically stable when $b > 0.7068$.
(A_2) $E_{1,2}$ is unstable for $b \in R^+$ as $a_1 a_2 - a_3 < 0$.

(B) When $b = 0.2$, system (2a), (2b), (2c), and (2d) has three equilibria for E_0 and $E_{1,2}$:

(B_1) E_0 is unstable for $m \in R^+$ as $a_1 < 0$.
(B_2) $E_{1,2}$ is asymptotically stable when $m > 0.5139$.

With the target of finding the effect of control parameters b of the new dynamic system of four dimensions, the simulation results are obtained by numerical simulation. According to conditions (A_2) and (B_1), some dynamic properties of system (2a), (2b), (2c), and (2d) can be analyzed through bifurcation diagrams.

3.2. An Analysis of System Bifurcation (2a), (2b), (2c), and (2d). Now we calculate the first Lyapunov coefficient in relation to Hopf bifurcation by employing the projection method [25]. Let l_1 be the first Lyapunov coefficient related to Hopf bifurcation. Firstly, consider the differential equation

$$\dot{X} = f(X, \mu), \tag{18}$$

in which $x \in R^4$ denotes vectors representing phase variables and $\mu \in R^6$ denotes control parameters. Suppose f is a class of C^∞ in $R^4 \times R^6$ and there is an equilibrium point in (18) $X = X_0$ at $\mu = \mu_0$. Let variable $X - X_0$ be X, and we can write

$$F(X) = f(X, \mu_0) \tag{19}$$

as

$$F(X) = AX + \frac{1}{2}B(X, X) + \frac{1}{6}C(X, X, X) + O\left(\|X\|^4\right), \tag{20}$$

where $A = f_x(0, \mu_0)$ and, for $i = 1, 2, 3$,

$$\begin{aligned} B(X, Y) &= \sum_{j,k=1}^{3} \left.\frac{\partial^2 F_i(\xi)}{\partial \xi_i \partial \xi_k}\right|_{\xi=0} X_j Y_k, \\ C(X, Y, Z) &= \sum_{j,k,l=1}^{3} \left.\frac{\partial^3 F_i(\xi)}{\partial \xi_j \partial \xi_k \partial \xi_l}\right|_{\xi=0} X_j Y_k Z_l. \end{aligned} \tag{21}$$

The following considerations are supposed: A has a pair of complex eigenvalues on the imaginary axis $\lambda_{2,3} = \pm i\omega$ ($\omega_0 > 0$), which are the only eigenvalues with $\mathrm{Re}\,\lambda = 0$, T^c is the generalized eigenspace of A with regard to $\lambda_{2,3}$, and $p, q \in C^3$ are vectors such that

$$\begin{aligned} Aq &= i\omega_0 q, \\ A^T p &= -i\omega_0 p, \\ \langle p, q \rangle &= 1, \end{aligned} \tag{22}$$

in which A^{T} is the transposition of the matrix A.

Vector $y \in T^c$ can be showed as $y = \omega q + \overline{\omega}\,\overline{q}$ with $\omega = \langle p, y \rangle \in C$. The two-dimensional center manifold related to the eigenvalues $\lambda_{2,3}$ is parameterized by ω and $\overline{\omega}$, with an immersion of the form $X = H(\omega, \overline{\omega})$, where $H : C^2 \to R^3$ is a Taylor expansion of the form

$$H(\omega, \overline{\omega}) = \omega q + \overline{\omega}\,\overline{q} + \sum_{2 \le j+k \le 3} \frac{1}{j!k!} h_{jk} \omega^j \overline{\omega}^k + o\left(|\omega|^4\right), \tag{23}$$

with $h_{jk} \in C^3$ and $h_{jk} = \overline{h}_{kj}$. Substituting (23) into (19), the following differential equation could be reached:

$$H_\omega \omega' + H_{\overline{\omega}} \overline{\omega}' = F(H(\omega, \overline{\omega})). \tag{24}$$

By solving the system of linear equations defined by the coefficients of (19), we can get the complex vectors h_{ij}. Given the coefficient F, system equation (19) can be written on the chart ω for a central manifold as

$$\dot{\omega} = i\omega_0 \omega + \frac{1}{2} G_{21} \omega |\omega|^2 + O\left(|\omega|^4\right), \tag{25}$$

where $G_{21} \in C$.

Denote the first Lyapunov coefficient as

$$l_1 = \frac{1}{2} R_e G_{21}, \tag{26}$$

in which $G_{21} = \langle p, C(q, q, \overline{q}) + B(\overline{q}, h_{20}) + 2B(q, h_{11}) \rangle$.

A Hopf bifurcation point (X_0, μ_0) is an equilibrium point of (18), a pair of purely imaginary eigenvalues $\pm i\omega_0$ $(\omega > 0)$ and another eigenvalue with nonzero real part only exists in the Jacobian matrix A. A two-dimensional center manifold is well defined at a Hopf point, which is invariant under the flow produced by (18) and can continue with arbitrarily high class of differentiability to nearby parameter values.

If the parameter-dependent complex eigenvalues cross the imaginary axis with nonzero derivative, then a Hopf point is called transversal. In the area of a transversal Hopf point with $l_1 \neq 0$, the dynamic behavior of system (18) can decrease to a family of parameter-dependent continuations of the center manifold and is topologically orbital equivalent to the complex normal form

$$\omega' = (\eta + i\omega)\,\omega + l_1 \omega\,|\omega|^2, \tag{27}$$

where $\omega \in C$ and η, ω, and l_1 are real functions with arbitrarily higher order derivatives, which are continuations of $0, \omega_0$, and the first Lyapunov coefficient at the Hopf point [23]. When $l_1 < 0$ $(l_1 > 0)$, we can find one family of stable (unstable) periodic orbits on this manifolded family, contracting to an equilibrium point at the Hopf point.

The remaining part of this section employs the four-dimensional Hopf bifurcation theory and uses symbolic computations to carry out the analysis of parametric variations concerning dynamical bifurcations. Because the system has only one equilibrium, the bifurcation of system (2a), (2b), (2c), and (2d) will be our only concern, and then we get Theorem 3.

3.2.1. Hopf Bifurcation at E_0

Theorem 3. *With system (2a), (2b), (2c), and (2d) and $a = 0.9$, $c = 1.5$, $d = 0.2$, $k = 0.05$, and $m = 0.005$, the first Lyapunov coefficient at E_0 for critical value $b = b_0 = 0.7068$ is given by*

$$l_1 = -0.1568 < 0. \tag{28}$$

Therefore, there exists a transversal Hopf point at E_0 of system (2a), (2b), (2c), and (2d), and thus this point is stable. Moreover, for each $b < b_0$, but close to b_0, there is a stable limit cycle close to the unstable equilibrium point E_0.

Proof. As to the parameters $(a, c, d, k, m) = (0.9, 1.5, 0.2, 0.05, 0.005)$ and $b = b_0 = 0.7068$, we have

$$\begin{aligned} \lambda_1 &= -1.0351, \\ \lambda_2 &= -0.7068, \\ \lambda_{3,4} &= \pm 0.5309i. \end{aligned} \tag{29}$$

Under this condition, it is easy to know the transverse condition $\lambda'(b = b_0) < 0$. Accordingly, there exists a Hopf bifurcation at E_0. The stability of E_0 can be decided by the value of the first Lyapunov coefficient l_1 and l_1 can show the stability of E_0 and the occurred periodic orbits. Making use of the notation of the section above, the multilinear symmetrical functions could be written as

$$\begin{aligned} &B(x, y) \\ &\quad = \left(x_1 y_3 + x_3 y_1, -2x_1 y_1, 0, -dx_1 y_2 - dx_2 y_1\right), \end{aligned} \tag{30a}$$

$$C(x, y, z) = (0, 0, 0, 0). \tag{30b}$$

Moreover, the following results are obtained:

$$\begin{aligned} p = (&0.142675 + 0.581567i, 0, -0.0353347 \\ &+ 0.375204i, -0.70668), \end{aligned} \tag{31a}$$

$$\begin{aligned} q = (&0.522813 + 1.01926i, 0, -0.810362 \\ &- 0.247239i, -0.561461 + 0.218144i), \end{aligned} \tag{31b}$$

$$h_{11} = (-0.370497, -3.71333, 1.54211, 1.94266), \tag{31c}$$

$$\begin{aligned} h_{20} = (&-2.77049 + 1.20144i, -0.726017 \\ &- 1.92509i, 0.494102 - 1.6501i, -0.277134 \\ &- 0.749036i). \end{aligned} \tag{31d}$$

Then the following value is computed:

$$\begin{aligned} G_{21} &= -0.313594 - 2.65646i, \\ l_1 &= \frac{1}{2} R_e G_{21} = -0.1568. \end{aligned} \tag{32}$$

Therefore, the theorem is proved. Near the unstable equilibrium point E_0, we can find a stable periodic solution for $b < b_0$. □

3.2.2. Hopf Bifurcation at $E_{1,2}$

Theorem 4. *With system (2a), (2b), (2c), and (2d) and $a = 0.9$, $c = 1.5$, $d = 0.2$, $k = 0.05$, and $b = 0.2$, the first Lyapunov coefficient at $E_{1,2}$ for critical value $m = m_0 = 0.5139$ is given by*

$$l_1 = -0.3045 < 0. \tag{33}$$

Therefore, system (2a), (2b), (2c), and (2d) has a transversal Hopf point at $E_{1,2}$, and thus this point is stable. Furthermore, for each $m < m_0$, but close to m_0, a stable limit cycle exists near the unstable equilibrium point $E_{1,2}$.

Proof. Because of symmetry, E_1 will be considered. Since the parameters satisfy $(a, c, d, k, b) = (0.9, 1.5, 0.2, 0.05, 0.2)$ and $m = m_0 = 0.5139$, we have

$$\begin{aligned} \lambda_1 &= -0.8279, \\ \lambda_2 &= -0.3307, \\ \lambda_{3,4} &= \pm 1.4120i. \end{aligned} \tag{34}$$

Under this condition, it is easy to know the transverse condition $\lambda'(m = m_0) < 0$. Accordingly, Hopf bifurcation

appears. There exists a Hopf bifurcation at E_0. The value of the first Lyapunov coefficient l_1 can decide the stability of E_0. It demonstrates the stability of the periodic orbits and the equilibrium point. Making use of the notation obtained from the section above, the multilinear symmetric functions could be written as

$$B(x,y) = \left(x_1y_3 + x_3y_1, -2x_1y_1, 0, -dx_1y_2 - dx_2y_1\right), \tag{35a}$$

$$C(x,y,z) = (0,0,0,0). \tag{35b}$$

Then, the following results are obtained:

$$p = (0.741494, -0.0915377 + 0.445225i, 0.331105 - 0.22946i, -0.154015, -0.239956i) \tag{36a}$$

$$q = (0.6928 - 0.277114i, -0.208195 - 0.851544i, -0.192858 + 0.428759i, -0.201872 + 0.0937186i), \tag{36b}$$

$$h_{11} = (0.542254, -1.02525, -0.674678, -0.469763), \tag{36c}$$

$$h_{20} = (0.218437 + 0.0754352i, 0.304126 + 0.177492i, -0.0578508 + 0.0199395i, 0.075354 - 0.0580204i). \tag{36d}$$

Then the following values are computed:

$$G_{21} = -0.608777 + 1.36819i,$$
$$l_1 = \frac{1}{2}R_eG_{21} = -0.3045. \tag{37}$$

Therefore, the theorem is justified. We can find a stable periodic solution close to the unstable equilibrium point E_1 for $m < m_0$. □

4. Four-Dimensional Estimate of Ultimate Bound and Positively Invariant Set

Let $X = [x_1, x_2, x_3, x_4]^{\mathrm{T}}$. Define $X(t, t_0, X_0)$ as the solution to system as

$$\dot{X} = f(X, \mu), \quad X \in R^4, \tag{38}$$

and $X(t, t_0, X_0) = X_0$ at the initial time t_0 and initial state X_0, which is denoted as $X(t)$ for simplicity. $\Omega \in R^4$ is assumed as a compact set, and the distance between the solution $X(t)$ and the set Ω by $\rho(X(t), \Omega) = \inf_{Y\in\Omega}\|X(t) - y\|$ is defined and denoted as $\Omega_\varepsilon = \{X \mid \rho(X, \Omega) < \varepsilon\}$.

Definition 5 (see [26, 27]). Supposing a compact set $\Omega \in R^4$. If, for every $X_0 \in R^4/\Omega$, $\lim_{t\to\infty}\rho(X(t), \Omega) = 0$, that means, for any $\varepsilon > 0$, there is $T > t_0$, such that, for $t > T$, $X(t, t_0, X_0) \in \Omega_\varepsilon$, and then the set Ω is named an ultimate bound for system (36a), (36b), (36c), and (36d); if for any $X_0 \in \Omega$ and all $t \geq t_0$, $X(t, t_0, X_0) \subset \Omega$, then Ω is called the positively invariant set for system (38).

Since quadratic polynomial type Lyapunov functions are simple both in form and in application, we mainly probe into the bounds of chaotic systems by using conicoids. So we choose Lyapunov function as

$$p(X) = X^{\mathrm{T}}PX + \zeta X + a_0, \tag{39}$$

in which $P = (a_{ij})_{4\times4} \in R^{4\times4}$, $\zeta = (\zeta_1, \zeta_2, \zeta_3, \zeta_4) \in R^{4\times4}$, and $a_0 \in R$ are parameters to determine. Deriving $p(X)$ along system (38) and deleting the terms with three or higher degrees, we get

$$\dot{p} = X^{\mathrm{T}}QX + \eta X + b_0. \tag{40}$$

Here $Q = (b_{ij})_{4\times4} \in R^{4\times4}$, $\eta = (\eta_1, \eta_2, \eta_3, \eta_4) \in R^{4\times4}$, and $b_0 \in R$.

If P is positive definite and Q is negative definite, then $\dot{p} = 0$ must be a bounded sphere in R^4; and now that chaotic systems are bounded, $p(X)$ reaches the maximum or minimum values under the solution set of (18), whereas it is necessary that $\dot{p} = 0$. So, in order to assess the ultimate bounds of system equation (18), the following optimization problem should only be solved:

$$\begin{aligned} &\text{Maximum (or minimum)} \quad p(X) \\ &\qquad = X^{\mathrm{T}}PX + \zeta X + a_0 \\ &\qquad X^{\mathrm{T}}QX + \eta X + b_0 = 0. \end{aligned} \tag{41}$$

If the above discussed conditions are satisfied, then the above optimization problem has a solution supposing $p_{\min} \leq p(X) \leq p_{\max}$, and then set $\Omega = \{X \in R^4 \mid p_{\min} \leq p(X) \leq p_{\max}\}$ would be our desired ultimate bounds.

Making use of the above method, we talk about the ultimate bound and positively invariant set for system (2a), (2b), (2c), and (2d) with $d = 0$.

Theorem 6. *Denote* $\Omega = \{(x, y, z, u) \mid mx^2 + m(y-h)^2 + mz^2 + u^2 \leq R^2\}$, *where*

$$R^2 = \begin{cases} \dfrac{m}{4a(b-a)}, & b \geq 2a \\ \dfrac{m}{4k(b-k)}, & b \geq 2k \\ \dfrac{m}{4c(b-c)}, & b \geq 2c \\ \dfrac{m}{b^2}, & b < 2a,\ b < 2k,\ b < 2c. \end{cases} \tag{42}$$

If parameters of the system satisfy $m > 0$, $a > 0$, $b > 0$, $c > 0$, and $k > 0$, then system (38) would have an ultimate bound and positively invariant set: hyperellipsoid Ω.

Proof. First the following generalized positive definite and radially unbounded Lyapunov function are defined as

$$V(x, y, z, u) = mx^2 + my^2 + mz^2 + u^2, \tag{43}$$

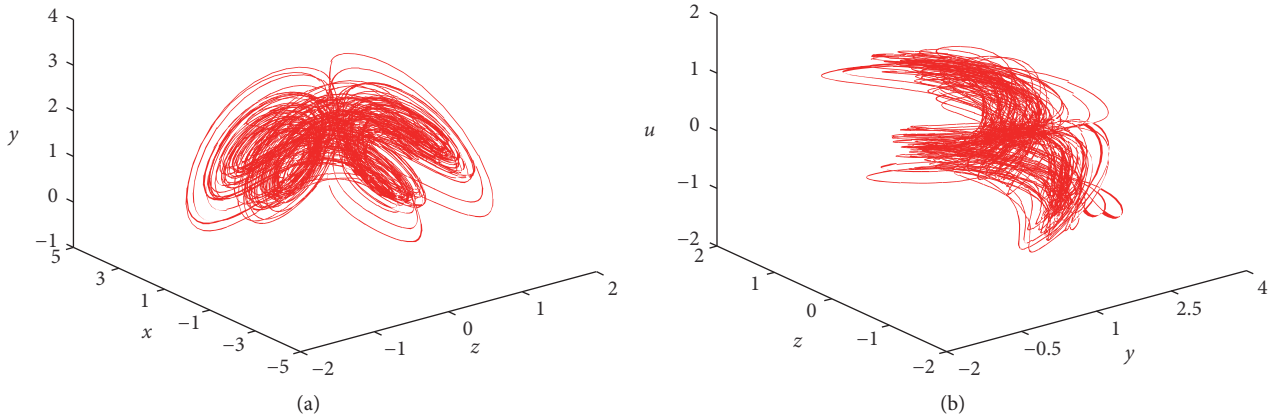

FIGURE 1: Hyperchaotic attractor for the four-dimensional financial system (2a), (2b), (2c), and (2d) with parameter values $a = 0.9$, $b = 0.2$, $c = 1.5$, $d = 0.2$, $k = 0.05$, and $m = 0.005$ and the initial condition $(0, 1, -0.5, 0)$. (a) The phase portrait in (x, y, z) space and $u = 0$; (b) the phase portrait in (y, z, u) space and $x = 0$.

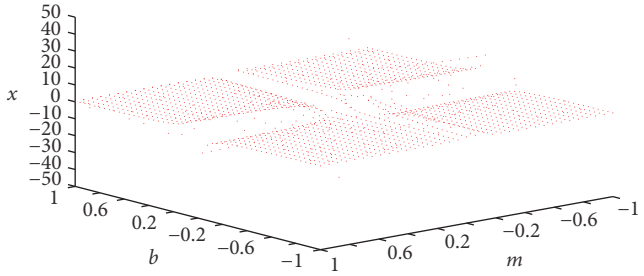

FIGURE 2: The bifurcation set of system (2a), (2b), (2c), and (2d) with parameter values $a = 0.9$, $c = 1.5$, $d = 0.2$, and $k = 0.05$, and $b \in [-1, 1]$ and $m \in [-1, 1]$.

where $m > 0$ and $h \in R$. Calculating the derivative of $V(x, y, z, u)$ along with a track of (2a), (2b), (2c), and (2d), we have

$$\frac{1}{2}\frac{V(x, y, z, u)}{dt} = -amx^2 - mb\left(y - \frac{1}{2b}\right)^2 - cmz - ku^2 + \frac{m}{4b}. \tag{44}$$

It is easy to see that, for $m > 0, a > 0, b > 0, c > 0$, and $k > 0$, $V(x, y, z, u)$ is positive definite and the quadratic principal part of $V(x, y, z, u)/dt$ is negative definite. $V(x, y, z, u) = 0$, which indicates the surface

$$\Gamma = \left\{(x, y, z, u) \mid amx^2 + mb\left(y - \frac{1}{2b}\right)^2 + cmz + ku^2 = \frac{m}{4b}\right\} \tag{45}$$

is an ellipsoid in the space of four dimensions for certain σ, k, b, d, and k. Outside of Γ, $V(x, y, z, u)/dt < 0$, and, inside of Γ, $V(x, y, z, u)/dt > 0$. Thus, system (2a), (2b), (2c), and (2d) would reach its ultimate bound on Γ.

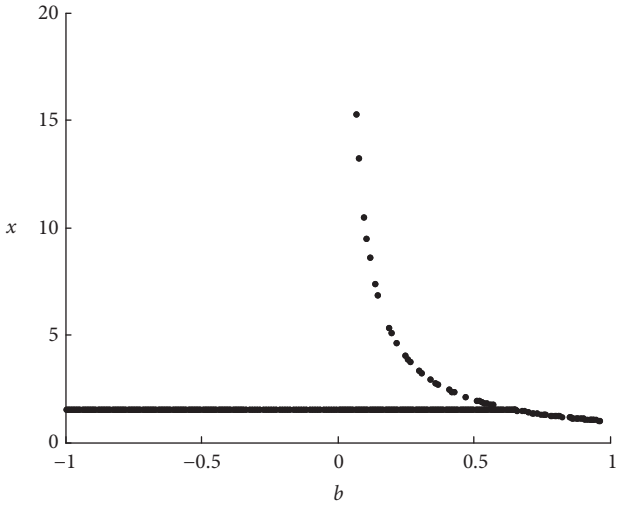

FIGURE 3: The bifurcation curve of system (2a), (2b), (2c), and (2d) with parameter values $a = 0.9$, $c = 1.5$, $d = 0.2$, $k = 0.05$, and $m = 0.005$, and the bifurcation point occurs when $b = 0.68$.

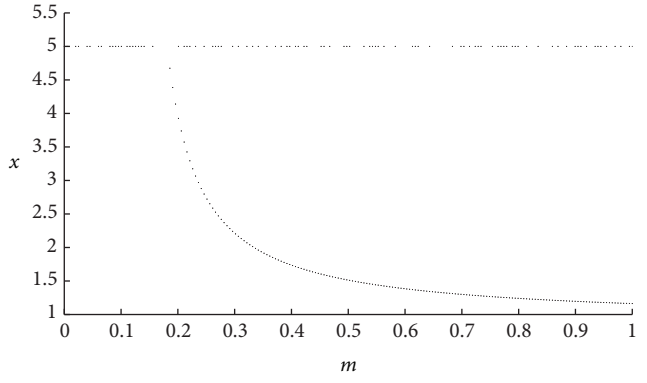

FIGURE 4: The bifurcation curves of system (2a), (2b), (2c), and (2d) with parameter values $a = 0.9$, $c = 1.5$, $d = 0.2$, $k = 0.05$, and $b = 0.2$, and the bifurcation point occurs when $m = 0.21$.

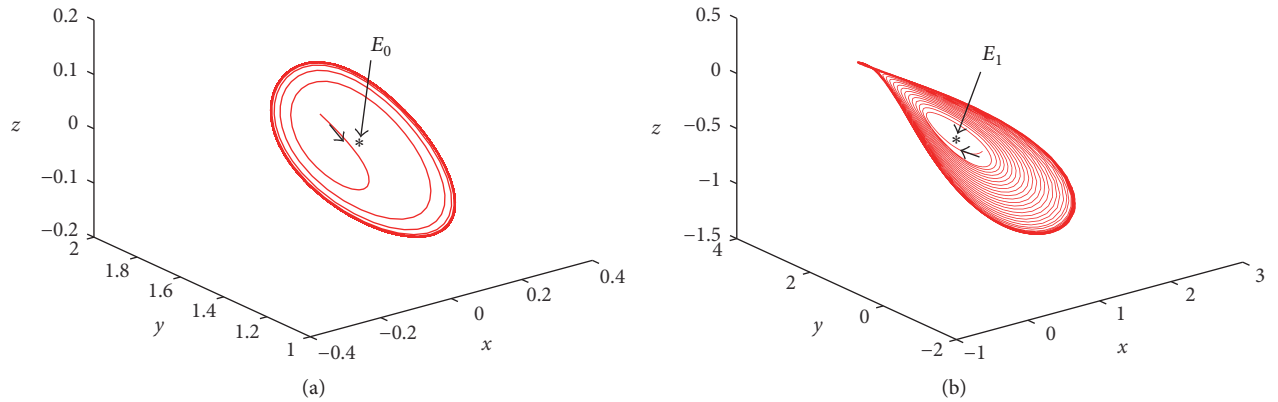

FIGURE 5: The stable periodic solution of system (2a), (2b), (2c), and (2d) with $(a, c, d, k) = (0.9, 1.5, 0.2, 0.05)$ and (a) $b = 0.68$; (b) $m = 0.49$.

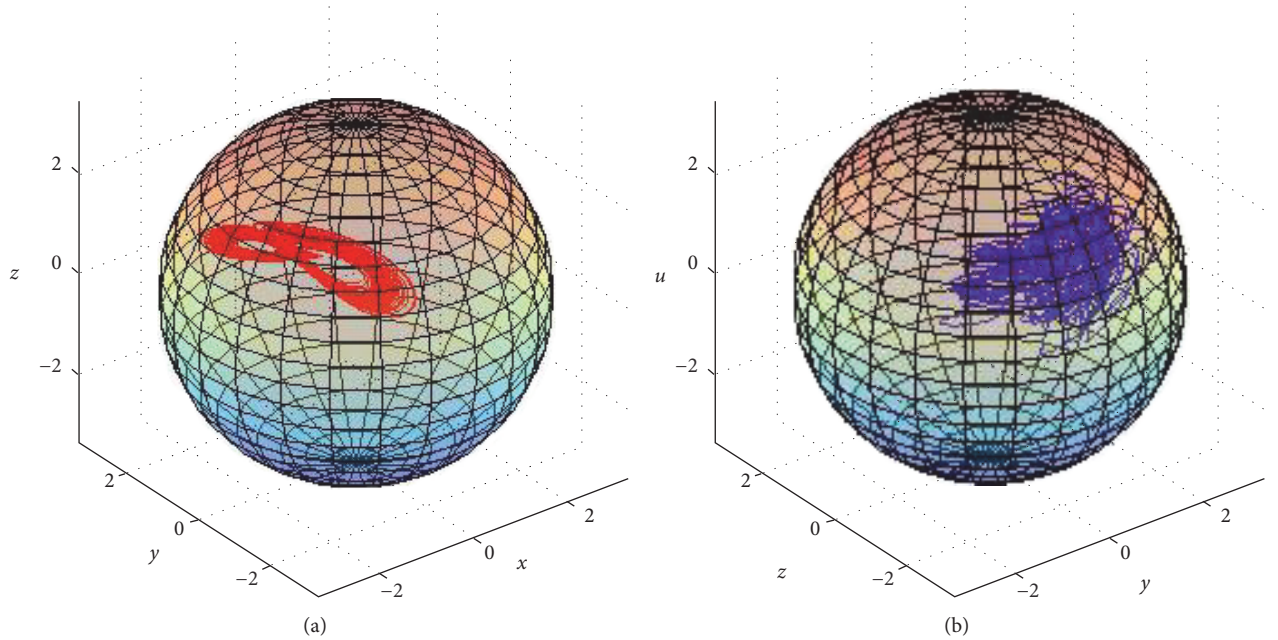

FIGURE 6: The projections of the bound estimated for system (2a), (2b), (2c), and (2d) with $a = 0.9$, $b = 0.3$, $c = 1.5$, $d = 0$, $k = 0.05$, and $m = 0.005$, (a) the phase portrait in (x, y, z) space and $u = 0$, and (b) the phase portrait in (y, z, u) space and $x = 0$.

Next we can obtain the maximum of V on Γ by expressions (2a), (2b), (2c), and (2d) according to employing the Lagrange multiplier method. Define

$$F = mx^2 + m(y-h)^2 + mz^2 + u^2 + \tau\left[amx^2 + mb\left(y - \frac{1}{2b}\right)^2 + cmz + ku^2 - \frac{m}{4b}\right], \tag{46}$$

$$\frac{1}{2}F'_x = m(1 + a\tau)x = 0, \tag{47a}$$

$$\frac{1}{2}F'_y = m\left[y + \tau\left(by - \frac{1}{2}\right)\right] = 0, \tag{47b}$$

$$\frac{1}{2}F'_z = m(1 + c\tau)z = 0, \tag{47c}$$

$$\frac{1}{2}F'_u = (1 + k\tau)u = 0, \tag{47d}$$

$$\frac{1}{2}F'_\tau = amx^2 + mb\left(y - \frac{1}{2b}\right)^2 + cmz + ku^2 - \frac{m}{4b} = 0. \tag{47e}$$

□

(1) If $\tau \neq -1/a$, $\tau \neq -1/c$, and $\tau \neq -1/k$, we have $(x, y, z, u) = (0, 0, 0, 0)$ or $(0, 1/b, 0, 0)$ and

$$V(x, y, z, u)_{\max} = \frac{m}{b^2}. \tag{48a}$$

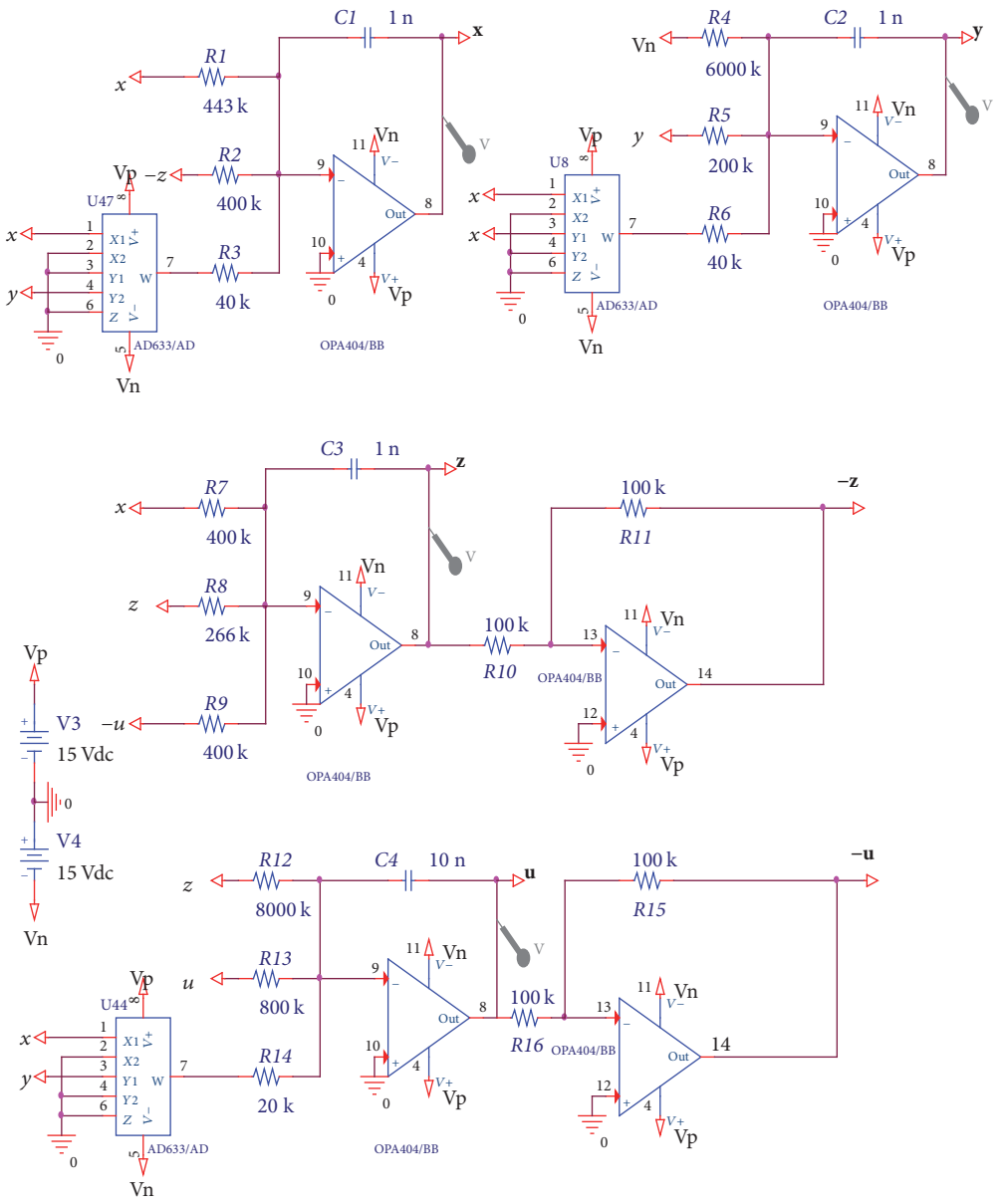

Figure 7: The electronic circuit schematic of the 4D financial system (2a), (2b), (2c), and (2d).

(2) If $\tau = -1/a$, $\tau = -1/c$, $\tau \neq -1/k$, and $b \geq 2a$, we have $(x, y, z, u) = (\pm(1/2)\sqrt{(b-2a)/a(a-b)^2}, 1/2(b-a), 0, 0)$ and

$$V(x, y, z, u)_{\max} = \frac{m}{4a(b-a)}. \tag{48b}$$

(3) If $\tau = -1/c$, $\tau = -1/a$, $\tau \neq -1/k$, and $b \geq 2c$, we have $(x, y, z, u) = (0, 1/2(b-c), \pm 1/2(c-b)\sqrt{(b-2c)/c}, 0)$ and

$$V(x, y, z, u)_{\max} = \frac{m}{4a(b-a)}. \tag{48c}$$

(4) If $\tau = -1/k$, $\tau \neq -1/a$, $\tau \neq -1/c$, and $b \geq 2a$, we have $(x, y, z, u) = (0, 1/2(b-k), 0, \pm 1/2(k-b)\sqrt{m(b-2k)/k})$ and

$$V(x, y, z, u)_{\max} = \frac{m}{4k(b-k)}. \tag{48d}$$

(5) If $\tau = -1/a$, $a = k$, $k \neq c$, and $b \geq 2a$, we have $(y, u) = (1/2(b-a), 0)$, $x^2 + z^2 = (b-2a)/4a(a-b)^2$, and

$$V(x, y, z, u)_{\max} = \frac{m}{4a(b-a)}. \tag{48e}$$

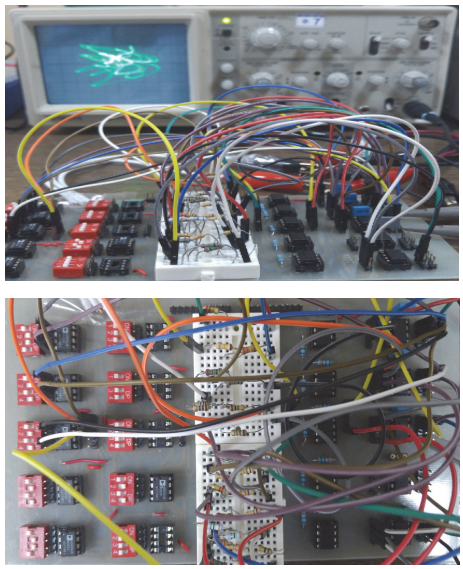

Figure 8: The experimental circuit of the hyperchaotic circuit.

(6) If $\tau = -1/a$, $a = c$, $k \neq c$, and $b \geq 2a$, we have $(y, u) = (1/2(b-a), 0)$, $mx^2 + u^2 = m(b-2a)/4a(a-b)^2$, and

$$V(x, y, z, u)_{\max} = \frac{m}{4a(b-a)}. \tag{48f}$$

(7) If $\tau = -1/k$, $a = k = q$, $k \neq a$, and $b \geq 2k$, we have $y = 1/2(b-k)$, $x^2 + z^2 = (b-2a)/4a(a-b)^2$, and

$$V(x, y, z, u)_{\max} = \frac{m}{4k(b-k)}. \tag{48g}$$

(8) If $\tau = -1/k$, $a = c$, $k \neq c$, and $b \geq 2a$, we have $(y, u) = (1/2(b-a), 0)$, $u^2 + mx^2 + mz^2 = m(b-2k)/4k(b-k)^2$, and

$$V(x, y, z, u)_{\max} = \frac{m}{4k(b-k)}. \tag{48h}$$

Figure 6 performs the corresponding ultimate bound and positively invariant set Ω with $u = 0$ or $x = 0$ ($a = 0.9, b = 0.2$, $c = 1.5$, $d = 0$, $k = 0.05$, and $m = 0.005$). We see that the estimated bounds in Theorem 6 are feasible.

5. Numerical Simulation

In the previous twenty years, different tools were developed to tap the periodic responses of nonlinear dynamical systems. The periodic responses can be spotted by several traditional criteria such as bifurcation diagrams and phase portraits. In this section, we use these techniques to illustrate the existence of the periodic motions for the financial system. Based on the four-dimensional nonlinear financial system (2a), (2b), (2c), and (2d), numerical simulations have been conducted in this paper. Using MATLAB software, a numerical approach is utilized to show the nonlinear dynamic behavior in the financial system.

The red in Figure 1 shows the hyperchaotic attractors for the four-dimensional financial system (2a), (2b), (2c), and (2d) with parameter values $a = 0.9$, $b = 0.2$, $c = 1.5$, $d = 0.2$, $k = 0.05$, and $m = 0.005$ and the initial condition $(0, 1, -0.5, 0)$. Figure 1(a) is the phase portrait in (x, y, z) space and $u = 0$, and Figure 1(b) is the phase portrait in (y, z, u) space and $x = 0$. It shows that the corresponding Lyapunov exponents are $L_1 = 0.03003$, $L_2 = 0.01448$, $L_3 = -0.0003$, and $L_4 = -1.2318$, and the system has complex dynamics. Figure 2 implies the bifurcation set of system (2a), (2b), (2c), and (2d) when the values of parameters are set as $a = 0.9$, $c = 1.5$, $d = 0.2$, $k = 0.05$, $b \in [-1, 1]$, and $m \in [-1, 1]$, and the bifurcation set divides the space into three regions with three solutions above the bifurcation set, one solution in the bifurcation set, and none under the set, which is consistent with the theoretical results. Figure 3 illustrates the bifurcation curve when $a = 0.9, c = 1.5, d = 0.2, k = 0.05$, and $m = 0.005$, and the point of Hopf bifurcation is $b = 0.68$.

The bifurcation curve in Figure 4 shows the bifurcation with $a = 0.9$, $c = 1.5$, $d = 0.2$, $k = 0.05$, $b = 0.2$, and altering system parameter m, and the point of Hopf bifurcation is $m = 0.49$. Figure 5(a) shows that there is a stable periodic solution near the unstable equilibrium point E_0 for $(a, c, d, k) = (0.9, 1.5, 0.2, 0.05)$ and $b = 0.68$. There is a stable periodic solution near the unstable equilibrium point E_1 for $m = 0.21$ shown in Figure 5(b). Figure 6 shows the corresponding ultimate bound and positively invariant set Ω with $u = 0$ or $x = 0$ ($a = 0.9, b = 0.3, c = 1.5, d = 0, k = 0.05$, and $m = 0.005$). Figure 6(a) is the phase portrait in (x, y, z) space and $u = 0$. Figure 6(b) is the phase portrait in (y, z, u) space and $x = 0$. The trajectories of system (2a), (2b), (2c), and (2d) are all in the domain of the estimated bound.

6. Physical Realization for the 4D Financial System (2a), (2b), (2c), and (2d)

In this section, the 4D hyperchaotic financial system will be applied for its application using the electronic circuit which has been designed on the oscilloscope. The hyperchaotic system is studied by using an electronic circuit design. The numerical simulation and the oscilloscope outputs were obtained for the similar shaped phase portraits [28–30].

The electronic circuit of the 4D financial system was designed in OrCAD-PSpice. Figure 7 shows the electronic circuit schematic of the system. Experimental electronic circuit of the 4D financial system was implemented for parameters $a = 0.9$, $c = 1.5$, $d = 0.2$, $k = 0.05$, and $m = 0.005$ and initial conditions $(0, 1, -0.5, 0)$. $R1$= 443 Kohm, $R2 = R7 = R9 = 400$ Kohm, $R3 = R6 = 40$ Kohm, $R4 = 6000$ Kohm, $R5 = 200$ Kohm, $R8 = 266$ Kohm, $R10 = R11 = R15 = R16 = 100$ Kohm, $R12 = 8000$ Kohm, $R13 = 800$ Kohm, $R14 = 20$ Kohm, $C1 = C2 = C3 = 1$ nF, $C4 = 10$ nF, $Vn = -15$ V, and $Vp = 15$ V were chosen. Real-time application of the 4D financial system was realized with electronic components on electronic card in Figure 8. The OrCAD-PSpice simulation outputs and oscilloscope outputs of 4D financial system, for parameters $a = 0.9$, $c = 1.5$, $d = 0.2$, $k = 0.05$, and $m = 0.005$, are seen in Figures 9 and 10.

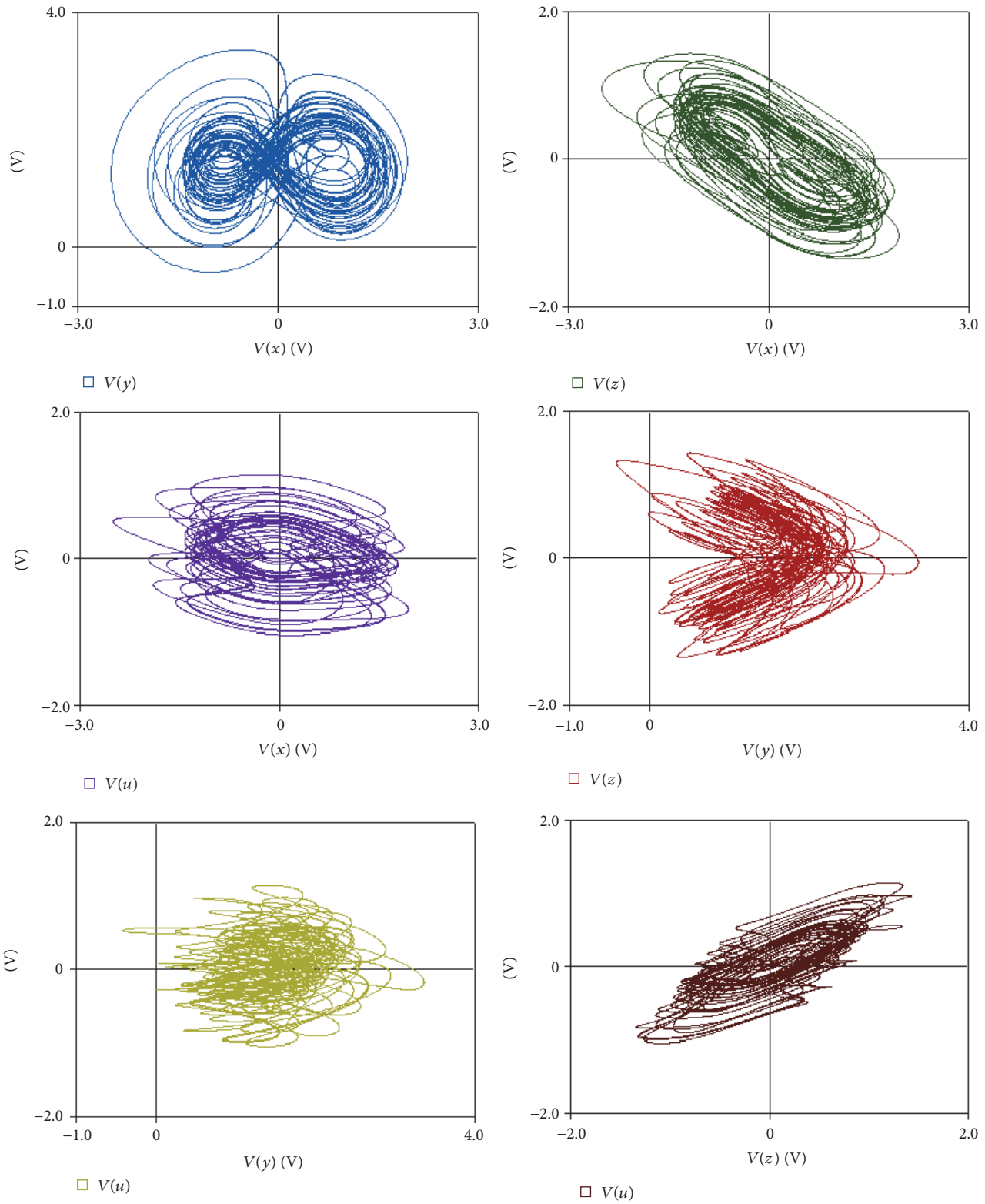

FIGURE 9: The phase portraits of 4D financial system (2a), (2b), (2c), and (2d) with $a = 0.9$, $b = 0.2$, $c = 1.5$, $d = 0.2$, $k = 0.05$, and $m = 0.005$ in ORCAD-PSpice.

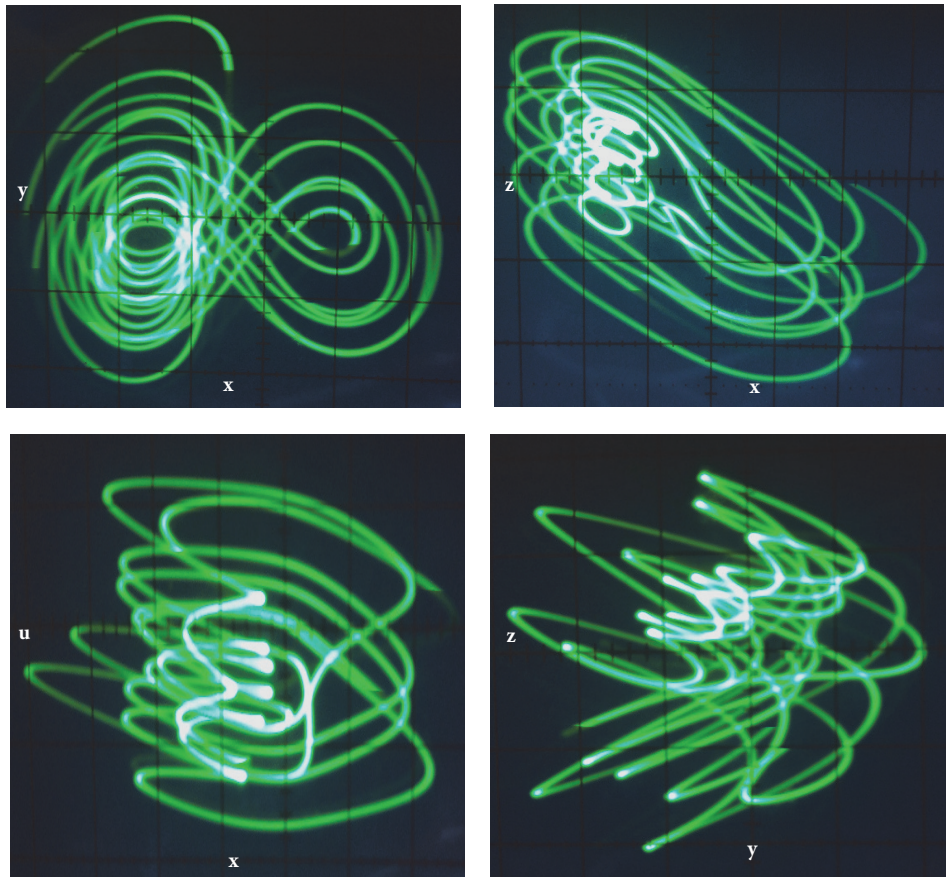

Figure 10: The phase portraits of 4D financial system (2a), (2b), (2c), and (2d) with $a = 0.9$, $b = 0.2$, $c = 1.5$, $d = 0.2$, $k = 0.05$, and $m = 0.005$ on the oscilloscope.

7. Conclusion

In our paper, the proposed financial system, which is generated from three-dimensional classical financial system, greatly expands the list of hyperchaotic financial attractors. The sufficient conditions for nonexistence of chaotic and hyperchaotic behaviors are derived theoretically, and the solutions of equilibria are obtained. For each equilibrium, its stability and existence of Hopf bifurcation are validated. Besides, based on its corresponding first Lyapunov coefficient, the analytic proof of the existence of periodic solutions is exhibited. Then the research has got the ultimate bound and positively invariant set for the proposed hyperchaotic financial system. The direction and stability of the bifurcating periodic solutions can be determined, and some numerical solutions are obtained to verify the theoretical results. In addition, the hyperchaotic financial system is extended to an electronic circuit implementation for real-time application.

We can understand the functions of financial policies and reveal the true geometrical structure of the attractors by the results of this paper. Since the global dynamics and geometrical structure of this system are not presented completely, more detailed theoretical simulation and investigations are expected in the forthcoming study.

Conflicts of Interest

The authors declare that they have no conflicts of interest.

Acknowledgments

The authors gratefully acknowledge the support of National Natural Science Foundation of China (NNSFC) through Grant nos. 11290152, 11427801, and 11401543, the Funding Project for Academic Human Resources Development in Institutions of Higher Learning under the Jurisdiction of Beijing Municipality (PHRIHLB), Beijing Postdoctoral Research Foundation (no. 2015ZZ17), the China Postdoctoral Science Foundation funded project (no. 2014M560028 and no. 2015T80029), the Government of Chaoyang District Postdoctoral Research Foundation (no. 2015ZZ-7), and Sakarya University Scientific Research Projects Unit under Grants 2016-09-00-008 and 2016-50-01-026.

References

[1] J. Alvarez-Ramirez and C. Ibarra-Valdez, "Modeling stock market dynamics based on conservation principles," *Physica A: Statistical Mechanics and Its Applications*, vol. 301, no. 1–4, pp. 493–511, 2001.

[2] Q. Gao and J. Ma, "Chaos and Hopf bifurcation of a finance system," *Nonlinear Dynamics*, vol. 58, no. 1-2, pp. 209–216, 2009.

[3] J. H. Ma and Y. S. Chen, "Study for the bifurcation topological structure and the global complicated character of a kind of nonlinear finance system. I," *Applied Mathematics and Mechanics*, vol. 22, no. 11, pp. 1240–1251, 2001.

[4] J. H. Ma, Y. Q. Cui, and L. X. Liu, "Hopf bifurcation and chaos of financial system on condition of specific combination of parameters," *Journal of Systems Science and Complexity*, vol. 21, no. 2, pp. 250–259, 2008.

[5] C. Ma and X. Wang, "Hopf bifurcation and topological horseshoe of a novel finance chaotic system," *Communications in Nonlinear Science and Numerical Simulation*, vol. 17, no. 2, pp. 721–730, 2012.

[6] X.-D. Zhang, X.-D. Liu, Y. Zheng, and C. Liu, "Chaotic dynamic behavior analysis and control for a financial risk system," *Chinese Physics B*, vol. 22, no. 3, Article ID 030509, 2013.

[7] J. A. Holyst and K. Urbanowicz, "Chaos control in economical model by time-delayed feedback method," *Physica A: Statistical Mechanics and its Applications*, vol. 287, no. 3-4, pp. 587–598, 2000.

[8] K. Pyragas, "Continuous control of chaos by self-controlling feedback," *Physics Letters A*, vol. 170, no. 6, pp. 421–428, 1992.

[9] W.-C. Chen, "Dynamics and control of a financial system with time-delayed feedbacks," *Chaos, Solitons and Fractals*, vol. 37, no. 4, pp. 1198–1207, 2008.

[10] Y. Ding and J. Cao, "Bifurcation analysis and chaos switchover phenomenon in a nonlinear financial system with delay feedback," *International Journal of Bifurcation and Chaos*, vol. 25, no. 12, pp. 155–165, 2015.

[11] J. Yang, E. Zhang, and M. Liu, "Bifurcation analysis and chaos control in a modified finance system with delayed feedback," *International Journal of Bifurcation and Chaos*, vol. 26, no. 6, Article ID 1650105, 2016.

[12] J. Yoshida, "Improved criteria for hyperbolic-elliptic motion in the general three-body problem," *Publications of the Astronomical Society of Japan*, vol. 24, pp. 391–408, 1972.

[13] G. Seifert, "Positively invariant closed sets for systems of delay differential equations," *Journal of Differential Equations*, vol. 22, no. 2, pp. 292–304, 1976.

[14] B. Kalitine, "The stability of compact positively invariant sets of dynamic systems," *RAIRO Automatique*, vol. 16, no. 3, pp. 275–286, 1982.

[15] J. Fu, L. Wang, and M. Chen, "Invariant set based sliding mode control for near-space vehicles with attitude constraints," *Proceedings of the Institution of Mechanical Engineers Part G: Journal of Aerospace Engineering*, vol. 230, no. 5, pp. 793–804, 2015.

[16] A. Weiss, C. Petersen, M. Baldwin, R. S. Erwin, and I. Kolmanovsky, "Safe positively invariant sets for spacecraft obstacle avoidance," *Journal of Guidance, Control, and Dynamics*, vol. 38, no. 4, pp. 720–732, 2015.

[17] S. V. Rakovic and R. H. Gielen, "Positively invariant families of sets for interconnected and time-delay discrete-time systems," *SIAM Journal on Control and Optimization*, vol. 52, no. 4, pp. 2261–2283, 2014.

[18] A. Algaba, F. F. Sanchez, M. Merino, and A. J. Rodriguez-Luis, "Comment on 'estimating the ultimate bound and positively invariant set for a synchronous motor and its application in chaos synchronization'," *Chaos Solitons and Fractals*, vol. 44, pp. 137–144, 2011.

[19] F. Zhang, Y. Shu, H. Yang, and X. Li, "Estimating the ultimate bound and positively invariant set for a synchronous motor and its application in chaos synchronization," *Chaos, Solitons and Fractals*, vol. 44, no. 1–3, pp. 137–144, 2011.

[20] J. Wang, Q. Zhang, Z. Chen, and H. Li, "Local bifurcation analysis and ultimate bound of a novel 4D hyper-chaotic system," *Nonlinear Dynamics*, vol. 78, no. 4, pp. 2517–2531, 2014.

[21] Z. Wei and W. Zhang, "Hidden hyperchaotic attractors in a modified Lorenz-Stenflo system with only one stable equilibrium," *International Journal of Bifurcation and Chaos in Applied Sciences and Engineering*, vol. 24, no. 10, Article ID 1450127, 14 pages, 2014.

[22] C. Du, Y. Liu, and W. Huang, "A class of three-dimensional quadratic systems with ten limit cycles," *International Journal of Bifurcation and Chaos*, vol. 26, no. 9, Article ID 1650149, 2016.

[23] M. Prakash and P. Balasubramaniam, "Stability and Hopf bifurcation analysis of novel hyperchaotic system with delayed feedback control," *Complexity*, vol. 21, no. 6, pp. 180–193, 2016.

[24] H. Yu, G. Cai, and Y. Li, "Dynamic analysis and control of a new hyperchaotic finance system," *Nonlinear Dynamics*, vol. 67, no. 3, pp. 2171–2182, 2012.

[25] J. Sotomayor, L. F. Mello, and D. C. Braga, "Bifurcation analysis of the Watt governor system," *Computational & Applied Mathematics*, vol. 26, no. 1, pp. 19–44, 2007.

[26] D. Li, X. Wu, and J.-A. Lu, "Estimating the ultimate bound and positively invariant set for the hyperchaotic Lorenz-Haken system," *Chaos, Solitons & Fractals*, vol. 39, no. 3, pp. 1290–1296, 2009.

[27] Z. Wei, P. Yu, W. Zhang, and M. Yao, "Study of hidden attractors, multiple limit cycles from Hopf bifurcation and boundedness of motion in the generalized hyperchaotic Rabinovich system," *Nonlinear Dynamics*, vol. 82, no. 1-2, pp. 131–141, 2015.

[28] A. Akgul, I. Moroz, I. Pehlivan, and S. Vaidyanathan, "A new four-scroll chaotic attractor and its engineering applications," *Optik*, vol. 127, no. 13, pp. 5491–5499, 2016.

[29] A. Akgul, H. Calgan, I. Koyuncu, I. Pehlivan, and A. Istanbullu, "Chaos-based engineering applications with a 3D chaotic system without equilibrium points," *Nonlinear Dynamics*, vol. 84, no. 2, pp. 481–495, 2016.

[30] A. Akgul and I. Pehlivan, "A new three-dimensional chaotic system without equilibrium points, its dynamical analyses and electronic circuit application," *Tehnicki Vjesnik*, vol. 23, no. 1, pp. 209–214, 2016.

Hindawi
Mathematical Problems in Engineering
Volume 2017, Article ID 5292494, 9 pages
https://doi.org/10.1155/2017/5292494

Research Article

Complexity Analysis of a Triopoly Cooperation-Competition Game Model in Convergence Product Market

Liming Zhao, Xiaofeng Liu, and Ning Ji

College of Management and Economics, Tianjin University, Tianjin 300072, China

Correspondence should be addressed to Ning Ji; ningji@tju.edu.cn

Received 30 September 2016; Accepted 19 December 2016; Published 15 January 2017

Academic Editor: Eric Campos-Canton

This work considered a tripartite cooperation-competition game model for the convergence product market, whose products are compounds of two base products or services. An early convergence product firm monopoly in this market and two potential entrants from the base products decide to cooperate with another to compete with the monopolist. We analyzed factors that affect existence and local stability of the Nash equilibrium. Rich nonlinear dynamic behaviors like bifurcation, chaos, and attractors are presented to explain the complex relationships between the three players. Results showed that the pulling effect on profit for the united R&D activity can significantly enlarge the stable region. Too frequently adjusted price strategy will bring the system into chaos. A parameter feedback control method is given to control the chaotic system and we numerically verified its effectiveness. This study has significant values to understand the fluctuations in related convergence product market.

1. Introduction

Convergence is a dominant paradigm in the contemporary industry innovation, which allows the introduction of seemingly disparate attributes or functionalities products into other existing industrial categorized products. As in China, the flourishing "Internet Plus" strategy, which means the conventional industries adopt the application of the Internet and other information technologies to reform the existing mode of products, is regarded as an important way to produce its new economic form and promote emerging industry [1].

For abbreviations, the base products are called BPs and the newly formed convergence products are called CPs. In a newly built CPs market, relying on its information, differentiation characteristics, and prior advantages over the competitors, an early entry firm is easy to monopoly the whole market [2]. With the fast growing CPs industry, owing to the similar product type and alternative functionalities, firms in BPs industry are the most probable potential entrants to compete with the monopolist, separately [3], while, in the context of CPs, because of the product segment in CPs industry which brings entry barrier for potential entrants, firms in BPs tend to complement and upgrade its product line to take a share in the rising CPs [4, 5]. The competitive structure and cooperative trend in CPs market will be changed.

Many researchers have contributed incremental values to extend the classical Cournot game and Bertrand game into different forms with practical variations in real economy [6, 7]. In [8], researchers built a duopoly game model for two zonal electricity firms which is an administrative monopolist granted by the bureaucracy in separate market and investigated its complex dynamics. Chen et al. [9] proposed a dynamic triopoly game model in Chinese 3G telecommunication market, which is a typical natural monopolized market. For the published literature, researchers interest on monopoly game has transformed from duopoly game [7, 10, 11] to triopoly game [8, 12, 13]. And the basic assumption has been modified from complete rational to bounded rational [13, 14]. In [15], the existence of chaotic dynamics for a triopoly game model with different decisional mechanism was rigorously proved by the "Stretching along the Paths (SAP)" method. However, for the third types of monopoly, the economic monopoly, which means firms acquire the monopoly status relying on powerful economic strength,

enormous paten ownership, and successful marketing strategy, is always regarded as the product of free completion and progress in science and technology. Under the background of economic globalization, the economic monopoly seems more acceptable by enhancing the competitiveness of a country, but it is also unsupported by government if it has touched fairness of the market. For instance, the US government has repeatedly inquired Microsoft on its monopoly and tying conduct [16].

In the process of industry convergence, the compounding characteristics of CPs and strong user stickiness can considerably cause monopoly in this market. On the one hand, convergence has accelerated the pace of breaking up boundaries and disintegrating of monopolists in existing industry [17]. On the other hand, by adding new functionalities to existing product to realize complementary goals, firms in CPs market achieved powerful marketing and sales benefits. For example, iPhones have helped Apple Inc. in monopolizing most of the profits in high-end smart phone industry, which is a revolutionary convergence in telecommunication and other Internet services [18]. Because of the natural strengths in transforming single products by introducing the complementary attributes and lack of experiences in the opposite field, firms in BPs will be guided to cooperate with its complementary firms to exploit in CPs. Thus, if the two united firms successfully fulfill their product transformation, the complex cooperation and competition behaviors among the three firms can form a triopoly cooperation-competition game in CPs market.

In this paper, we develop the complexity of convergence theory to build a three-dimensional discrete cooperation-competition game model in CPs market. A price adjustment dynamic strategy is used to investigate the complex dynamic features of this model and the stability of the Nash equilibrium. Our result aims to show the influence of the cooperation-competition behaviors on CPs market and find out proper strategies to control chaos when this system enters into chaos state.

The rest of this paper is organized as follows: In Section 2, we describe the triopoly cooperation-competition game model with bounded rationality. In Section 3, we discuss the existence and local stability of the Nash equilibrium. In Section 4, the numerical simulations of the dynamical behaviors for this model are investigated. Finally, conclusions are given in Section 5.

2. The Triopoly Cooperation-Competition Game Model

We consider two potential entrants from the basic markets (denoted by firm 1 and firm 2), who consist of the two aspects of the compounding attributes for CPs, and an early entry firm in CPs market (denoted by firm 3). Having seeing the fast rising of excess profits in CPs market and similar product structure, the two firms from BPs decided to cooperate with each other to research and develop new CPs in continuous periods by adding the complementary functionality into its existing products. The expenditure of research and development (R&D) will prorate between the two united firms and the proportion depends on the preexisting R&D ability and the effort level in the cooperation process. For firm 3, on the one hand, the excellent characteristics of CPs and the accumulative experience in CPs market provide it with a huge amount of demand and a relatively low cost. On the other hand, the newly launched products from the two cooperative firms bring a rise in publicity and an overall sales improvement for CPs. For the sake of risk aversion in R&D, firm 3 decides to hold its product line unchanged and expects to get a free ride of rise in demand. Thus, the new products of firms 1 and firm 2 will gradually form a substitution for products of firm 3 in CPs.

Let $q_i(t)$ denote the output of products by firm i at period t and $p_i(t)$ denote the corresponding prices ($i = 1, 2, 3$). Since the product of each firm has complementary attributes in CPs market, according to [10], the demand function of the three firms can be given as

$$\begin{aligned} q_1(t) &= a_1 - b_1 p_1(t) + c_1 p_2(t) + d_1 p_3(t), \\ q_2(t) &= a_2 - b_2 p_2(t) + c_2 p_1(t) + d_2 p_3(t), \\ q_3(t) &= a_3 - b_3 p_3(t) + c_3 p_1(t) + d_3 p_2(t), \end{aligned} \tag{1}$$

where a_i is the maximum demand in the market, b_i is the price elasticity of demand $q_i(t)$ regarding on product i, and c_i and d_i are the cross-price elasticity of demand $q_i(t)$ regarding on the complementary product j and product k ($j, k = 1, 2, 3$, $j, k \neq i$, and $j \neq k$). All the parameters above are positive and satisfy the restrict conditions of $0 < b_i, c_i, d_i \leq 1$, $b_i > c_i$, and $b_i > d_i$; that is, the ownership price effect is greater than the complementary cross-price effect.

The innovative activities to develop new CPs will raise the cost of firm 1 and firm 2. We suppose that the R&D cost for the cooperative union is a linear function of the production. It can be given as

$$E = (e - r)(q_1 + q_2), \tag{2}$$

where $e - r$ represents the marginal cost of R&D, e represents the present marginal R&D cost, and r represents the effort level in collaborative R&D activity. The R&D cost is proportional to the total output. It means that the innovation activity becomes more difficult in a larger scale of production. Considering the intrinsic fixed cost and variable cost of firm 1 and firm 2, the total cost function can be written as

$$\begin{aligned} C_1 &= f_1 + g_1 q_1 + \theta E = f_1 + g_1 q_1 + \theta (e - r)(q_1 + q_2), \\ C_2 &= f_2 + g_2 q_2 + (1 - \theta) E \\ &= f_2 + g_2 q_2 + (1 - \theta)(e - r)(q_1 + q_2), \end{aligned} \tag{3}$$

where f_1 and f_2 are the fixed costs, g_1 and g_2 are coefficients of the variable costs, and θ and $1 - \theta$ denote the proportion of the R&D cost between the union.

With the above assumption, the cost function of firm 3 is given by

$$C_3 = f_3 + g_3 q_3, \tag{4}$$

where $f_3 < f_1$ and $f_3 < f_2$, which denote the cost advantage for the early entry firm.

Let λ denote the pulling effect on profit for the united R&D activity of firm 1 and firm 2. I_i is the indicator function that takes value 1 for $i = 1, 2$ and takes value 0 for $i = 3$. Then we can get the profit function of firm i at period t:

$$\pi_i(t) = p_i(t)\left(1 + \lambda I_i\right) q_i - C_i, \quad i = 1, 2, 3. \tag{5}$$

We assume that this is an incomplete information market. All of the three firms choose the bounded rational adjustment strategy based on the marginal profit in the next period:

$$\begin{aligned} p_1(t+1) &= p_1(t) + \alpha p_1(t) \frac{\partial \pi_1(t)}{\partial p_1(t)}, \\ p_2(t+1) &= p_2(t) + \beta p_2(t) \frac{\partial \pi_2(t)}{\partial p_2(t)}, \\ p_3(t+1) &= p_3(t) + \gamma p_3(t) \frac{\partial \pi_3(t)}{\partial p_3(t)}, \end{aligned} \tag{6}$$

where $\alpha > 0$, $\beta > 0$, and $\gamma > 0$ are the adjustment speed for the three firms, respectively. By substituting (5) into (6), we obtain the dynamic model of a triopoly cooperation-competition game model in the convergence product market:

$$\begin{aligned} p_1(t+1) &= p_1(t) + \alpha p_1(t) \\ &\quad \times \left[(1+\lambda)\left(a_1 - b_1 p_1(t) + c_1 p_2(t) + d_1 p_3(t)\right)\right. \\ &\quad \left. - b_1(1+\lambda) p_1(t) - (e-r)\left(c_2 - b_1\right)\theta + b_1 g_1\right], \\ p_2(t+1) &= p_2(t) + \beta p_2(t) \\ &\quad \times \left[(1+\lambda)\left(a_2 - b_2 p_2(t) + c_2 p_1(t) + d_2 p_3(t)\right)\right. \\ &\quad \left. - b_2(1+\lambda) p_2(t) - (e-r)\left(c_1 - b_2\right)(1-\theta) + b_2 g_2\right], \\ p_3(t+1) &= p_3(t) + \gamma p_3(t)\left[a_3 + b_3 g_3 + c_3 p_1 + d_3 p_2\right. \\ &\quad \left. - 2b_3 p_3\right]. \end{aligned} \tag{7}$$

3. The Complex Dynamic Behaviors

3.1. The Nash Equilibrium and Stability Analysis. In system (7), we can get that this discrete system has eight equilibrium points with forms of $(0,0,0)$, $(p_1^1, 0, 0)$, $(0, p_2^1, 0)$, $(0, 0, p_3^1)$, $(0, p_2^2, p_3^2)$, $(p_1^2, 0, p_3^2)$, $(p_1^2, p_2^2, 0)$, and (p_1^*, p_2^*, p_3^*). The three firms in the game will not supply any production to the market at price 0.

Hence, the nontrivial equilibrium point (p_1^*, p_2^*, p_3^*) is the only Nash equilibrium with positive component values. It can be found that values of the nontrivial equilibrium point are parameter dependent in system (7) except for α, β, and γ. For denotations, we numerically give out values in Section 3.2.

In order to study the stability of the system at (p_1^*, p_2^*, p_3^*), the Jacobian matrix of (7) can be given as

$$J\left(p_1^*, p_2^*, p_3^*\right) = \begin{bmatrix} j_{11} & j_{12} & j_{13} \\ j_{21} & j_{22} & j_{23} \\ j_{31} & j_{32} & j_{33} \end{bmatrix}, \tag{8}$$

where

$$\begin{aligned} \Delta_1 &= \alpha\left[(1+\lambda)\left(a_1 - b_1 p_1^* + c_1 p_2^* + d_1 p_3^*\right)\right. \\ &\quad \left. - b_1(1+\lambda) p_1^* - (e-r)\left(c_2 - b_1\right)\theta + b_1 g_1\right] \\ &\quad - 2\alpha b_1(1+\lambda) p_1^*, \\ \Delta_2 &= \beta\left[(1+\lambda)\left(a_2 - b_2 p_2^* + c_2 p_1^* + d_2 p_3^*\right)\right. \\ &\quad \left. - b_2(1+\lambda) p_2^* - (e-r)\left(c_1 - b_2\right)(1-\theta) + b_2 g_2\right] \\ &\quad - 2\beta b_2(1+\lambda) p_2^*, \\ \Delta_3 &= \gamma\left[a_3 + b_3 g_3 + c_3 p_1^* + d_3 p_2^* - 2b_3 p_3^*\right] - 2\gamma b_3 p_3^*; \\ j_{11} &= 1 + \Delta_1, \\ j_{12} &= \alpha c_1(1+\lambda) p_1^*, \\ j_{13} &= \alpha d_1(1+\lambda) p_1^*; \\ j_{21} &= \beta c_2(1+\lambda) p_2^*, \\ j_{22} &= 1 + \Delta_2, \\ j_{23} &= \beta d_2(1+\lambda) p_2^*; \\ j_{31} &= \gamma c_3 p_3^*, \\ j_{32} &= \gamma d_3 p_3^*, \\ j_{33} &= 1 + \Delta_3. \end{aligned} \tag{9}$$

Hence, the characteristic equation of system (7) at (p_1^*, p_2^*, p_3^*) is given by

$$f(\lambda) = \lambda^3 + A\lambda^2 + B\lambda + C, \tag{10}$$

where $A = -(j_{11} + j_{22} + j_{33})$, $B = -(-j_{11}j_{22} - j_{11}j_{33} + j_{21}^2 - j_{22}j_{33} + j_{23}j_{32} + j_{31}^2)$, and $C = -j_{11}j_{22}j_{33} + j_{11}j_{23}j_{32} + j_{21}^2 j_{33} - j_{21}j_{23}j_{31} - j_{21}j_{31}j_{32} + j_{22}j_{31}^2$.

According to the Jury conditions in [19], the Nash equilibrium (p_1^*, p_2^*, p_3^*) of system (7) is locally stable if and only if the following conditions hold:

$$\begin{aligned} f_1 &= A + B + C + 1 > 0, \\ f_2 &= A - B + C - 1 < 0, \\ f_3 &= 1 - C^2 > 0, \\ f_4 &= \left(1 - C^2\right)^2 - (B - AC)^2 > 0. \end{aligned} \tag{11}$$

In this case, prices in the CPs market will reach the Nash equilibrium after limited rounds of games with random initial values. The Nash point is stable in the region consisting of the adjusted speed parametric space (α, β, γ).

3.2. Numerical Simulations. In this triopoly game, the three firms choose the optimal price strategy to maximize their profits in the CPs market and adjust the price according to the marginal profit in the next period. While changes of the

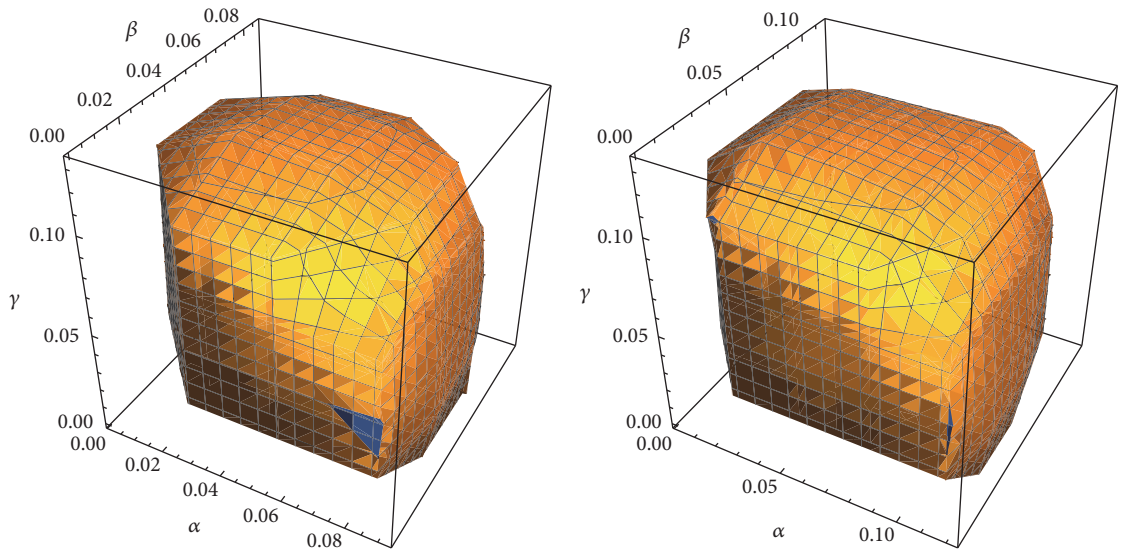

(a) The stable region with $\lambda = 0.2$ (b) The stable region with $\lambda = 0.8$

FIGURE 1: The stable region of the equilibrium with different values of the pulling effect.

adjustment speed α, β, and γ will not influence the values of the Nash equilibrium, we discuss the complex dynamic behaviors of these parameters.

Given a group of parameters $a_1 = a_2 = 6.5, a_3 = 8.25, b_1 = b_2 = b_3 = 1, c_1 = c_2 = 0.30, c_3 = d_1 = 0.35, d_2 = d_3 = 0.40, f_1 = f_2 = 6.50, f_3 = 6, g_1 = g_2 = 2, g_3 = 1.40, e = 0.75, r = 0.46, \lambda = 0.8$, and $\theta = 0.5$. The positive solutions of system (7) are $p_1^* = 6.00, p_2^* = 6.16$, and $p_3^* = 7.11$. In the above analysis, we know that different values of λ can affect the stability of the triopoly cooperation-competition game (7).

As shown in Figure 1, it is noted that the stable region surrounded by the yellow volume is irregular and asymmetric for approximate critical values of $\alpha < 0.08$, $\beta < 0.08$, and $\gamma < 0.11$. The stable region is larger for $\lambda = 0.8$ than that of $\lambda = 0.2$, which means that larger pulling effect on profit for the united R&D activity is conductive to enlarge the stable region of the CPs market.

For given values of $\beta = 0.075$ and $\gamma = 0.08$, Figure 2 shows the price bifurcation diagram of the three firms by taking the adjustment speed α as bifurcating parameter. According to definitions of Lyapunov exponent given in [20], Figure 3 shows the corresponding diagram of the largest Lyapunov exponent. We can see that, for $\alpha < 0.08342$, the Nash equilibrium is locally stable and the largest Lyapunov exponents are negative. The system generates the first flip bifurcation at $\alpha = 0.08342$. With the increase of α, the system turns to be more complicated. When $\alpha > 0.1151$, system (7) has a positive largest Lyapunov exponent, which indicates that the system has entered into chaos state. It means that if the firm 1 from BPs market makes excessive adjustment to adapt itself in the CPs market, this market will gradually become unpredictable and uncontrollable.

The strange attractor is another characteristic of a chaotic system. As shown in Figure 4 when $\beta = 0.075$, $\gamma = 0.08$, and $\alpha = 0.1233$, the system is in chaos and exhibits a fractal

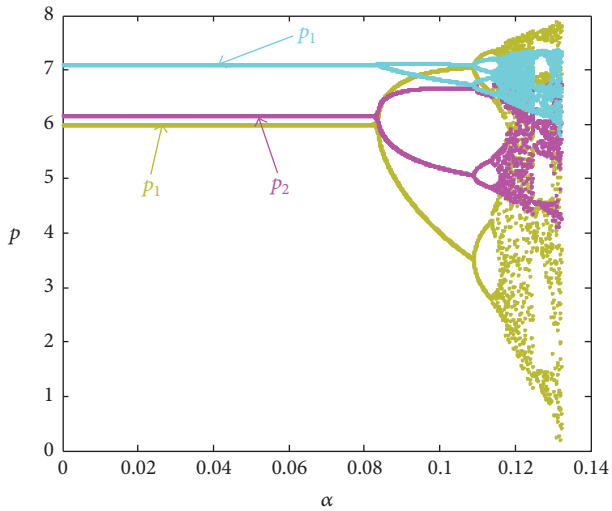

FIGURE 2: The bifurcation diagram of system (7) when $\beta = 0.075$, $\gamma = 0.08$, and $\alpha \in (0, 0.14)$.

structured type. It means that the cooperation-competition relationship in CPs market is disordered and inefficient. If the triopoly system remains in chaotic state, the three firms have to change their pricing mechanism instead of bounded rational adjustment strategy. Since we assume that this is an incomplete information market, information asymmetry and the changed strategy will lead firms to a suboptimal choice to pursue maximum and steady profit.

Figure 5 is the bifurcation diagram of parameter β for firm 2, when given values are $\alpha = 0.075$ and $\gamma = 0.08$. Combined with Figure 6 which is the largest Lyapunov exponent diagram, we obtain similar results of firm 1. For values of $\beta < 0.08156$, the largest Lyapunov exponents are

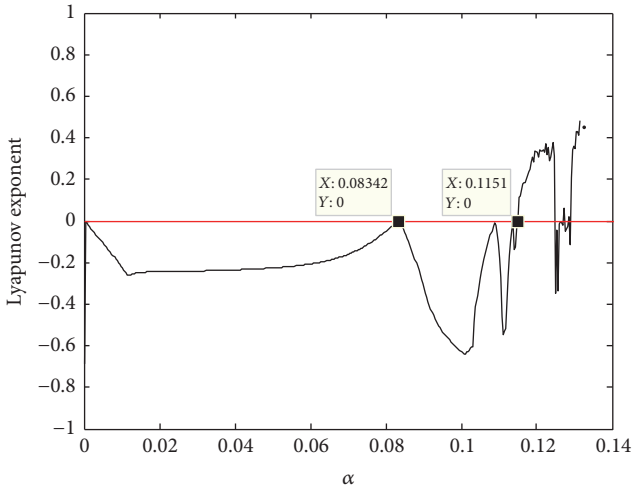

Figure 3: The largest Lyapunov exponent diagram of system (7) when $\beta = 0.075$, $\gamma = 0.08$, and $\alpha \in (0, 0.14)$.

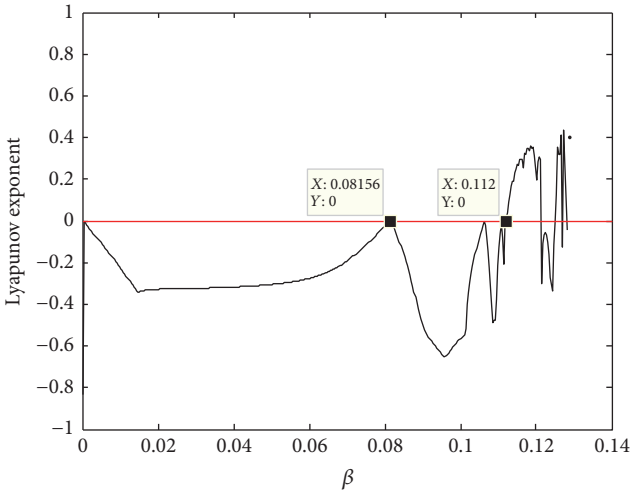

Figure 6: The largest Lyapunov exponent diagram of system (7) when $\alpha = 0.075$, $\gamma = 0.08$, and $\beta \in (0, 0.14)$.

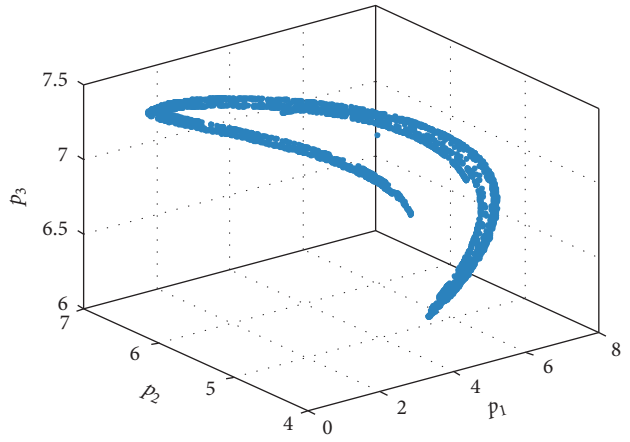

Figure 4: The chaotic attractor diagram of system (7) when $\beta = 0.075$, $\gamma = 0.08$, and $\alpha = 0.1233$.

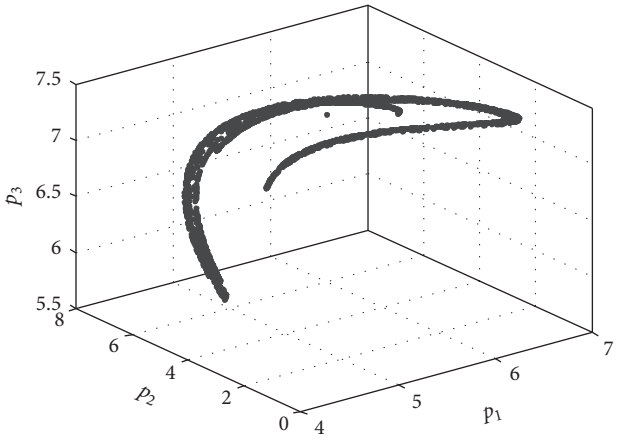

Figure 7: The chaotic attractor diagram of system (7) when $\alpha = 0.075$, $\gamma = 0.08$, and $\beta = 0.121$.

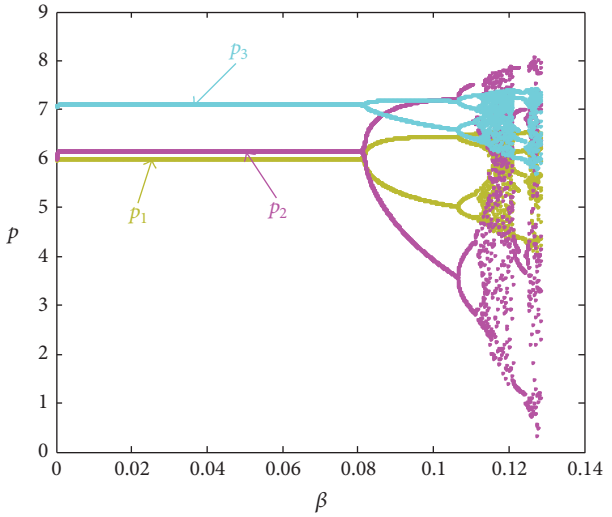

Figure 5: The bifurcation diagram of system (7) when $\alpha = 0.075$, $\gamma = 0.08$, and $\beta \in (0, 0.14)$.

negative, so the Nash equilibrium is locally stable in this case. With increases of β, the Nash equilibrium turns to be unstable and the price decisions for the three firms are continually bifurcating from the equilibrium and eventually enter into chaos when $\beta > 0.112$. The chaos attractor diagram in Figure 7 also illustrates the chaotic phenomenon for adjustment parameter of firm 2 when $\alpha = 0.075$, $\gamma = 0.08$, and $\beta = 0.121$.

Figure 8 shows the bifurcation diagram of firm 3, which is the initial monopolist in CPs and keeps its product line unchanged to expect a rise in demand against the united R&D activity of firm 1 and firm 2. Combined with Figures 9 and 10, it is noted that the critical values of the adjustment speed, where the system passes through bifurcations to chaos, are distinctively larger than that of firms from BPs. The first bifurcating value for γ is 0.117 and system (7) becomes chaotic when $\gamma = 0.1761$.

For more analysis, it can be seen that the cooperation between firm 1 and firm 2 provides a complementary

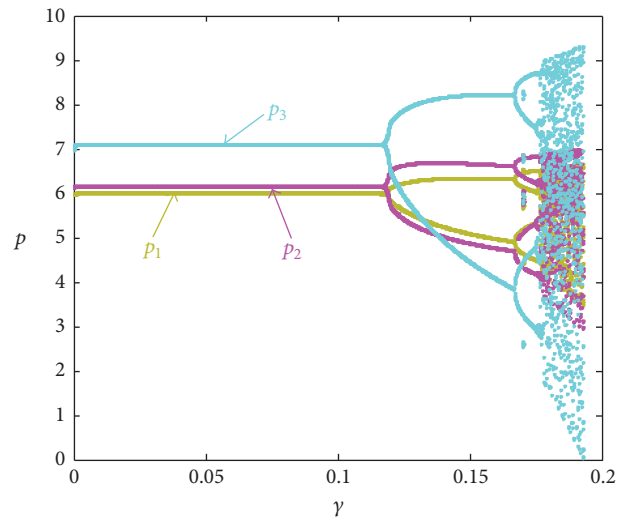

Figure 8: The bifurcation diagram of system (7) when $\alpha = \beta = 0.075$ and $\gamma \in (0, 0.20)$.

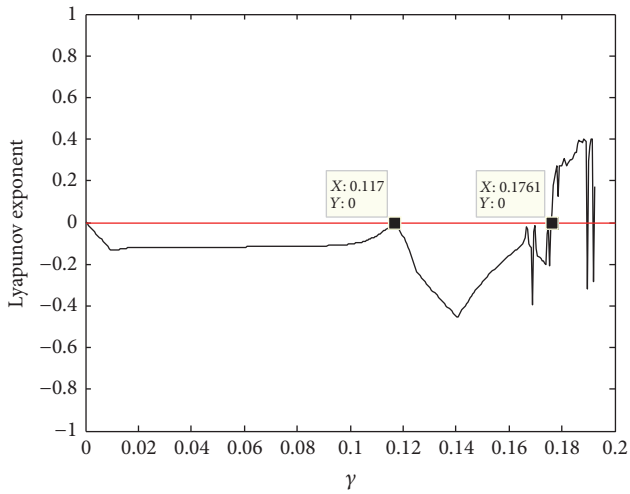

Figure 9: The largest Lyapunov exponent diagram of system (7) when $\alpha = \beta = 0.075$ and $\gamma \in (0, 0.20)$.

opportunity to compete with firm 3 in CPs market. But the players' adjustment speed from both sides of BPs can significantly influence stability of the CPs market. Besides, it proves that the market shows higher tolerance to the adjustment strategy of firm 3 which is an early monopolist in the market. An early entry can build up valuable advantages from aspects like the huge potential demands, the industry-leading technologies and standards, good brand reputations, and so forth. Therefore, in a competitive CPs environment, it is also advisable for enterprises to take an opening strategic attitude to acquire the first-mover advantages.

4. Chaos Control

In CPs market, all the three players are expected to achieve maximum and steady profit. But the price adjustment strategy

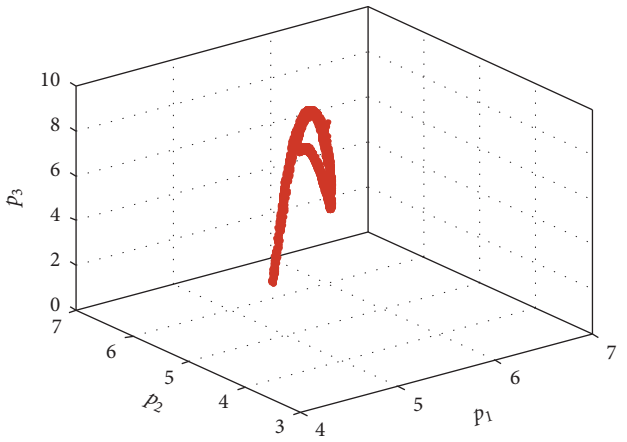

Figure 10: The chaotic attractor diagram of system (7) when $\alpha = \beta = 0.075$ and $\gamma = 0.179$.

should not be independent for the three firms. With increase of the adjustment parameters, the system generates bifurcations and eventually falls into chaos state, which means disorder and difficulty in making arrangement for enterprises in this field. In this section, we choose the parameter feedback method to control chaos in system (7), which is often used in other literatures to eliminate or delay chaos in general discrete systems.

The original triopoly cooperation-competition can be written as

$$p_i(t+1) = f_i\left(p_1(t), p_2(t), p_3(t)\right). \tag{12}$$

We introduce the controlling parameter μ ($\mu \in [0,1]$) into this system. Then the controlled system can be given as $p_i(t+1) = (1-\mu) f_i(p_1(t), p_2(t), p_3(t)) + \mu p_i(t)$; that is,

$$\begin{aligned}
p_1(t+1) &= (1-\mu)\{p_1(t) + \alpha p_1(t) \\
&\quad \times [(1+\lambda)(a_1 - b_1 p_1(t) + c_1 p_2(t) + d_1 p_3(t)) \\
&\quad - b_1(1+\lambda) p_1(t) - (e-r)(c_2 - b_1)\theta + b_1 g_1]\} \\
&\quad + \mu p_1(t), \\
p_2(t+1) &= (1-\mu)\{p_2(t) + \beta p_2(t) \\
&\quad \times [(1+\lambda)(a_2 - b_2 p_2(t) + c_2 p_1(t) + d_2 p_3(t)) \\
&\quad - b_2(1+\lambda) p_2(t) - (e-r)(c_1 - b_2)(1-\theta) \\
&\quad + b_2 g_2]\} + \mu p_2(t), \\
p_3(t+1) &= (1-\mu)\{p_3(t) + \gamma p_3(t)[a_3 + b_3 g_3 + c_3 p_1 \\
&\quad + d_3 p_2 - 2 b_3 p_3]\} + \mu p_3(t).
\end{aligned} \tag{13}$$

When $\mu = 0$, the controlled system degenerated to the original uncontrolled system. When $\mu = 0$, system (13) becomes $p_i(t+1) = p_i(t)$. In this case, the players take simple price strategy as in last period but lose the opportunity to achieve more profits in the market.

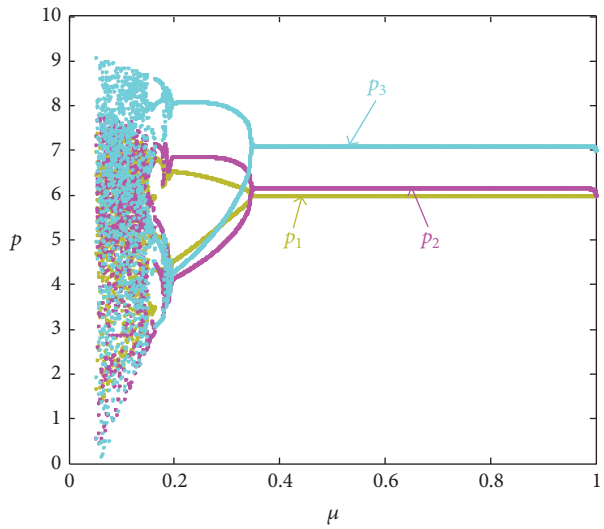

Figure 11: Chaos controlling performance with parameter μ.

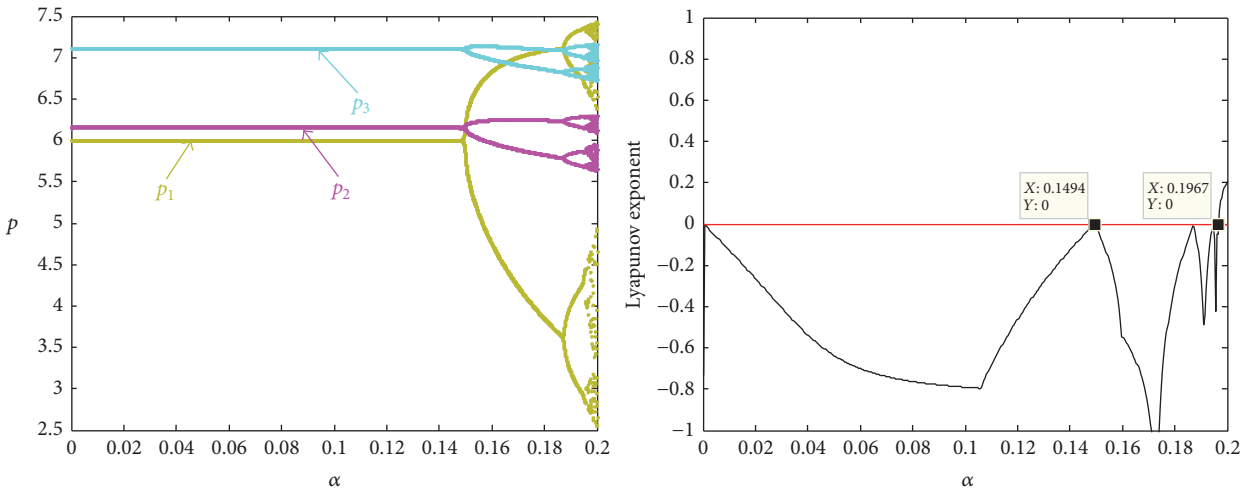

Figure 12: Performance of the controlled system on parameter α.

Substituting (7) into (13), we use numerical simulations to illustrate the effect of μ on the stable region of the Nash equilibrium and the chaos controlling performance for system (7). Take $\alpha = \beta = 0.115$ and $\gamma = 0.18$ and other parameters are the same as in Section 3. In this case, system (7) is in chaos state and Figure 11 gives the bifurcation diagram of the three firms' price range regarding on controlling parameter μ.

It can be seen from Figure 11 that the original system has been controlled from chaos to periodic bifurcations with the increase of μ and eventually recovered to stable state when $\mu > 0.35$, which indicates that the chaotic system is effectively controlled with the controlling parameter. Take $\mu = 0.4$, and the bifurcation diagrams and the largest Lyapunov exponent diagrams of the controlled system (13) with respect to α, β, and γ are given in Figures 12–14. It shows that the controlled system (13) can be stabilized to the Nash equilibrium and chaos has been significantly eliminated or delayed for parameters in its feasible basin. Compared with the numerical simulation results in Section 3, the critical value of the price adjustment speed α where system (7) occurs as the first flip bifurcation has been increased from 0.8342 to 0.1494, and the turning point where system (7) transforms from multiperiodic orbits to chaos has been delayed from 0.11151 to 0.1967. The stability analysis of parameters β and γ also proved the controlling performance on chaotic system. In this case, the stable region of system (7) is enlarged for a wider range of α, β, and γ, where the system converges to the Nash equilibrium.

In an associated economic system, a chaos state means disordered and inefficient competition in the market. The controlling performance of μ on the chaotic system shows that reasonable interventions or regulations on CPs are necessary and the learning ability or adaptability can be considered when making price decisions by analyzing the

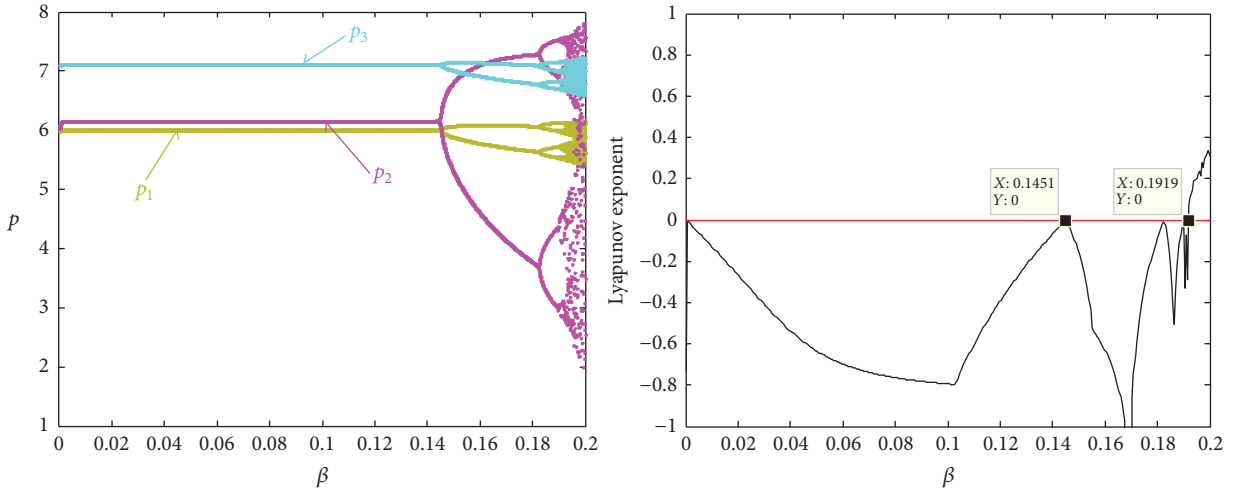

Figure 13: Performance of the controlled system on parameter β.

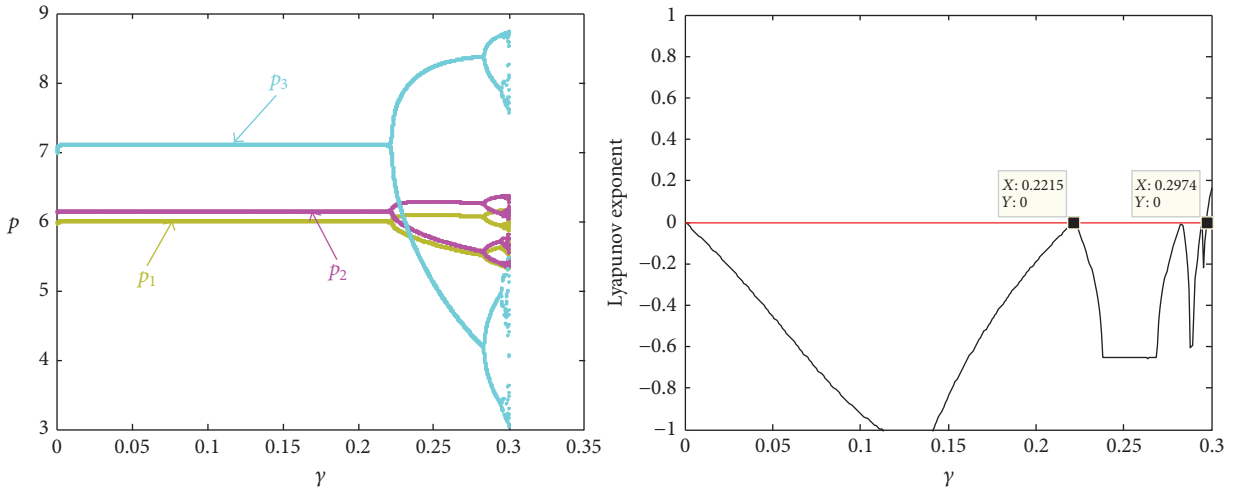

Figure 14: Performance of the controlled system on parameter γ.

past information for enterprises in this market. In addition, in an incomplete information market, the firms have limited information on output and pricing strategy of its competitors. So the three firms should be more cautious to make a decision. The price adjustment speed for each firm is not independently decided; it needs collaborative cooperation for all the three firms to pull the chaotic system back into stability.

5. Conclusions

In this paper, we investigate the complexity property of a triopoly game model in the convergence product market which contains three players: an early entry monopolist and two potential entrants from the base product market. Because of the nonindependent price decision mechanism and intentions to pursue the maximum profits, the cooperation and competition behaviors among the players will lead to complex dynamic results in this system. The cost-sharing competition for the two cooperative BPs firms and the alternative competition among the CPs and BPs firms will be eventually reflected in their price decision strategies. We find that the pulling effect on profit form R&D activity can affect the stable range of the Nash equilibrium. So the first-mover strategy is recommended for enterprises who are preparing for entering a convergence product market. The system presents complex bifurcation and chaos behaviors if the adjustment speed exceeds a critical value. An effective parameter feedback control method can be applied to delay or eliminate the chaos state for the system, which supports the idea of reasonable interventions and regulation measures. Parameter values in real case scenarios rely on more empirical studies with variations of composition and structure analysis for specific convergence product. This study helps to better understand the fluctuations in general convergence product market and has theoretical and practical meaning when

making price decision and strategy selection for enterprises in related fields.

Competing Interests

The authors declare that there is no conflict of interests regarding the publication of this paper.

References

[1] Z. Wang, C. Chen, B. Guo, Z. Yu, and X. Zhou, "Internet plus in China," *IT Professional*, vol. 18, no. 3, pp. 5–8, 2016.

[2] A. Fishman and R. Rafael, "Product innovation by a durable-good monopoly," *The RAND Journal of Economics*, vol. 31, no. 2, pp. 237–252, 2000.

[3] E. Danneels, "The dynamics of product innovation and firm competences," *Strategic Management Journal*, vol. 23, no. 12, pp. 1095–1121, 2002.

[4] T. Gill, "Convergent products: what functionalities add more value to the base?" *Journal of Marketing*, vol. 72, no. 2, pp. 46–62, 2008.

[5] E. M. Okada, "Upgrades and new purchases," *Journal of Marketing*, vol. 70, no. 4, pp. 92–102, 2006.

[6] H. N. Agiza and A. A. Elsadany, "Nonlinear dynamics in the Cournot duopoly game with heterogeneous players," *Physica A. Statistical Mechanics and its Applications*, vol. 320, no. 1-4, pp. 512–524, 2003.

[7] G. Symeonidis, "Comparing Cournot and Bertrand equilibria in a differentiated duopoly with product R&D," *International Journal of Industrial Organization*, vol. 21, no. 1, pp. 39–55, 2003.

[8] H. Yang, M. Zhang, and M. Lai, "Complex dynamics of Cournot game with bounded rationality in an oligopolistic electricity market," *Optimization and Engineering*, vol. 12, no. 4, pp. 559–582, 2011.

[9] F. Chen, J. H. Ma, and X. Q. Chen, "The study of dynamic process of the triopoly games in chinese 3G telecommunication market," *Chaos, Solitons and Fractals*, vol. 42, no. 3, pp. 1542–1551, 2009.

[10] C. H. Tremblay and V. J. Tremblay, "The Cournot-Bertrand model and the degree of product differentiation," *Economics Letters*, vol. 111, no. 3, pp. 233–235, 2011.

[11] S. S. Askar, A. M. Alshamrani, and K. Alnowibet, "The arising of cooperation in Cournot duopoly games," *Applied Mathematics and Computation*, vol. 273, pp. 535–542, 2016.

[12] A. A. Elsadany, "Competition analysis of a triopoly game with bounded rationality," *Chaos, Solitons & Fractals*, vol. 45, no. 11, pp. 1343–1348, 2012.

[13] E. M. Elabbasy, H. N. Agiza, and A. A. Elsadany, "Analysis of nonlinear triopoly game with heterogeneous players," *Computers and Mathematics with Applications*, vol. 57, no. 3, pp. 488–499, 2009.

[14] S. K. Ethiraj and D. Levinthal, "Bounded rationality and the search for organizational architecture: an evolutionary perspective on the design of organizations and their evolvability," *Administrative Science Quarterly*, vol. 49, no. 3, pp. 404–437, 2004.

[15] M. Pireddu, "Chaotic dynamics in three dimensions: a topological proof for a triopoly game model," *Nonlinear Analysis. Real World Applications*, vol. 25, pp. 79–95, 2015.

[16] D. A. Heiner, "Microsoft: a remedial success?" *Antitrust Law Journal*, vol. 78, no. 2, pp. 329–362, 2012.

[17] J. M. Pennings and P. Puranam, "Market convergence & firm strategy: new directions for theory and research," in *Proceedings of the ECIS Conference, The Future of Innovation Studies*, Eindhoven, The Netherlands, 2001.

[18] M. Lee and Y. Cho, "Consumer perception of a new convergence product: a theoretical and empirical approach," *Technological Forecasting and Social Change*, vol. 92, pp. 312–321, 2015.

[19] S. Elaydi, *An Introduction to Difference Equations*, Springer, 2005.

[20] E. Beltrami, *Mathematics for Dynamic Modeling*, Academic Press, Boston, Mass, USA, 1987.

Hindawi Publishing Corporation
Mathematical Problems in Engineering
Volume 2016, Article ID 9506795, 9 pages
http://dx.doi.org/10.1155/2016/9506795

Research Article

Uncertain Unified Chaotic Systems Control with Input Nonlinearity via Sliding Mode Control

Zhi-ping Shen,[1] Jian-dong Xiong,[1] and Yi-lin Wu[2]

[1] *Henan Engineering Laboratory for Big Data Statistical Analysis and Optimal Control, School of Mathematics and Information Sciences, Henan Normal University, Xinxiang, Henan 453007, China*
[2] *Department of Computer Science, Guangdong University of Education, Guangzhou, Guangdong 510310, China*

Correspondence should be addressed to Zhi-ping Shen; zpshen@htu.cn

Received 1 July 2016; Revised 27 August 2016; Accepted 4 September 2016

Academic Editor: Jesus M. Munoz-Pacheco

This paper studies the stabilization problem for a class of unified chaotic systems subject to uncertainties and input nonlinearity. Based on the sliding mode control theory, we present a new method for the sliding mode controller design and the control law algorithm for such systems. In order to achieve the goal of stabilization unified chaotic systems, the presented controller can make the movement starting from any point in the state space reach the sliding mode in limited time and asymptotically reach the origin along the switching surface. Compared with the existing literature, the controller designed in this paper has many advantages, such as small chattering, good stability, and less conservative. The analysis of the motion equation and the simulation results all demonstrate that the method is effective.

1. Introduction

"Chaos" in contemporary English language refers to the meaning of "Unzucht and Unordnung"; its meaning is close to "determinacy for random phenomena" in nonlinear systemic theory. Thus, chaos is borrowed to call these anomalies. In the eyes of appearance, chaos movement looks like random process, but, in fact, there is a distinction between chaotic motion and stochastic process. Chaos has the following features [1]: initial value sensitivity, boundedness, randomness, ergodicity, universality, fractal dimension and positive maximum Lyapunov index, and so forth. It should be pointed out that the identification of chaos is still a topic that is not completely solved till now.

The existence of the chaotic motion can be observed in many cases because chaotic signal has the properties of the inherent continuous broadband power spectra and noise like and so forth. It provides a highly classified secret communication method; chaos control and synchronization and its application in secret communication have attracted many researchers' attention [1–13]. However, due to the fact that the chaotic system is extremely sensitive to initial value and long time unpredictability, chaos control has become the key link of chaotic application. Since 1987, Alekseevv and Loskutov [14] published papers about the controlling chaos, and, in 1989, Hubler et al. [15, 16] proposed OGY method; international and domestic academics have proposed many different methods of chaos control, and the main research results of the chaos control basically have the following categories: feedback control method [17, 18], adaptive control method [19, 20], neural network control method [21], sliding mode control method [6, 22, 23], and so on.

In 2002, Lü et al. proposed a new chaotic system: the system connects the Lorenz attractor and Chen attractor; Lü system is a special case; hence, it is called the unified chaotic system [24]. Controlling the unified chaotic system had attracted many researchers' attention from the beginning for its special properties; for example, its form is very simple and it only has one parameter, its dynamics behavior can be analyzed using energy barriers principle, it connects the Lorenz attractor and Chen attractor, and it realizes continuous evolution of one system and another system in the whole parameters spectrum. Literature [25] studied the feedback control and synchronization problem of unified chaotic system; literature [26] studied the projective synchronization and control problems of unified chaotic system. In view of

the system equation containing the unknown parameters, literature [27] studied the stabilization of equilibrium points using the sliding mode variable structure control; literature [28] designed a constraint controller to stabilize the system states to unstable equilibrium points of the unified chaotic system by using the Minimum Principle of Pontryagin, and the paper also presented a combination of Bang-Bang control and logic switching to overcome the limitation of Bang-Bang control; literature [29] proposed a passive equivalent control scheme to realize the stability control of different equilibrium for the unified chaotic system using the passive control theory. Literature [30] proposed a sliding mode controller to synchronize two different chaotic systems with unknown bounded uncertainties. Reference [31] proposed a discontinuous Lyapunov functional approach to achieving asymptotic robust synchronization of uncertain chaotic systems using sampled-data control with stochastically varying sampling intervals. However, there is not an overall and only effective control method in presented methods so far.

This paper studies the stabilization problem of a class of unified chaotic systems with parameter uncertainty and nonlinear input based on the sliding mode variable structure control. A sufficient condition under which the sliding mode system is quadratically stable, a new control method, and the time during which the system states can reach the sliding manifold are given. The designed control law algorithms in this paper and in literature [22] are all able to ensure that the motion of the system can reach the switching surface and thus can make the closed-loop system asymptotically stable, but the control law in paper [22] cannot provide the arrival speed, cannot guarantee rapidity, and had a big conservative, but the control law in this paper can improve the rapidity of the system's trajectories to reach the sliding mode and effectively weaken the chattering of the sliding mode. Simulation results verify that the method is feasible, and the improvement of the dynamic property is prominent.

2. Problem Formulation

A class of unified chaotic systems is shown in

$$\begin{aligned} \dot{x}_1 &= (25\alpha + 10)\left(x_2 - x_1\right), \\ \dot{x}_2 &= (28 - 35\alpha)\, x_1 + (29\alpha - 1)\, x_2 - x_1 x_3, \\ \dot{x}_3 &= x_1 x_2 - \frac{8+\alpha}{3} x_3, \end{aligned} \tag{1}$$

where $\alpha \in [0, 1]$, system (1) is always chaotic when $\alpha \in [0, 1]$; when α increases from 0 to 1, system (1) gradually transits from Lorenz system to Chen system. According to the definition in literature [24], system (1) belongs to generalized Lorenz chaotic system when $\alpha \in [0, 0.8)$, satisfying $a_{12}a_{21} > 0$; system (1) belongs to generalized Chen chaotic system when $\alpha \in (0.8, 1]$, satisfying $a_{12}a_{21} < 0$; and when $\alpha = 0.8$, system (1) satisfying $a_{12}a_{21} = 0$ plays an important role in connecting generalized Lorenz chaotic system to generalized Chen chaotic system. The systems offer the study of chaos control and synchronization of a new mathematical model and make chaos synchronization based on the unified models

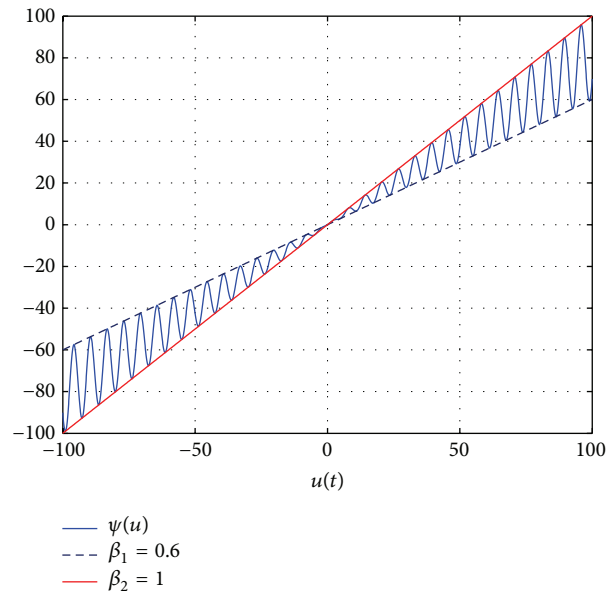

Figure 1: Nonlinear function $\psi(u(t)) = [0.8 + 0.2\sin(u(t))]u(t)$.

that have already gained practical application in secure communications; however, there are still many problems that should be further studied, for example, combining the synchronization methods of the unified chaotic system with the advanced control methods, improving the synchronization performance of a unified chaotic system, and studying nonlinear circuits communication based on unified chaotic system.

The controlled system is as follows:

$$\begin{aligned} \dot{x}_1 &= (25\alpha + 10)\left(x_2 - x_1\right), \\ \dot{x}_2 &= (28 - 35\alpha)\, x_1 + (29\alpha - 1)\, x_2 - x_1 x_3 \\ &\quad + \Delta f\left(x_1, x_2, x_3\right) + \psi(u), \\ \dot{x}_3 &= x_1 x_2 - \frac{8+\alpha}{3} x_3, \end{aligned} \tag{2}$$

where Δf is the system uncertainty, satisfying $|\Delta f| \le \gamma\|x\|$, γ a positive real number, and nonlinear control $\psi(u)$ satisfies

$$\beta_1 u^2 \le u\psi(u) \le \beta_2 u^2, \quad 0 < \beta_1 < \beta_2, \tag{3}$$

for example,

$$\psi(u(t)) = [0.8 + 0.2\sin(u)]\, u(t). \tag{4}$$

The figure of the above nonlinear control is shown in Figure 1.

The aim of this paper is to design a controller which can make the closed-loop system stable; therefore, the stabilization problem of system (1) can be transformed into the asymptotic stability problem of system (2); that is,

$$\lim_{t\to\infty} x(t) = 0. \tag{5}$$

3. Sliding Mode Design

Considering the uncertainties in system (2), a sliding mode control method is adopted in this paper to achieve $\lim_{t\to\infty} x(t) = 0$ through its strong robustness on the sliding surface. In order to prove the main results, some lemmas are given.

Lemma 1. *If A is a stable and diagonal matrix; then there exists λ, satisfying*

$$\left\|e^{At}\right\| \le e^{-\lambda t}. \tag{6}$$

Proof. Diagonal matrix A can be rewritten as follows:

$$A = \operatorname{diag}\{\lambda_1, \lambda_2, \ldots, \lambda_n\}, \tag{7}$$

where $\lambda_i,\ i = 1, 2, \ldots, n$ are the diagonal elements and also are eigenvalues of diagonal matrix A; let

$$\lambda_{\max} = \max\{\lambda_1, \lambda_2, \ldots, \lambda_n\}; \tag{8}$$

then, according to the matric exponential function properties, we can get

$$e^{At} = \operatorname{diag}\left\{e^{\lambda_1 t}, e^{\lambda_2 t}, \ldots, e^{\lambda_n t}\right\}; \tag{9}$$

thereby,

$$\left\|e^{At}\right\| = \left\|\operatorname{diag}\left\{e^{\lambda_1 t}, e^{\lambda_2 t}, \ldots, e^{\lambda_n t}\right\}\right\| \le e^{\lambda_{\max} t}. \tag{10}$$

Let

$$\lambda = -\lambda_{\max} > 0; \tag{11}$$

then,

$$\left\|e^{At}\right\| \le e^{-\lambda t}. \tag{12}$$

□

Lemma 2. *If A is a stable and diagonal matrix and $f(x,t)$ satisfies*

$$\left\|f(x,t)\right\| \le \beta e^{-\zeta t}, \quad \beta > 0,\ \zeta > 0, \tag{13}$$

then the following system is asymptotically stable:

$$\dot{x} = Ax + f(x,t). \tag{14}$$

Proof. Solving (14), we can obtain

$$x(t) = e^{At}x(0) + \int_0^t e^{A(t-\tau)} f(x(\tau), \tau)\, d\tau; \tag{15}$$

hence,

$$\begin{aligned}\|x(t)\| &\le \left\|e^{At}\right\| \cdot \|x(0)\| \\ &\quad + \int_0^t \left\|e^{A(t-\tau)}\right\| \cdot \left\|f(x(\tau), \tau)\right\| d\tau.\end{aligned} \tag{16}$$

Let $-\lambda$ be the maximum real part of the eigenvalues of matrix A, and from Lemma 1, we can get

$$\begin{aligned}\|x(t)\| &\le \|x(0)\| e^{-\lambda t} + \frac{\beta}{\lambda - \zeta} e^{-\lambda t} e^{(\lambda-\zeta)\tau}\Big|_0^t \\ &= e^{-\lambda t}\|x(0)\| + \frac{\beta}{\lambda - \zeta}\left(e^{-\zeta t} - e^{-\lambda t}\right) \longrightarrow 0.\end{aligned} \tag{17}$$

Based on the above lemmas, we shall propose the sliding mode design. □

Theorem 3. *If we choose the following switching function:*

$$s(t) = -(1-\delta)x_1(t) + x_2(t), \quad \delta > 0, \tag{18}$$

then, the sliding mode equation is asymptotically stable.

Proof. Choose a switching function as

$$s(t) = c_1 x_1(t) + c_3 x_3(t) + x_2(t), \tag{19}$$

where c_1, c_3 are parameters to be determined.

On switching surface $s(t) = 0$, from (19), we can get

$$x_2(t) = -c_1 x_1(t) - c_3 x_3(t), \tag{20}$$

substituting (20) to the first and the third equalities of state equation (2); the sliding mode equation is obtained:

$$\begin{aligned}\dot{x}_1 &= -(25\alpha + 10)(c_1 + 1)x_1 - (25\alpha + 10)c_3 x_3, \\ \dot{x}_3 &= -(c_1 x_1 + c_3 x_3)x_1 - \frac{8+\alpha}{3}x_3.\end{aligned} \tag{21}$$

The above equation can be rewritten as a vector form:

$$\begin{pmatrix}\dot{x}_1 \\ \dot{x}_3\end{pmatrix} = \begin{pmatrix}-\Upsilon(c_1+1) & -\Upsilon c_3 \\ 0 & -\dfrac{8+\alpha}{3}\end{pmatrix}\begin{pmatrix}x_1 \\ x_3\end{pmatrix} - \begin{pmatrix}0 \\ \bigwedge\end{pmatrix}, \tag{22}$$

where $\Upsilon = (25\alpha + 10)$, $\bigwedge = x_1(c_1 x_1 + c_3 x_3)$.

Choose $c_1 = -1 + \delta$, $\delta > 0$, and $c_3 = 0$; then (22) becomes

$$\begin{pmatrix}\dot{x}_1 \\ \dot{x}_3\end{pmatrix} = \begin{pmatrix}-\Upsilon\delta & 0 \\ 0 & -\dfrac{8+\alpha}{3}\end{pmatrix}\begin{pmatrix}x_1 \\ x_3\end{pmatrix} - \begin{pmatrix}0 \\ (c_1 x_1)x_1\end{pmatrix}. \tag{23}$$

Solving the first equality of (23), we obtain

$$x_1(t) = x_1(0)\, e^{-(25\alpha+10)\delta t} \longrightarrow 0; \tag{24}$$

hence, $x_1(t)$ is exponentially stable, and because

$$\left\|(c_1 x_1(t))\, x_1(t)\right\| \le \left\|c_1 x_1(t)\right\| \cdot \left\|x_1(t)\right\|, \tag{25}$$

then $c_1 x_1^2(t)$ converges exponentially to zero; thus, from Lemma 2, we obtain

$$\lim_{t\to\infty}\left[x_1, x_3\right]^T = 0, \tag{26}$$

which completes the theorem. □

4. Variable Structure Control Law Design

Theorem 3 discusses the stability of the system on the switching surface; we now resort to present the sliding controller that can make the movement starting from any point in state space reach the switching surface in limited time.

Theorem 4. *If we choose the controller as*

$$u = \frac{1}{2}\left(u^{+} + u^{-}\right) + \frac{1}{2}\left(u^{+} - u^{-}\right)\operatorname{sgn}\left(s\left(t\right)\right), \tag{27}$$

where

$$\begin{aligned} u^{+} = & -\frac{1}{2\beta_1}\left(|ks| + \epsilon + \Gamma\left(s,x\right) + \gamma\left\|x\right\|\right) \\ & - \frac{1}{2\beta_1}\left|\Gamma\left(s,x\right) + \gamma\left\|x\right\| + |ks| + \epsilon\right|, \end{aligned} \tag{28}$$

$$\begin{aligned} u^{-} = & \frac{1}{2\beta_1}\left(|ks| + \epsilon - \Gamma\left(s,x\right) + \gamma\left\|x\right\|\right) \\ & + \frac{1}{2\beta_1}\left|-\Gamma\left(s,x\right) + \gamma\left\|x\right\| + |ks| + \epsilon\right|, \end{aligned} \tag{29}$$

$$\begin{aligned} \Gamma\left(s,x\right) = & -\left(1-\delta\right)\left(25\alpha + 10\right)\left(x_2 - x_1\right) - x_1 x_3 \\ & + \left(29\alpha - 1\right)x_2 + \left(28 - 35\alpha\right)x_1, \end{aligned} \tag{30}$$

and parameters $k > 0$, $\epsilon > 0$, and $s(t)$ are the switching surface as in (18), then the movement starting from any point in the state space can reach the switching surface in limited time, and the time to reach the switching surface is

$$T \le \frac{1}{k}\ln\left(\frac{k}{\epsilon}\left|s\left(0\right)\right| + 1\right). \tag{31}$$

Proof. We shall first prove that the movement starting from any point in the state space can reach the switching surface in limited time.

It is easy to verify that (28) and (29) can be rewritten as

$$u^{+} = \min\left\{\frac{1}{\beta_1}\left(-|ks| - \epsilon - \Gamma\left(s,x\right) - \gamma\left\|x\right\|\right), 0\right\}, \tag{32}$$

$$u^{-} = \max\left\{\frac{1}{\beta_1}\left(|ks| + \epsilon - \Gamma\left(s,x\right) + \gamma\left\|x\right\|\right), 0\right\}. \tag{33}$$

Because switching surface $s(t) = 0$ divides the state space into two parts $s(t) > 0$ and $s(t) < 0$, we should consider the following two scenarios:

(1) When $s(t) > 0$, from (27), we can get $u = u^{+}$, and, then from (32), we can easily get $u = u^{+} \le 0$, and, since

$$\beta_1 u^2 \le u\psi\left(u\right) \le \beta_2 u^2, \quad 0 < \beta_1 < \beta_2, \tag{34}$$

both sides of the above equation are divided by $u < 0$, and we obtain

$$\beta_2 u \le \psi\left(u\right) \le \beta_1 u. \tag{35}$$

Therefore, by (2), we can get

$$\begin{aligned} \dot{s} = & -\left(1-\delta\right)\dot{x}_1 + \dot{x}_2 \\ = & -\left(1-\delta\right)\left(25\alpha + 10\right)\left(x_2 - x_1\right) + \Phi x_1 - x_1 x_3 \\ & + \left(29\alpha - 1\right)x_2 + \psi\left(u\right) + \Delta f\left(x,t\right) \\ \le & -\left(1-\delta\right)\left(25\alpha + 10\right)\left(x_2 - x_1\right) + \Phi x_1 + \beta_1 u \\ & + \left(29\alpha - 1\right)x_2 - x_1 x_3 + \left|\Delta f\left(x,t\right)\right| \\ \le & \Gamma\left(s,x\right) + \beta_1 u^{+} + \gamma\left\|x\right\| \\ \le & \Gamma\left(s,x\right) + \gamma\left\|x\right\| - |ks| - \epsilon - \Gamma\left(s,x\right) - \gamma\left\|x\right\| \\ = & -|ks| - \epsilon, \quad s > 0, \end{aligned} \tag{36}$$

where $\Phi = (28 - 35\alpha)$.

(2) When $s(t) < 0$, from (27), we can get $u = u^{-}$, and, then, from (33), we can easily get $u = u^{-} \ge 0$, so, from (3), we have $\psi(u) \ge \beta_1 u$, and, then

$$\begin{aligned} \dot{s} = & -\left(1-\delta\right)\left(25\alpha + 10\right)\left(x_2 - x_1\right) + \psi\left(u\right) - x_1 x_3 \\ & + \left(28 - 35\alpha\right)x_1 + \left(29\alpha - 1\right)x_2 + \Delta f\left(x,t\right) \\ \ge & -\left(1-\delta\right)\left(25\alpha + 10\right)\left(x_2 - x_1\right) - x_1 x_3 + \beta_1 u \\ & + \left(28 - 35\alpha - x_3^{0}\right)x_1 + \left(29\alpha - 1\right)x_2 - \gamma\left\|x\right\| \\ = & \Gamma\left(s,x\right) - \gamma\left\|x\right\| + \beta_1 u^{-} \\ \ge & \Gamma\left(s,x\right) - \gamma\left\|x\right\| + |ks| + \epsilon - \Gamma\left(s,x\right) + \gamma\left\|x\right\| \\ \ge & |ks| + \epsilon, \quad s < 0, \end{aligned} \tag{37}$$

from (36) and (37); we can obtain that the movement starting from any point in the state space can reach the switching surface in limited time.

In the sequel, solve the time to reach the switching surface.

For the time to reach the switching surface, through solving (36) and (37), we obtain

$$\begin{aligned} \dot{s} \le & -|ks| - \epsilon, \quad s > 0, \\ \dot{s} \ge & |ks| + \epsilon, \quad s < 0. \end{aligned} \tag{38}$$

When $s(t) > 0$, the first equality in (38) is

$$\dot{s} \le -ks - \epsilon. \tag{39}$$

Letting $w(t)$ be the solution of the following linear differential equation,

$$\begin{aligned} \dot{w}\left(t\right) = & -kw\left(t\right) - \epsilon, \\ w\left(0\right) = & s\left(0\right). \end{aligned} \tag{40}$$

We conclude by the comparison lemma [32] that

$$s\left(t\right) \le w\left(t\right) = s\left(0\right)e^{-kt} - \epsilon\int_0^t e^{-k(t-\tau)}d\tau. \tag{41}$$

Similarly, when $s(t) < 0$, we have

$$s(t) \le s(0)\, e^{-kt} + \epsilon \int_0^t e^{-k(t-\tau)} d\tau. \tag{42}$$

So, we get

$$\begin{aligned} s(t) &\le s(0)\, e^{-kt} - \epsilon \int_0^t e^{-k(t-\tau)} d\tau, \\ &\qquad s(0) > 0,\ s(t) \ge 0; \\ s(t) &\ge s(0)\, e^{-kt} + \epsilon \int_0^t e^{-k(t-\tau)} d\tau, \\ &\qquad s(0) < 0,\ s(t) \le 0. \end{aligned} \tag{43}$$

Let the time to reach the switching surface be T, since, on switching surface surface $s(t) = 0$ and from the above equation, one has

$$\begin{aligned} 0 &\le s(0)\, e^{-kT} - \frac{\epsilon}{k}\left(1 - e^{-kT}\right), \quad s(0) > 0,\ s(t) = 0; \\ 0 &\ge s(0)\, e^{-kT} + \frac{\epsilon}{k}\left(1 - e^{-kT}\right), \quad s(0) < 0,\ s(t) = 0. \end{aligned} \tag{44}$$

Consequently, we have

$$T \le \frac{1}{k} \ln\left(\frac{k}{\epsilon} |s(0)| + 1\right). \tag{45}$$

This completes the proof. □

Remark 5. The designed control law algorithms in Theorem 4 and in literature [22] are all able to ensure that the motion of the system can reach the switching surface and hence can make the closed-loop system asymptotically stable, whereas the control law in Theorem 4 has the following advantages:

(1) The designed control law algorithm in literature [22] can only guarantee $s(t)\dot{s}(t) < 0$ and cannot provide arrival speed and cannot guarantee rapidity, while the designed control law algorithm in Theorem 4 can guarantee

$$\begin{aligned} \dot{s} &\le -|ks| - \epsilon, \quad s > 0, \\ \dot{s} &\ge |ks| + \epsilon, \quad s < 0, \end{aligned} \tag{46}$$

and the time to reach switching surface T is

$$T \le \frac{1}{k} \ln\left(\frac{k}{\epsilon} |s(0)| + 1\right); \tag{47}$$

hence, the system has good rapidity.

(2) The designed control law algorithm in literature [22] uses $|\Gamma(s,x)|$, while, in Theorem 4, $\Gamma(s,x)$ is employed, which results in small chattering, good stability, and less conservative.

5. An Improved Control Law

The designed control law algorithm in Theorem 4 only limits the minimum speed in which the movement starting from any point in state space reaches the switching surface:

$$|\dot{s}| \ge |ks| + \epsilon, \tag{48}$$

but does not limit the maximum speed, which may result in too fast to reach the switching surface, as a result, the sliding mode control may cause severe chattering, for example,

when $s > 0$, and

$$\begin{aligned} &\Gamma(s,x) + \gamma \|x\| \ll -|ks| - \epsilon, \\ &-|ks| - \epsilon - \Gamma(s,x) - \gamma \|x\| > 0, \end{aligned} \tag{49}$$

$\ll$ denoting "much less than," we have $u = u^+ = 0$, and from (27) and (32), one has

$$\dot{s} \le \Gamma(s,x) + \gamma \|x\| \ll -|ks| - \epsilon, \quad s > 0. \tag{50}$$

Similarly, when $s < 0$, and

$$\begin{aligned} &\Gamma(s,x) - \gamma \|x\| \gg |ks| + \epsilon, \\ &0 > |ks| + \epsilon - \Gamma(s,x) + \gamma \|x\|, \end{aligned} \tag{51}$$

we have $u = u^- = 0$, and from (27) and (33), one has

$$\dot{s} \ge \Gamma(s,x) - \gamma \|x\| \gg |ks| + \epsilon, \quad s < 0. \tag{52}$$

Equations (50) and (52) indicate that the controller designed by (27)–(30) may lead to

$$\begin{aligned} \dot{s} &\ll -|ks| - \epsilon, \quad s > 0, \\ \dot{s} &\gg |ks| + \epsilon, \quad s < 0; \end{aligned} \tag{53}$$

that is to say, the movement starting from any point in the state space reaches the switching surface too fast, which may cause that the sliding mode produces severe chattering and the system dynamic quality is poor. In order to avoid these disadvantages, we shall make the following improvement for the control law in Theorem 4; choose

$$\begin{aligned} u_*^+ &= -\frac{1}{2}\left(\frac{1}{\beta_1} + \frac{1}{\beta_2}\right)\left(|ks| + \epsilon + \Gamma(s,x) + \gamma \|x\|\right) \\ &\quad - \frac{1}{2}\left(\frac{1}{\beta_1} - \frac{1}{\beta_2}\right)\left|\Gamma(s,x) + \gamma \|x\| + |ks| + \epsilon\right|, \\ u_*^- &= -\frac{1}{2}\left(\frac{1}{\beta_1} + \frac{1}{\beta_2}\right)\left(-|ks| - \epsilon + \Gamma(s,x) - \gamma \|x\|\right) \\ &\quad - \frac{1}{2}\left(\frac{1}{\beta_2} - \frac{1}{\beta_1}\right)\left|\Gamma(s,x) - \gamma \|x\| - |ks| - \epsilon\right|, \end{aligned} \tag{54}$$

which is to say that we shall present the following improved controller theorem which can avoid the above disadvantages.

Theorem 6. *If we choose the controller as*

$$u = \frac{1}{2}\left(u_*^+ + u_*^-\right) + \frac{1}{2}\left(u_*^+ - u_*^-\right) \operatorname{sgn}(s(t)), \tag{55}$$

then the movement starting from any point in the state space can reach the switching surface in limited time, and the time to reach the switching surface is

$$T \le \frac{1}{k} \ln\left(\frac{k}{\epsilon} |s(0)| + 1\right). \tag{56}$$

Meanwhile, the movement starting from any point in the state space reaches the switching surface not too fast.

Proof. Consider the following four scenarios.

(1) When $s > 0$ and $|ks| + \epsilon + \Gamma(s,x) + \gamma\|x\| > 0$, we have

$$u_*^+ = \frac{1}{\beta_1}\left(-|ks| - \epsilon - \Gamma(s,x) - \gamma\|x\|\right) < 0; \tag{57}$$

hence, from the switching surface equation, we obtain

$$\begin{aligned}\dot{s} &\le \Gamma(s,x) + \beta_1 u_*^+ + \gamma\|x\| \\ &\le \Gamma(s,x) + \gamma\|x\| - |ks| - \epsilon - \Gamma(s,x) - \gamma\|x\| \\ &\le -k|s| - \epsilon.\end{aligned} \tag{58}$$

(2) When $s > 0$ and $|ks| + \epsilon + \Gamma(s,x) + \gamma\|x\| < 0$, we have

$$u = u_*^+ = -\frac{1}{\beta_2}\left(|ks| + \epsilon + \Gamma(s,x) + \gamma\|x\|\right) > 0. \tag{59}$$

From (3), we get $\psi(u) \le \beta_2 u$, substituting it into the switching surface equation; we obtain

$$\begin{aligned}\dot{s} &\le \Gamma(s,x) + \psi(u) + \gamma\|x\| \le \Gamma(s,x) + \beta_2 u_*^+ + \gamma\|x\| \\ &\le \Gamma(s,x) + \gamma\|x\| - |ks| - \epsilon - \Gamma(s,x) - \gamma\|x\| \\ &\le -|ks| - \epsilon.\end{aligned} \tag{60}$$

(3) When $s < 0$ and $-|ks| - \epsilon + \Gamma(s,x) - \gamma\|x\| > 0$, we get

$$u = u_*^- = \frac{1}{\beta_2}\left(|ks| + \epsilon - \Gamma(s,x) + \gamma\|x\|\right) < 0. \tag{61}$$

From (3), we get $\psi(u) \ge \beta_2 u$, substituting it into the switching surface equation, and we obtain

$$\begin{aligned}\dot{s} &\ge \Gamma(s,x) + \psi(u) - \gamma\|x\| \ge \Gamma(s,x) + \beta_2 u_*^- - \gamma\|x\| \\ &\ge \Gamma(s,x) - \gamma\|x\| + |ks| + \epsilon - \Gamma(s,x) + \gamma\|x\| \\ &\ge |ks| + \epsilon.\end{aligned} \tag{62}$$

(4) When $s < 0$ and $-|ks| - \epsilon + \Gamma(s,x) - \gamma\|x\| < 0$, we get

$$u_*^- = \frac{1}{\beta_1}\left(|ks| + \epsilon - \Gamma(s,x) + \gamma\|x\|\right) > 0. \tag{63}$$

From the above equation, we get $\psi(u) \ge \beta_1 u$, substituting it into the switching surface equation, and we obtain

$$\begin{aligned}\dot{s} &\ge \Gamma(s,x) + \psi(u) - \gamma\|x\| \ge \Gamma(s,x) + \beta_2 u_*^- - \gamma\|x\| \\ &\ge \Gamma(s,x) - \gamma\|x\| + |ks| + \epsilon - \Gamma(s,x) + \gamma\|x\| \\ &\ge |ks| + \epsilon;\end{aligned} \tag{64}$$

hence, we can obtain Theorem 6 from (58)–(64). □

Comparison between the Control Law in Theorems 4 and 6. From the proofs of Theorems 4 and 6, we can see that when

$$\begin{aligned}&s > 0, \quad -|ks| - \epsilon - \Gamma(s,x) - \gamma\|x\| < 0, \\ &s < 0, \quad -|ks| - \epsilon + \Gamma(s,x) - \gamma\|x\| > 0,\end{aligned} \tag{65}$$

the speed of reaching the switching surface is obtained by the control laws in Theorem 4, and its expression is

$$\begin{aligned}&\dot{s} \le \Gamma(s,x) + \beta_1 u^+ + \gamma\|x\| = -|ks| - \epsilon, \quad s > 0, \\ &\dot{s} \ge \Gamma(s,x) + \beta_2 u^- - \gamma\|x\| = |ks| + \epsilon, \quad s < 0,\end{aligned} \tag{66}$$

and the speed of reaching the switching surface is obtained by the control laws in Theorem 6, and its expression is

$$\begin{aligned}&\dot{s} \le \Gamma(s,x) + \beta_1 u_*^+ + \gamma\|x\| = -|ks| - \epsilon, \quad s > 0, \\ &\dot{s} \ge \Gamma(s,x) + \beta_2 u_*^- - \gamma\|x\| = |ks| + \epsilon, \quad s < 0,\end{aligned} \tag{67}$$

and we can see that the speeds obtained by the two control laws are identical from the above two equations, but, when

$$\begin{aligned}&s > 0, \quad \Gamma(s,x) + \gamma\|x\| \ll -|ks| - \epsilon, \\ &s < 0, \quad \Gamma(s,x) - \gamma\|x\| \gg |ks| + \epsilon,\end{aligned} \tag{68}$$

by the control law in Theorem 4, we get

$$u = u^- = u^+ = 0. \tag{69}$$

Substituting the above controller into the switching surface equation, we get

$$\begin{aligned}&\dot{s} \le \Gamma(s,x) + \beta_1 u + \gamma\|x\| \ll -|ks| - \epsilon, \quad s > 0, \\ &\dot{s} \le \Gamma(s,x) + \beta_2 u - \gamma\|x\| \gg |ks| + \epsilon, \quad s < 0,\end{aligned} \tag{70}$$

while, by the control law in Theorem 6, we get

$$u = u_*^+ = u_*^- = -\frac{|ks| + \epsilon + \Gamma(s,x) + \gamma\|x\|}{\beta_2} > 0. \tag{71}$$

Substituting the above controller into the switching surface equation, we get

$$\begin{aligned}&\dot{s} \le \Gamma(s,x) + \beta_2 u_*^+ + \gamma\|x\| = -|ks| - \epsilon, \quad s > 0, \\ &\dot{s} \ge \Gamma(s,x) + \beta_2 u_*^- - \gamma\|x\| = |ks| + \epsilon, \quad s < 0,\end{aligned} \tag{72}$$

and we can see that the improved control law can change the case that the movement starting from any point in the state space reaches the switching surface too fast from (70) and (72). We can improve the rapidity of the system's trajectories to reach the sliding mode, effectively weaken the chattering of sliding mode, and improve the system dynamic quality by choosing appropriate parameters $k > 0$ and $\epsilon > 0$.

6. Simulation Example

In this section, we shall give an example to demonstrate the effectiveness of the control law in Theorem 6 and meanwhile compare it with the control law in literature [22].

When $\alpha = 1$, the unified chaotic system (1) denotes Chen's chaotic system, that is

$$\begin{aligned}\dot{x}_1 &= 35(x_2 - x_1), \\ \dot{x}_2 &= -7x_1 + 28x_2 - x_1x_3, \\ \dot{x}_3 &= x_1x_2 - 3x_3,\end{aligned} \tag{73}$$

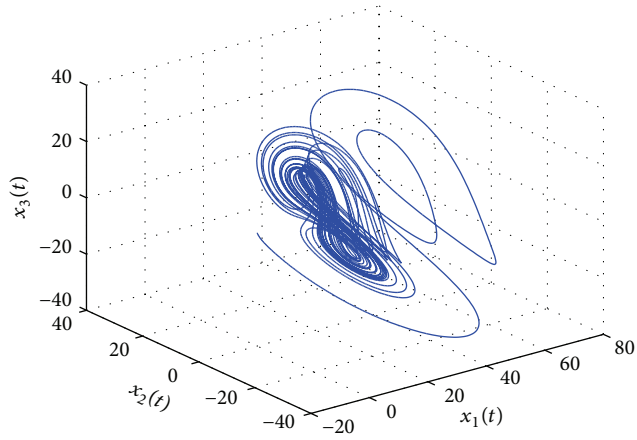

FIGURE 2: Phase portraits of Chen chaotic system.

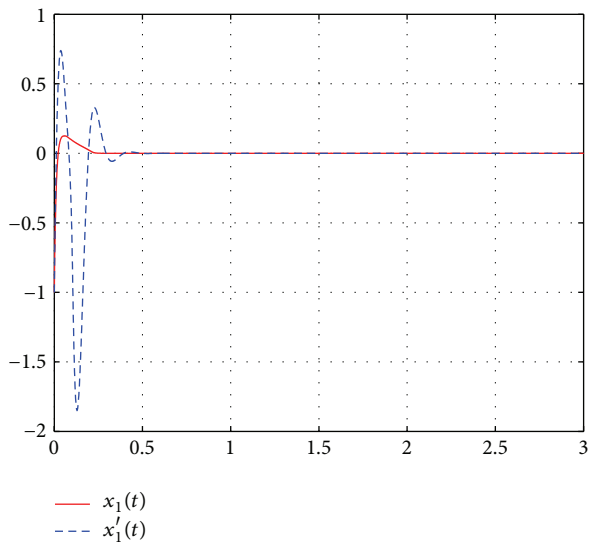

FIGURE 3: State variable $x_1(t) - t$.

by using Simulink, and Chen's chaotic attractor is shown in Figure 2, where we choose the initial values as $(x_1(0), x_2(0), x_3(0)) = (1.00, -1.00, -1.01)$.

The controlled system with disturbances is

$$\begin{aligned} \dot{x}_1 &= 35\left(x_2 - x_1\right), \\ \dot{x}_2 &= -7x_1 + 28x_2 - x_1x_3 + \Delta f\left(x, t\right) + \psi\left(u\right), \\ \dot{x}_3 &= x_1x_2 - 3x_3, \end{aligned} \tag{74}$$

where external disturbance $\Delta f = 0.5\cos(3\pi t)\|x\|$, $x = (x_1, x_2, x_3)^T$.

Obviously, parameter $\gamma = 0.5$. We choose nonlinear input as $\psi(u(t)) = [0.8 + 0.2\sin(u(t))]u(t)$; from (3), we can get parameters $\beta_1 = 0.6$ and $\beta_2 = 1.0$. Simulation results of nonlinear function $\psi(u(t))$ are shown in Figure 1.

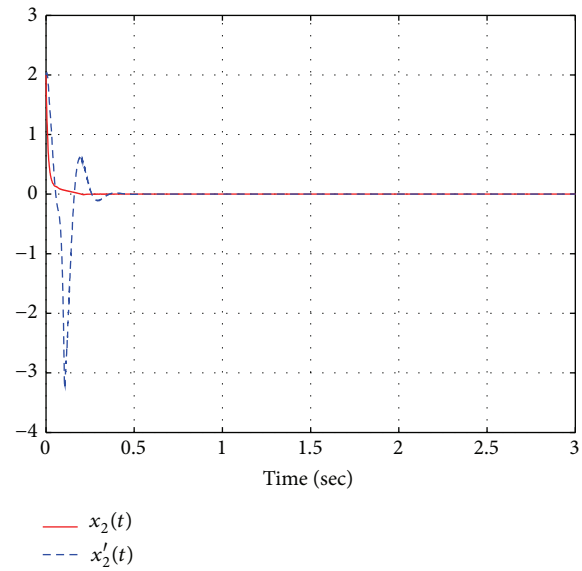

FIGURE 4: State variable $x_2(t) - t$.

6.1. Simulation Example by Using This Paper Control Law. According to Theorem 3 in this paper, we can choose the switching surface function as

$$s\left(t\right) = -\left(1 - \delta\right)x_1 + x_2, \tag{75}$$

where parameter $\delta = 2$, and, according to (55) in Theorem 6 and (30) and (54), we can choose the control law as

$$u\left(t\right) = \frac{1}{2}\left(u_*^+ + u_*^-\right) + \frac{1}{2}\left(u_*^+ - u_*^-\right)\operatorname{sgn}\left(s\left(t\right)\right), \tag{76}$$

where $k = 1$, $\epsilon = 0.5$, $c_1 = \delta - 1 = 1$ are chosen.

6.2. Simulation Example by Using the Control Law in Paper [22]. According to (5) and (6) in literature [22], we can choose the corresponding switching surface function as

$$\begin{aligned} s\left(t\right) &= x_2\left(t\right) + \rho\left(t\right), \\ \dot{\rho}\left(t\right) &= 35x_1 + x_1x_3 + 0.5x_2, \end{aligned} \tag{77}$$

and, according to (11) in Theorem 1 in literature [22], we can choose the control law as

$$\begin{aligned} u\left(t\right) &= -2\eta\operatorname{sgn}\left(s\left(t\right)\right), \\ \eta &= \left|28x_1 + 27x_2\right| + 0.5\left\|x\right\|. \end{aligned} \tag{78}$$

Simulink results are shown in Figures 3–7, where the red solid lines in all curves denote Simulink results obtained by the control law in this paper, the blue dashed lines in all curves denote Simulink results obtained by the control law in paper [22], which is to say, $x_1(t), x_2(t), x_3(t), s(t), u(t)$ denote Simulink results obtained by the control law in this paper and $x_1'(t), x_2'(t), x_3'(t), s'(t), u'(t)$ denote Simulink results obtained by the control law in paper [22] in all curves.

Figures 3–5 are the state curves with respect to time; we can see that the designed control law algorithm in this paper

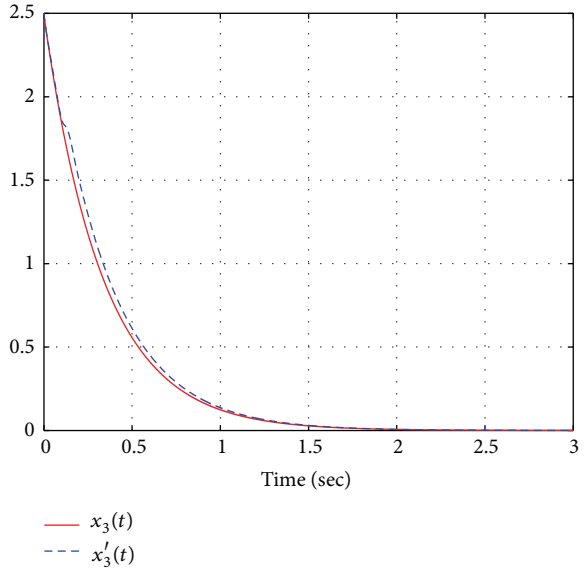

FIGURE 5: State variable $x_3(t) - t$.

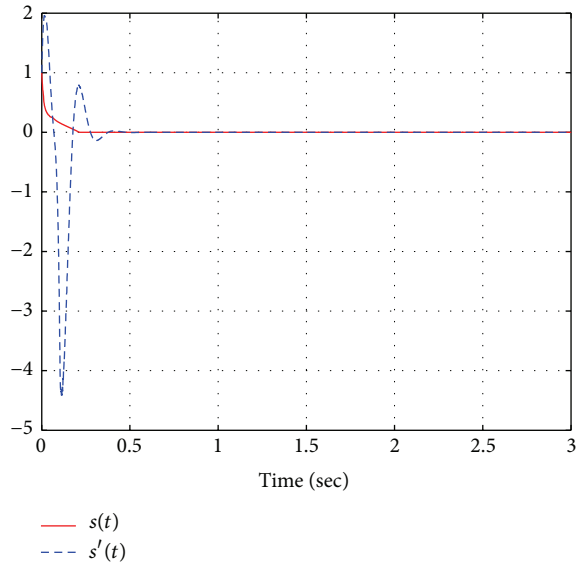

FIGURE 6: Sliding mode surface $s(t) - t$.

and in literature [22] are all able to control the state variable to the neighborhood of the equilibrium point, but the solid lines (the designed control law algorithm in this paper) are superior to the dashed lines (the control law in paper [22]) in rapidity and stationarity. Figure 6 is the switching function curve with respect to time, and it can be seen that the control law in this paper can effectively weaken the chattering of the sliding mode, the chattering obtained by the designed control law algorithm in this paper is much less than the chattering obtained by the designed control law algorithm in paper [22]. Figure 7 is the control function curve with respect to time, as can be seen by comparing; the controller designed in this paper has many advantages, such as small chattering, good stability, and less conservative.

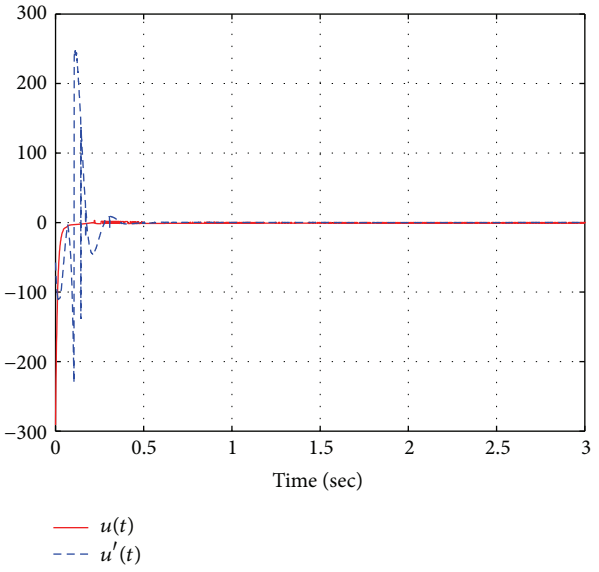

FIGURE 7: Input variable $u(t) - t$.

7. Conclusions

The designed control law algorithm in this paper can realize the stabilization of the chaotic system with external disturbances and has good inhibition to the uncertainty. Compared with the existing literature, the control law algorithm in this paper can improve the quickness of reaching the sliding mode and also effectively weaken the chattering of the sliding mode; meanwhile the algorithm also can reduce the conservatism of the parameter design of the controller, and both the analysis of the motion equation and simulation results confirm the effectiveness of the conclusion.

Competing Interests

The authors declare that they have no competing interests.

Acknowledgments

This work was supported by National Natural Science Foundation of China (60774057); Appropriative Researching Fund for Professors and Doctors, Guangdong University of Education (2014ARF25); Science and Technology Planning Project of Guangdong Province, China (2016A010106007); Applied Science and Technology Special Funds Project of Guangdong Province, China (2016B090927010); Foundation for Ph.D. of Henan Normal University, China (5101019170158); Key Scientific Research Project of Universities and Colleges in Henan, China (16A120005).

References

[1] F. H. Min, *Research Some Problems in Control and Synchronization of Chaotic Systems*, Nanjing University of Science and Technology, Nanjing, China, 2007.

[2] S.-Y. Li and Z.-M. Ge, "Fuzzy modeling and synchronization of two totally different chaotic systems via novel fuzzy model," *IEEE Transactions on Systems, Man, and Cybernetics, Part B: Cybernetics*, vol. 41, no. 4, pp. 1015–1026, 2011.

[3] M. Srivastava, S. P. Ansari, S. K. Agrawal, S. Das, and A. Y. Leung, "Anti-synchronization between identical and non-identical fractional-order chaotic systems using active control method," *Nonlinear Dynamics*, vol. 76, no. 2, pp. 905–914, 2014.

[4] L. Zhang and X. Liu, "The synchronization between two discrete-time chaotic systems using active robust model predictive control," *Nonlinear Dynamics*, vol. 74, no. 4, pp. 905–910, 2013.

[5] X. Yang, J. Cao, and J. Lu, "Synchronization of markovian coupled neural networks with nonidentical node-delays and random coupling strengths," *IEEE Transactions on Neural Networks and Learning Systems*, vol. 23, no. 1, pp. 60–71, 2012.

[6] M. Yahyazadeh, N. R. Noei, and R. Ghaderi, "Synchronization of chaotic systems with known and unknown parameters using a modified active sliding mode control," *ISA Transactions*, vol. 50, no. 2, pp. 262–267, 2011.

[7] X. Feng, F. Zhang, and W. Wang, "Global exponential synchronization of delayed fuzzy cellular neural networks with impulsive effects," *Chaos, Solitons & Fractals*, vol. 44, no. 1–3, pp. 9–16, 2011.

[8] J. Lu, D. W. C. Ho, J. Cao, and J. Kurths, "Exponential synchronization of linearly coupled neural networks with impulsive disturbances," *IEEE Transactions on Neural Networks*, vol. 22, no. 2, pp. 329–335, 2011.

[9] W. He, F. Qian, Q.-L. Han, and J. Cao, "Synchronization error estimation and controller design for delayed Lur'e systems with parameter mismatches," *IEEE Transactions on Neural Networks and Learning Systems*, vol. 23, no. 10, pp. 1551–1563, 2012.

[10] W. Zhou, D. Tong, Y. Gao, C. Ji, and H. Su, "Mode and delay dependent adaptive exponential synchronization in pth moment for stochastic delayed neural networks with Markovian switching," *IEEE Transactions on Neural Networks and Learning Systems*, vol. 23, no. 4, pp. 662–668, 2012.

[11] Z.-G. Wu, P. Shi, H. Su, and J. Chu, "Exponential synchronization of neural networks with discrete and distributed delays under time-varying sampling," *IEEE Transactions on Neural Networks and Learning Systems*, vol. 23, no. 9, pp. 1368–1376, 2012.

[12] H.-J. Zhu and C.-B. Zeng, "Scaling and mixed synchronization for different chaotic systems with totally unknown parameters," *Control Theory & Applications*, vol. 32, no. 3, pp. 341–346, 2015.

[13] Z.-B. Li and J.-S. Tang, "Chaotic synchronization with parameter perturbation and its secure communication scheme," *Control Theory & Applications*, vol. 31, no. 5, pp. 592–600, 2014.

[14] V. V. Alekseevv and A. Y. Loskutov, "Control of a system with a strange attractor through periodic parametric action," *Soviet Physics Doklady*, vol. 32, no. 4, pp. 1346–1348, 1987.

[15] A. W. Hubler, "Adaptive control of chaotic systems," *Helvetica Physica Acta*, vol. 62, no. 2, pp. 343–346, 1989.

[16] E. Ott, C. Grebogi, and J. A. Yorke, "Controlling chaos," *Physical Review Letters*, vol. 64, no. 11, pp. 1196–1199, 1990.

[17] J. A. Gallegos, "Nonlinear regulation of a Lorenz system by feedback linearization techniques," *Dynamics and Control*, vol. 4, no. 3, pp. 277–298, 1994.

[18] X.-S. Luo, B.-H. Wang, F. Jiang, and Y. Gao, "Using random proportional pulse feedback of system variables to control chaos and hyperchaos," *Chinese Physics*, vol. 10, no. 1, pp. 17–20, 2001.

[19] G.-G. Liu and Y. Zhao, "Adaptive control on a class of uncertain chaotic systems," *Chinese Physics Letters*, vol. 22, no. 5, pp. 1069–1071, 2005.

[20] R. Luo and Y. Zeng, "The adaptive control of unknown chaotic systems with external disturbance via a single input," *Nonlinear Dynamics*, vol. 80, no. 1-2, pp. 989–998, 2015.

[21] C.-T. Lin and C.-P. Jou, "Controlling chaos by GA-based reinforcement learning neural network," *IEEE Transactions on Neural Networks*, vol. 10, no. 4, pp. 846–859, 1999.

[22] T.-Y. Chiang, M.-L. Hung, J.-J. Yan, Y.-S. Yang, and J.-F. Chang, "Sliding mode control for uncertain unified chaotic systems with input nonlinearity," *Chaos, Solitons & Fractals*, vol. 34, no. 2, pp. 437–442, 2007.

[23] L. G. Zhang and Y. Yan, "Robust synchronization of two different uncertain fractional-order chaotic systems via adaptive sliding mode control," *Nonlinear Dynamics*, vol. 76, no. 3, pp. 1761–1767, 2014.

[24] J. Lü, G. Chen, D. Cheng, and S. Celikovsky, "Bridge the gap between the Lorenz system and the Chen system," *International Journal of Bifurcation and Chaos*, vol. 12, no. 12, pp. 2917–2926, 2002.

[25] C.-H. Tao, J.-A. Lu, and J.-H. Lü, "The feedback synchronization of a unified chaotic system," *Acta Physica Sinica*, vol. 51, no. 7, pp. 1500–1501, 2002.

[26] J. Liu, S. H. Chen, and J. A. Lu, "Projective synchronization in a unified chaotic system and its control," *Acta Physica Sinica*, vol. 52, no. 7, pp. 1595–1599, 2003.

[27] X.-P. Guan and Y.-H. He, "Stabilizing unstable equilibrium point of unified chaotic systems with unknown parameter using sliding mode control," *Chinese Physics Letters*, vol. 21, no. 2, pp. 227–229, 2004.

[28] Y. Z. Song, G. Z. Zhao, and D. L. Qi, "Some comments on constrained control of chaos," *Physics Letters A*, vol. 359, no. 6, pp. 624–626, 2006.

[29] D.-L. Qi, X.-R. Li, and G.-Z. Zhao, "Passive control of hybrid chaotic dynamical systems," *Journal of Zhejiang University*, vol. 38, no. 1, pp. 86–97, 2004.

[30] J. T. Li, W. L. Li, and Q. P. Li, "Sliding mode control for uncertain chaotic systems with input nonlinearity," *Communications in Nonlinear Science and Numerical Simulation*, vol. 17, no. 1, pp. 341–348, 2012.

[31] T. H. Lee, J. H. Park, S. M. Lee, and O. M. Kwon, "Robust synchronisation of chaotic systems with randomly occurring uncertainties via stochastic sampled-data control," *International Journal of Control*, vol. 86, no. 1, pp. 107–119, 2013.

[32] K. K. Hassan, *Nonlinear Systems*, Prentice Hall, 3rd edition, 2001.